İSTANBUL TECHNICAL UNIVERSITY ★ INSTITUTE OF SCIENCE AND TECHNOLOGY

APPLIED ROBUST MOTION CONTROL

Ph.D. Thesis by
Bilin AKSUN GÜVENÇ, M.Sc.

(503962002)

Date of submission : 14 February 2001

Date of defence examination: 20 July 2001

Supervisor (Chairman): Assoc. Prof. Dr. Levent GÜVENÇ

Members of the Examining Committee Prof.Dr. Aydın HIZAL (İ.T.Ü.)

Assoc.Prof.Dr. Metin GÖKAŞAN (İ.T.Ü.)

Prof.Dr. Osman TÜRKAY (B.Ü.)

Prof.Dr. Abdülkerim KAR (M.Ü.)

JULY 2001

İSTANBUL TEKNİK ÜNİVERSİTESİ ★ FEN BİLİMLERİ ENSTİTÜSÜ

UYGULAMALI GÜRBÜZ HAREKET KONTROLÜ

DOKTORA TEZİ

Y. Müh. Bilin AKSUN GÜVENÇ
(503962002)

Tezin Enstitüye Verildiği Tarih : 14 Şubat 2001
Tezin Savunulduğu Tarih : 20 Temmuz 2001

Tez Danışmanı :	**Doç.Dr. Levent GÜVENÇ**
Diğer Jüri Üyeleri	**Prof.Dr. Aydın HIZAL (İ.T.Ü.)**
	Doç.Dr. Metin GÖKAŞAN (İ.T.Ü.)
	Prof.Dr. Osman TÜRKAY (B.Ü.)
	Prof.Dr. Abdülkerim KAR (M.Ü.)

TEMMUZ 2001

FOREWORD

I would especially like to thank my advisor Assoc. Prof. Levent Güvenç for his valuable guidance during the course of my Ph.D. study. I am grateful to my dear parents Tanju and Alparslan Aksun for their great support throughout my life. In addition, I would also like to thank Prof. Jürgen Ackermann and the friends in the department of Robust Control at the Institute of Robotics and Mechatronics at German Aerospace Center-Oberpfaffenhofen (DLR-Oberpfaffenhofen) for allowing me to join their Robust Control Group during the year 2000. My thanks also go to my friends at İstanbul Technical University for the friendship and moral support they have provided me with during the course of my graduate studies.

Bilin AKSUN GÜVENÇ July 2001

TABLE OF CONTENTS

LIST OF ABBREVIATIONS

CG : Center of Gravity
EPTC : Extended Precision Tracking Control
MP : Minimum Phase
NMP : Nonminimum Phase
NP : Nominal Performance
OPTC : Optimal Precision Tracking Control
PTC : Precision Tracking Control
RHP : Right Half Plane
RP : Robust Performance
RS : Robust Stability
SSV : Structured Singular Value
TSA : Truncated Series Approximation
ZPET : Zero Phase Error tracking Control

LIST OF TABLES

Page No.

LIST OF FIGURES

Page No.

Page No.

LIST OF SYMBOLS

μ	: Coefficient of friction
ζ	: Damping ratio
θ^*	: Desired normalized tracking bandwidth
λ	: Eigenvalue
ω	: Frequency
δ_f	: Front wheel steering angle
$\overline{\sigma}$	: Maximum singular value
Δ_m	: Multiplicative model uncertainty
θ	: Normalized frequency
δ_r	: Real wheel steering angle
ρ	: Spectral radius
$\mu(M)$	: Structured singular value of M
τ	: Time constant
Δ	: Uncertainty
β	: Chassis side slip angle at vehicle CG
$\alpha_f\ (\alpha_r)$	: Front (rear) tire side slip angle
σ	: Singular value
$\boldsymbol{C}$	: Field of complex numbers
c_f	: Front wheel cornering stiffness
c_r	: Rear wheel cornering stiffness
d	: Disturbances
F_x, F_y	: Forces in the x and y directions
$F_f\ (F_r)$	: Lateral wheel force at front (rear) wheel
J	: The moment of inertia w.r.t. a vertical axis through the CG
L	: Loop gain
$l_f\ (l_r)$	: Distance from front (rear) axle to CG
m	: The mass of the vehicle
M_z	: Moment about the vertical axis z through the center of gravity (CG)
n	: Sensor noise
$\boldsymbol{R}$	: Field of real numbers
r	: Yaw rate
s	: Laplace transform variable
S	: Sensitivity function
T	: Complementary sensitivity function
T_s	: Sampling time
v	: Velocity
v_d	: Desired speed
W_S	: Sensitivity function weight

W_T : Complementary sensitivity function weight

APPLIED ROBUST MOTION CONTROL

SUMMARY

This thesis concentrates on the analysis and design of robust motion control systems with particular attention on some promising motion control algorithms. Mainly, a generic robust motion control structure is proposed and seen to work very well both theoretically and in the context of applications. This robust motion control architecture has what is known as a model regulator in an inner loop which can be used alone or in conjunction with a feedback controller. This structure can be further complemented by a preview based feedforward control block which is explained in detail in Chapters 2 and 3. This architecture and how it can be exploited to get better results in motion control applications as far as performance and robustness of performance are concerned is treated in detail in Chapters 4, 5 and 6. The main applications treated here are in the area of automobile dynamics control. The robust motion control concepts developed are applied to vehicle lateral control (yaw stabilization) and automated path following. Both of these applications are quite important in the automotive industry. The application of the robust motion control structure proposed here to these vehicle control problems is a new approach, resulting in the development of several application-induced design and structural enhancements. The simulation results obtained demonstrate the superior nature of the results in comparison to those previously reported in the literature. Noting that several practical motion control algorithms involve repetitive tasks or disturbances, this thesis also considers the related, more specific needs of such systems by treating a robust repetitive control architecture which is explained in detail in Chapter 7 also. This thesis ends with the conclusions being given in Chapter 8.

UYGULAMALI GÜRBÜZ HAREKET KONTROLÜ

ÖZET

Bu tez öncelikli olarak bazı ümit vaadeden hareket kontrolü algoritmaları olmak üzere gürbüz konum kontrolü sistemlerinin analiz ve tasarımı üzerinde yoğunlaşmıştır. Başlıca olarak bir genel gürbüz konum kontrolü yapısı öne sürülmüş ve teorik olarak da uygulama çerçevesi içinde de çok iyi çalıştığı görülmüştür. Bu gürbüz konum kontrolü yapısı tek başına veya bir geri besleme kontrolcüsü ile birlikte olmak üzere kullanılabilen bir model regülatörü içermektedir. Bu yapı ayrıca ikinci ve üçüncü bölümlerde ayrıntılı bir şekilde açıklanmış olan ön görülü ileri besleme kontrol bloğu ile de tamamlanabilmektedir. Bu kontrol yapısı ve konum kontrolü uygulamalarında performans ve performans gürbüzlüğü göz önünde bulundurularak daha iyi sonuçlar elde edebilmek için nasıl kulanılacağı detaylı olarak dördüncü, beşinci ve altıncı bölümlerde işlenmiştir. Burada ele alınan başlıca uygulamalar otomobil dinamiği kontrolü alanındadır. Geliştirilmiş olan gürbüz konum kontrolü kavramları araç yanal kontrolü (yalpalama stabilizasyonu) ve otomatik yörünge takibine uygulanmıştır. Bu iki uygulama da otomotiv endüstrisinde oldukça büyük bir önem arzetmektedir. Bu tezde öne sürülmüş ve araç kontrol problemlerine uygulanmış olan gürbüz konum kontrolü yapısı çeşitli uygulamaya yönelik tasarım gelişimi ve yapısal iyileştirmeler ile sonuçlanmış olan yeni bir yaklaşımdır. Elde edilen simülasyon sonuçları literatürde daha önce bildirilmiş olan sonuçlara göre daha üstünlük göstermektedir. Pratikte bir çok konum kontrolü algoritmasının tekrarlı görev ve tekrarlı bozucu etkenleri içerdiği dikkate alınarak bu tip sistemlerin belirli ihtiyaçlarına yönelik olan gürbüz tekrarlı kontrol yapısı da ayrıca yedinci bölümde ele alınmıştır. Bu tez sekizinci bölümde verilmiş olan sonuçlar ile sona ermektedir.

1. INTRODUCTION

This thesis is on applied robust motion control. Motion control has been a subject of great interest among control engineers as most applications of control theory involve control of some of the variables related to the motion, meaning position, angular orientation, velocity and acceleration of the process being controlled. Among the typical and widely studied motion control systems are linear positioning systems (x, xy stages, machine tools etc.) and robotics (joint control, end effector position and orientation control etc.). High-speed and high accuracy motion control is an important feature for increased productivity, improved quality of finished products and flexible operation of modern machine tools such as high speed machining centers. Some of the important considerations in attaining high speed and high accuracy motion control are the development and implementation of effective motion control algorithms to achieve precision positioning and tracking. Consequently, there have been an abundence of work on controller design for performance improvement in motion control systems. Matching the impetus on robustness issues in controller analysis and design after the 80's, the motion control industry has also seen a corresponding increase in research on and implementation of robust motion controllers in the 90's. This robust motion control analysis and design trend is presently continuing, since increasingly more performance is demanded from such systems even in the presence of model uncertainties. Model uncertainties can arise from various sources including for example the aging of components, differences from one set to another within a batch of manufactured motion control equipment and unmodeled high frequency dynamics, among others.

This thesis concentrates on the analysis and design of robust motion control systems. In this thesis, some promising motion control algorithms are treated. Mainly, a generic robust motion control structure is proposed and seen to work very well both theoretically and in the context of applications. This robust motion control architecture has what is known as a model regulator in an inner loop which can be used alone or in conjunction with a feedback controller. This structure can be further complemented by a preview based feedforward control block. This architecture and how it can be exploited to get better results in motion control applications as far as performance and robustness of performance are concerned is treated in detail in this thesis. Along with some standard, well known positioning applications, the main applications treated here come from the automotive industry. The robust motion control concepts developed are applied to vehicle lateral control (yaw stabilization) and automated path following. Both of these applications are quite important in the automotive industry. Further, the application of the robust motion control structure proposed here to these vehicle control problems is a new approach, resulting in the development of several application-induced design and structural enhancements. Noting that several practical motion control algorithms involve repetitive tasks or disturbances, this thesis also considers the related, more specific needs of such systems by treating a robust repetitive control architecture also.

The organization of the rest of the thesis is as follows. In Chapter 2, different preview based reference feedforward tracking control techniques are presented. The aim in reference feedforward tracking control is to increase tracking bandwidth beyond what is available with the feedback controller alone. In Chapter 3, the use of structured singular value (SSV) analysis along with a suitably chosen measure of performance is utilized to develop a useful tool for evaluating performance robustness of discrete time reference feedforward control systems. In Chapter 4, the model regulator, which is a two degree of freedom controller that provides desired model following and very good disturbance rejection along with a high level of robustness to unmodeled dynamics, is presented. The application of the model regulator architecture to vehicle lateral control (yaw stabilization) and automated path following are treated in Chapters 5 and 6, respectively. There is a group of applications where the motion control problem addressed has periodic reference inputs or periodic disturbances. Motion controllers that take into account the periodic nature of the exogenous input work much better for such applications. Repetitive control is such a motion control scheme that has been developed specifically for handling systems with repetitive references/disturbances and is treated in Chapter 7. The thesis ends with the conclusions being summarized in Chapter 8.

2. REFERENCE FEEDFORWARD TRACKING CONTROL

The aim in reference feedforward tracking control is to obtain a low pass filter of desired tracking bandwidth between the input and the output to reduce tracking error. A two degree of freedom controller architecture is used to achieve this purpose by cascading the closed loop system, already under feedback control, with its approximate inverse, as shown in Figure 2.1. The second degree of design freedom afforded by the feedforward control block $\tilde{G}_{fb}^{-1}$ is used to reduce tracking error below what is achievable with only the feedback controller C. While the feedback controller must be limited to causal filters, the approximate inverse filter $\tilde{G}_{fb}^{-1}$ is allowed to be noncausal since off-line computation and hence preview of the input signal R is possible in feedforward tracking control.

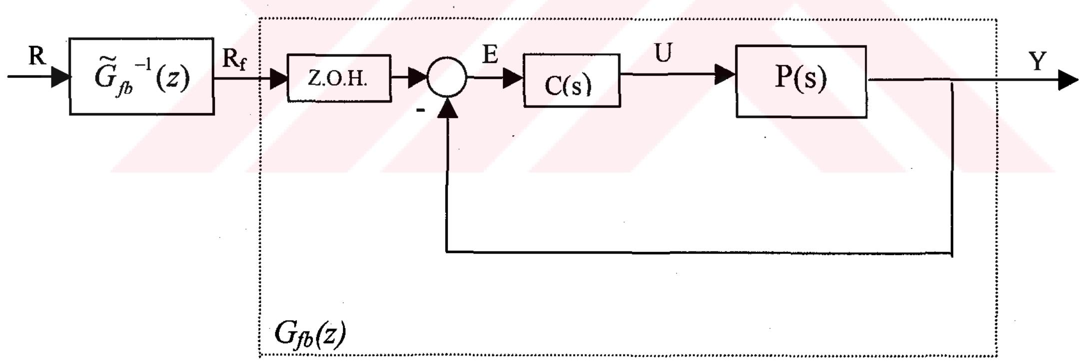

Figure 2.1 Discrete time reference feedforward tracking control

Seeking an exact inverse based on pole-zero cancellation to achieve perfect compensation of the plant or closed loop system is the ideal goal. This is not possible since nonminimum phase (NMP) zeros, if they exist, cannot be inverted directly. NMP zeros are quite common in models of process control systems with transport lag (Ogata, 1990) and flexible structures (Cannon and Schmitz, 1984). It is also a well known fact that even the zero order hold equivalent of a minimum phase continuous time plant with relative degree greater than two will always be NMP for large enough sampling rate (Aström et al, 1984). Due to the presence of high frequency modeling errors, exact inversion is not a good idea even for minimum phase systems and an approximate inverse should be used to achieve low pass filter characteristics between system input and output for better performance robustness.

2.1 Discrete Time NMP Zeros

Consider the zero-order-hold (ZOH) discretized version G(z) of a continuous time plant H(s) that is illustrated in Figure 2.2. For H(s) with n poles and m zeros, G(z) has n poles and n-1 zeros, some of which may be at infinity. Even though poles p_i of H(s) are transformed simply into poles $e^{p_i T_s}$ of G(z), the transformation of the zeros is much more complicated. In the limiting case of small sampling time T_s, the location of the zeros of G(z) are governed by the following theorem.

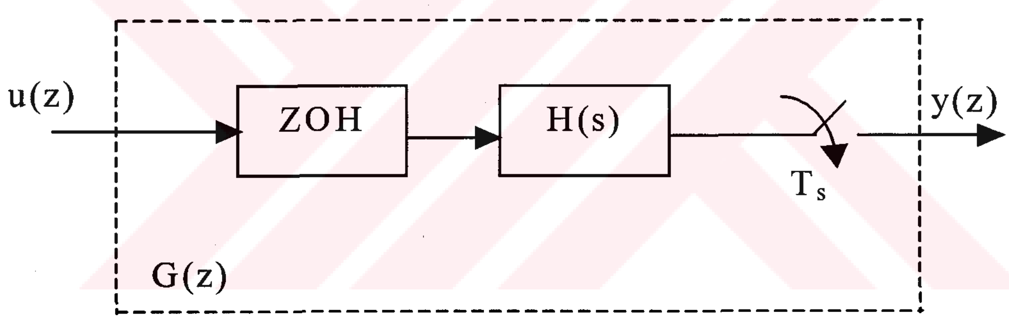

Figure 2.2 ZOH discrete time equivalent

Theorem 2.1 (Aström et al, 1984): Let H(s) be the rational function

$$H(s) = K\frac{(s-z_1)(s-z_2)...(s-z_m)}{(s-p_1)(s-p_2)...(s-p_n)}; \quad m < n \tag{2.1}$$

and G(z) the corresponding pulse transfer function. Then, as $T_s \to 0$, m zeros of G(z) go to 1 as $e^{z_i T_s}$ and the remaining n-m-1 zeros of G(z) go to zeros of the polynomial $B_{n-m}(z)$.

The polynomials $B_{n-m}(z)$ are given in Jury (1964) and Aström et al (1984) and have both MP and NMP real zeros for n-m≥2. None of the NMP zeros of $B_{n-m}(z)$ are complex. So, G(z) corresponding to H(s) with relative degree greater than or equal to 2 (n-m≥2) will necessarily have real NMP zeros coming from $B_{n-m}(z)$ for small sampling time. Complex NMP zeros, if they exist, occur in complex conjugate pairs since G(z) is real rational. The conditions under which complex NMP zeros occur for small sampling time can be determined using Theorem 2.1 and are summarized by the following corollary.

Corollary 2.1: For small T_s, the m_c ($2m_c<m$) complex conjugate zero pairs of H(s) in (2.1), if any, result in m_c complex conjugate zero pairs of G(z) which go to 1 as $e^{z_i T_s} = e^{T_s \operatorname{Re}(z_i)} e^{jT_s \operatorname{Im}(z_i)}$ as $T_s \to 0$.

Some remarks that follow from Theorem 2.1 and its corollary are listed below.

Remark 1: For small T_s, complex zeros of G(z) are only possible for H(s) with m≥2.

Remark 2: For small T_s, G(z) will have complex NMP zeros if and only if H(s) has complex NMP zeros.

The locations of zeros of G(z) in the limiting case of large sampling time are characterized by the following theorem.

Theorem 2 (Aström et al, 1984): Let H(s) be a strictly proper, stable and rational transfer function with H(0)≠0. Then all zeros of G(z) go to 0 as $T_s \to \infty$.

Note that for large sampling time, complex zeros of H(s) may become real zeros of G(z). Also, it is not possible for G(z) to have NMP zeros for large enough sampling time if H(s) satisfies the conditions of Theorem 2. A conservative condition to guarantee minimum phase G(z) is given in Aström et al (1984). Less conservative conditions can be found in Fu and Dumont (1989) and Ishitobi (1992).

The conditions under which NMP zeros can occur for large sampling time can be determined using Theorem 2 and are summarized by the following corollary.

Corollary 2.2: For large enough sampling time, G(z) can have NMP zeros if and only if H(s) satisfies one or more of the conditions: H(s) unstable, biproper or H(0)=0.

Example 2.1: Consider the continuous time transfer function

$$H(s) = \frac{(s^2 - 4s + 8)}{s(s^2 + 2s + 5)} \tag{2.2}$$

with two complex NMP zeros at $s_1, \bar{s}_1 = 2 \pm j2$. Figure 2.3 shows a plot of the zeros of G(z) corresponding to H(s) in (2.2) as T_s is varied. It is seen that G(z) has a complex conjugate NMP zero pair for small T_s as predicted by the corollary to Theorem 2.1. For large T_s, these zeros go to 0 as predicted by Theorem 2.2.

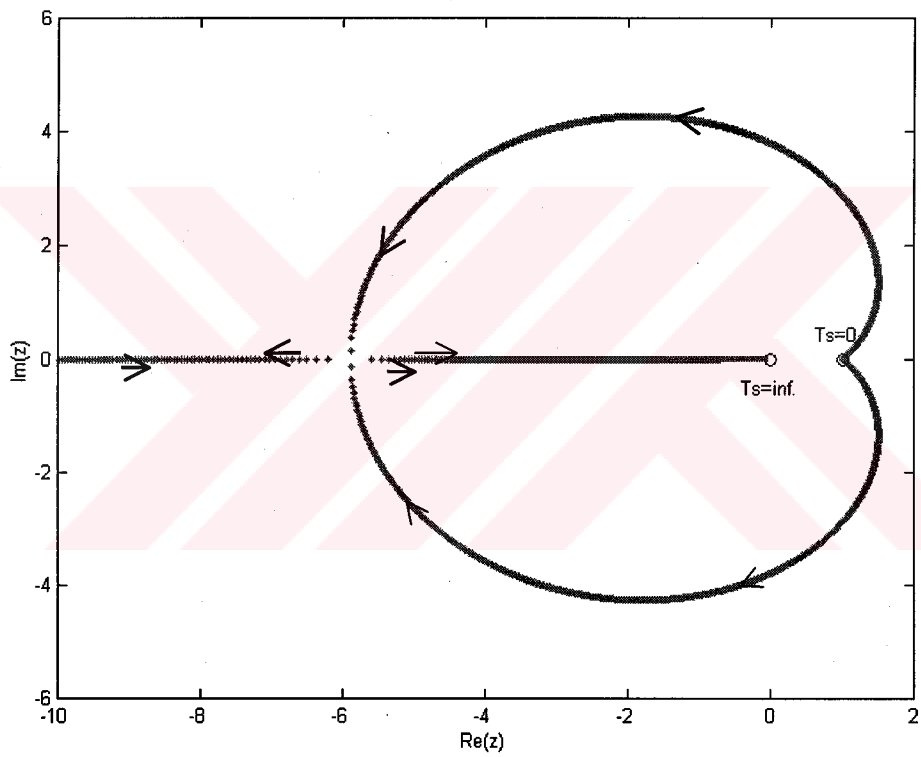

Figure 2.3 Location of zeros in example 1 for T_s: $0 \rightarrow \infty$

Example 2.2 (Aström et al, 1984): Consider

$$H(s) = \frac{1}{(s+1)(s^2+1)} \tag{2.3}$$

which has no zeros but two unstable poles on the imaginary axis. So, one of the conditions of Theorem 2.2 is not satisfied and G(z) can have NMP zeros for large enough sampling time by Corollary 2.2. G(z) has complex NMP zeros for some choices of T_s as shown in Figure 2.4. Note also that the zeros of G(z) do not go to zero as $T_s \to \infty$, since the conditions of Theorem 2 are not satisfied. In fact, the zeros start at $-2\pm\sqrt{3}$ for $T_s=0$, and traverse the complex plane periodically with a period in T_s of 2π (see Figure 2.4)

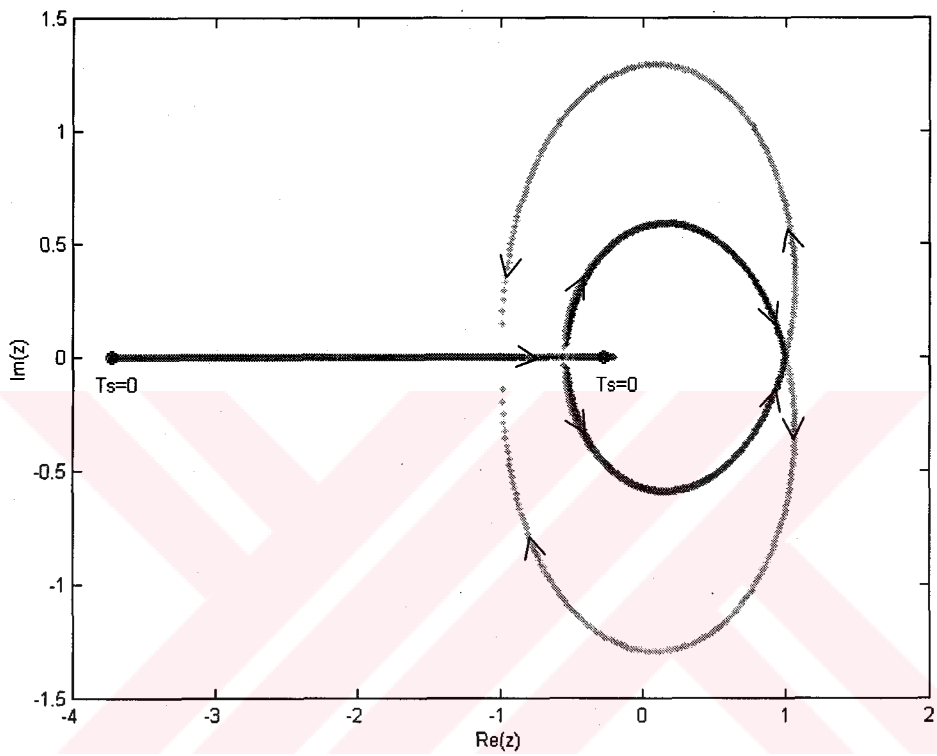

Figure 2.4 Location of zeros in example 2 for T_S: $0 \to \infty$

2.2 Different Feedforward Controller Designs

There are several methods that can be used to design non-causal approximate inverse filters for discrete-time systems with NMP zeros. Some of the important methods are introduced in this section. The earliest method of designing preview based reference feedforward controllers is the zero phase error tracking control (ZPET) scheme of Tomizuka (1987), where the phase error due to the NMP zeros is eliminated to achieve zero phase error trajectory tracking. Gain errors due to the NMP zeros still exist and can be compensated for by using the E filter (Haack and Tomizuka, 1991), the precision tracking control (PTC) method (Menq and Xia, 1990), the extended precision tracking control (EPTC) method (Güvenç et al, 1995) or the optimal precision tracking control (OPTC) method (Aksun Güvenç and Güvenç, 1999), among other methods, where additional gain compensating zeros are used to reduce the gain error for NMP zeros while keeping zero phase error characteristics. In the methods of PTC and EPTC, the gain compensating zero is determined using design equations based on a single point in the system frequency response to approximately obtain the desired bandwidth. The aim of OPTC is to design the gain compensating zero optimally. In the truncated series approximation (TSA) method of Gross et al (1994), polynomial long division is used to obtain a non-zero phase solution. This solution can also be obtained via an optimization approach.

2.2.1 Zero Phase Error Tracking (ZPET) Controller

The transfer function of the nominal feedback control architecture in Figure 2.1 can be expressed as

$$G_{fb}(z) = \frac{n_{mp}(z) n_{nmp}(z)}{d(z)} \tag{2.4}$$

where $n_{mp}(z)$ and $n_{nmp}(z)$ are the minimum and nonminimum phase parts, respectively, of the numerator. The nonminimum phase part of the numerator can be factored into

$$\begin{aligned} & n_{nmp}(z) = \prod_{k=1}^{m} (z - z_k) \\ & z_k \in \boldsymbol{C}, |z_k| \geq 1 \end{aligned} \tag{2.5}$$

where $\boldsymbol{C}$ denotes complex numbers. z_k's are thus the m nonminimum phase zeros of the feedback system. Noting that complex conjugation of factors of the form $z - z_k$ ($z_k \in \boldsymbol{C}$) over the unit circle amounts to

$$\overline{(z - z_k)\big|_{z=e^{j\theta}}} = (z^{-1} - \bar{z}_k)\big|_{z=e^{j\theta}} \tag{2.6}$$

the ZPET approximate inverse of $G_{fb}(z)$ is given by

$$\widetilde{G}_{ZPET}^{-1}(z) = \frac{d(z)}{n_{mp}(z)} \prod_{k=1}^{m} \frac{(z^{-1} - \bar{z}_k)}{(1 - z_k)(1 - \bar{z}_k)} \tag{2.7}$$

The first part of (2.7), $d(z)/n_{mp}(z)$, is the invertible part of $G_{fb}(z)$. The remaining part of (2.7) has been formulated so that the compensated system $\widetilde{G}_{ZPET}^{-1}(z)G_{fb}(z)$ has zero phase angle at all frequencies. Whatever can be inverted in $G_{fb}(z)$ has been inverted and the remaining nonminimum phase part has been multiplied by its complex conjugate in the frequency domain. The $(1-z_k)$ type terms in the denominator of (2.7) are introduced to make the d.c. gain of the feedforward compensated system equal to unity. The transfer function of the ZPET feedforward compensated system becomes

$$\widetilde{G}_{ZPET}^{-1}(z)G_{fb}(z) = \prod_{k=1}^{m} \frac{(z - z_k)(z^{-1} - \bar{z}_k)}{(1 - z_k)(1 - \bar{z}_k)} \tag{2.8}$$

This method assures that the phase shift between the reference input and the output becomes zero for all frequencies. However, while the phase errors are cancelled, this approach may increase the gain errors. Therefore, desired tracking control characteristics can be obtained only within a relatively small bandwidth. One should therefore combine the zero phase error of the ZPET method with a gain error compensation method.

Let's assume that z_k's which are the NMP zeros of the closed loop system are real.

$$\begin{gathered} n_{nmp}(z) = \prod_{k=1}^{m}(z - z_k) \\ z_k \in \boldsymbol{R}, |z_k| \geq 1 \end{gathered} \tag{2.9}$$

Consider only one of these real NMP zero terms and adjust for unity d.c. gain as

$$\frac{z - z_k}{1 - z_k} \tag{2.10}$$

Its frequency response is evaluated by letting $z = e^{j\theta}$ as

$$\frac{e^{j\theta} - z_k}{1 - z_k} \tag{2.11}$$

Here the angle θ with $0 \le \theta \le \pi$ is given by $\theta = \omega T_s$ where ω is the frequency and T_s is the sampling time. After manipulation, the frequency response magnitude and phase become

$$\left|\frac{z - z_k}{1 - z_k}\right|_{z=e^{j\theta}} = \sqrt{\frac{1 - 2z_k \cos\theta + z_k^2}{(1 - z_k)^2}} \tag{2.12}$$

$$\angle\left(\frac{z - z_k}{1 - z_k}\right)_{z=e^{j\theta}} = \tan^{-1}\frac{\sin\theta}{\cos\theta - z_k} \tag{2.13}$$

By examining equation (2.12), the NMP zeros are further divided into two types as type 1 and type 2 zeros based on whether they lie to the left or to the right of the unit circle (Menq and Xia, 1990). If $z_k < -1$, z_k is defined as a type 1 NMP zero and it is defined as a type 2 NMP zero if $z_k > 1$. The difference of these two types of NMP zeros can be seen from their amplitude Bode plots displayed in Figure 2.5. The first diagram in this figure shows that the gain of a type 1 NMP zeros attenuates from one as θ increases. On the other hand, the gain of a type 2 NMP zeros increases from one as θ increases. The presence of gain errors are evident from Figure 2.5. From the tracking viewpoint, these errors will severely degrade the tracking performance. The precision tracking control (PTC) method of Menq and Xia (1990) was formulated in order to compensate for the gain errors.

2.2.2 Precision Tracking Controller (PTC)

Gain errors due to type 1 NMP zeros can be compensated for by appropriately chosen type 2 NMP zeros in the feedforward compensator and vice versa. The zero phase error property is preserved in this method. The PTC feedforward compensator is given by

$$\tilde{G}_{PTC}^{-1}(z) = \frac{d(z)}{n_{mp}(z)} \prod_{k=1}^{m} \frac{(z^{-1} - \bar{z}_k)}{(1 - z_k)(1 - \bar{z}_k)} \frac{(z - z_k^*)(z^{-1} - \bar{z}_k^*)}{(1 - z_k^*)(1 - \bar{z}_k^*)} \tag{2.14}$$

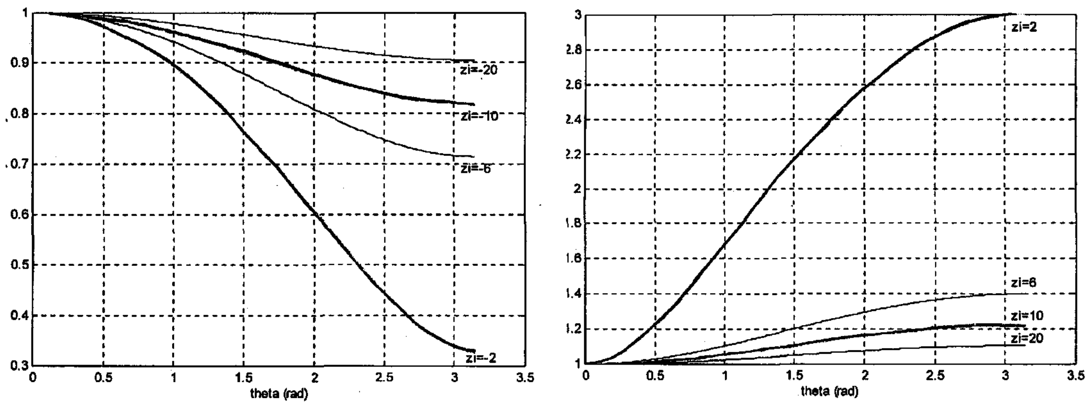

Figure 2.5 Normalized gain of type 1 (left) and type 2 (right) NMP zeros

where $z_k^* \in \boldsymbol{C}$ is the gain compensating zero corresponding to the NMP zero z_k. The PTC feedforward compensator in (2.14) adds gain compensating zero expressions adjusted for zero phase on top of the ZPET controller of (2.7). The transfer function of the feedforward compensated system becomes

$$\widetilde{G}_{PTC}^{-1}(z)G_{fb}(z) = \prod_{k=1}^{m} \frac{(z - z_k)(z^{-1} - \bar{z}_k)}{(1 - z_k)(1 - \bar{z}_k)} \frac{(z - z_k^*)(z^{-1} - \bar{z}_k^*)}{(1 - z_k^*)(1 - \bar{z}_k^*)} \tag{2.15}$$

and its frequency response is characterized by

$$\widetilde{G}_{PTC}^{-1}(z)G_{fb}(z)\Big|_{z=e^{j\theta}} = \prod_{k=1}^{m} \frac{(e^{j\theta} - z_k)(e^{-j\theta} - \bar{z}_k)}{(1 - z_k)(1 - \bar{z}_k)} \frac{(e^{j\theta} - z_k^*)(e^{-j\theta} - \bar{z}_k^*)}{(1 - z_k^*)(1 - \bar{z}_k^*)} \tag{2.16}$$

The gain compensating zeros are determined using

$$\left|\widetilde{G}_{PTC}^{-1}(e^{j\theta})G_{fb}(e^{j\theta})\right|_{\theta=\theta^*} = 1 \tag{2.17}$$

as the design equation. Here θ^* is the desired bandwidth. In the case of a real NMP zero and a real gain compensating zero, the following equation is derived for the purpose of finding z_k^* (Menq and Xia, 1990)

$$\cos\theta^* = \frac{1}{2}\left[\frac{(1-z_k)^2}{z_k} + \frac{(1-z_k^*)^2}{z_k^*}\right] + 1 \tag{2.18}$$

Using equation (2.18), the desired bandwidth θ^* can be achieved approximately by selecting an appropriate z_k^*. From the design viewpoint, if the desired bandwidth θ^* is specified, the following equation can be obtained from equation (2.18) to determine the corresponding z_k^* that should be used in the feedforward compensator.

$$\frac{(1-z_k^*)^2}{z_k^*} = -\left[\frac{(1-z_k)^2}{z_k} + 2(1-\cos\theta^*)\right] \tag{2.19}$$

From the result of equation (2.19), a PTC based feedforward controller which has zero phase shift and small gain error up to the desired bandwidth can be designed by substituting for z_k^* into (2.14).

By using PTC, the system tracking bandwidth can be assigned arbitrarily according to the tracking signal and the tracking accuracy can be greatly improved. But it should be kept in mind that even though the PTC design method usually results in satisfactory results, it is not an optimal method and there are situations where the desired bandwidth is not achieved. The PTC method has been extended by Güvenç et al (1995) to cope with pairs of complex conjugate NMP zeros as well. A characterization of complex nonminimum phase zeros is given in the next section.

2.2.3 Characterization of Complex Non Minimum Phase Zeros

As mentioned before, Menq and Xia (1990) have classified real NMP zeros as type 1 and type 2 zeros based on whether they lie to the left or to the right of the unit circle. Type 1 and type 2 NMP zeros have decreasing and increasing gain characteristics, respectively. Thus, the gain errors of type 1 zeros are compensated by introducing type 2 zeros and vice versa in the PTC method of feedforward compensation. While such simple characterization of complex NMP zeros is much more difficult because of the two coordinates involved rather than one, it is still useful to make some qualitative observations relating zero location in the complex plane to gain characteristics. For this purpose, the frequency response magnitude of the expression

$$[(z-z_1)(z-\bar{z}_1)]\left[\frac{1}{(1-z_1)(1-\bar{z}_1)}\right] \tag{2.20}$$

with complex NMP zero pair z_1 and $\bar{z}_1$ and where the second expression is for unity gain at zero frequency is considered. This is illustrated in Figure 2.6 where the magnitudes of $(z-z_1)$ and $(z-\bar{z}_1)$ are multiplied and recorded in a sweep of the point $z=e^{j\theta}$ with $\theta=\omega T_s$ from 0 to the Nyquist frequency of π radians to obtain the magnitude frequency response. Based on Figure 2.6, purely imaginary NMP zeros will have a valley at $\theta=\pi/2$ in their magnitude frequency response that will get deeper as the zero approaches the unit circle (A in Figure 2.6). This phenomenon is observed in Figure 2.7 which shows the effect of NMP zero pair location on frequency response gain characteristics. Magnitude frequency responses of (2.20) at several different locations in the complex plane can be observed in Figure 2.7.

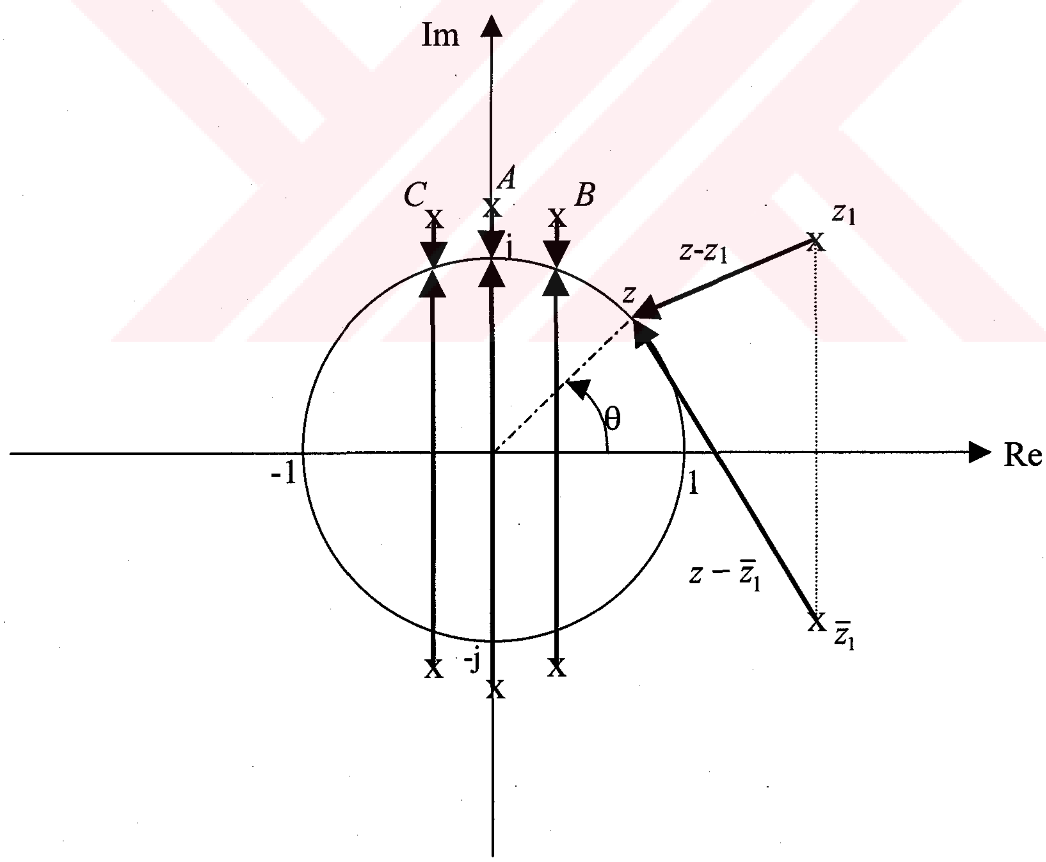

Figure 2.6 Illustration of discrete time magnitude frequency response calculation for (2.20)

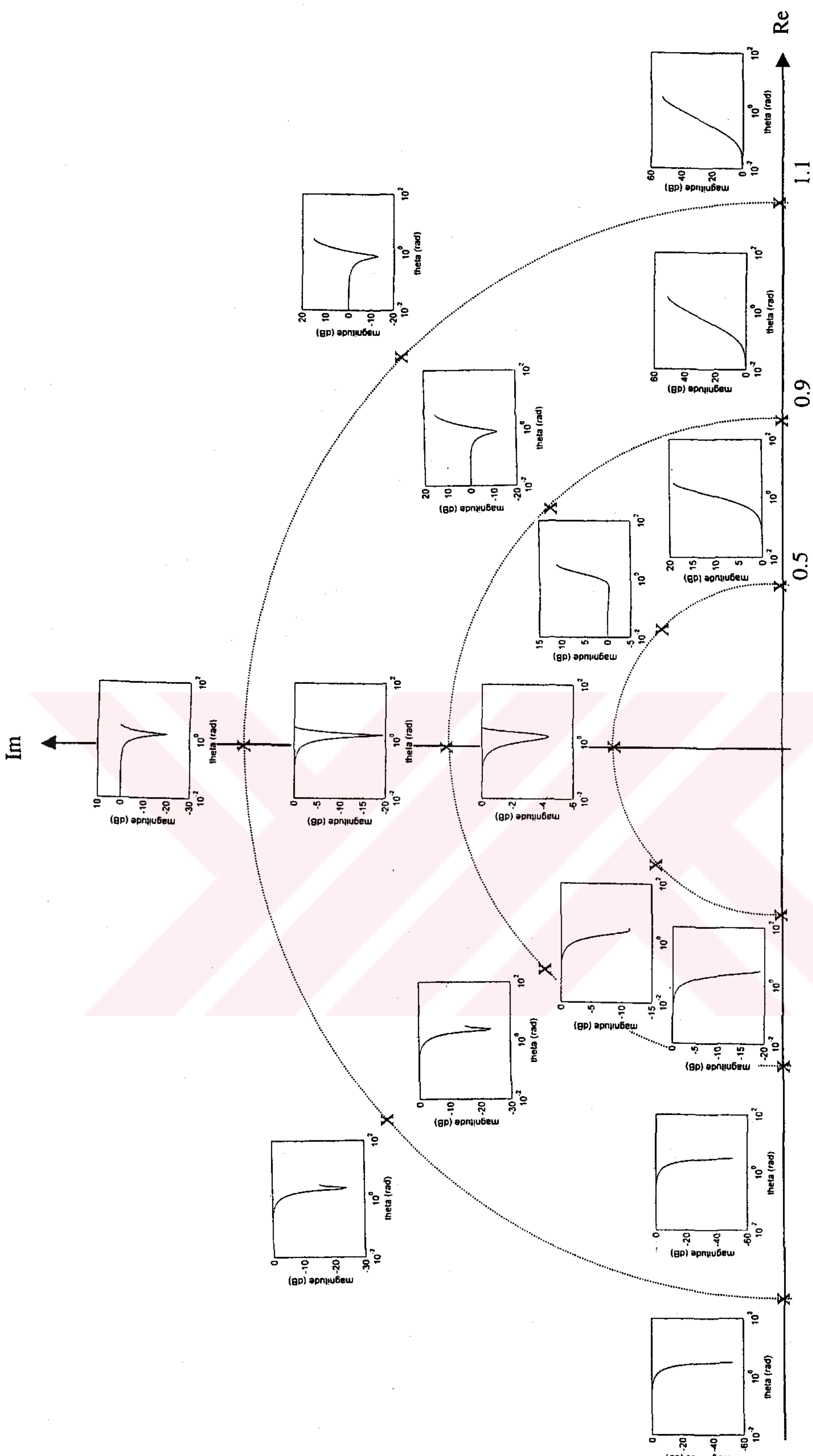

Figure. 2.7a Effect of zero location on magnitude frequency response (2.20) (not to scale)

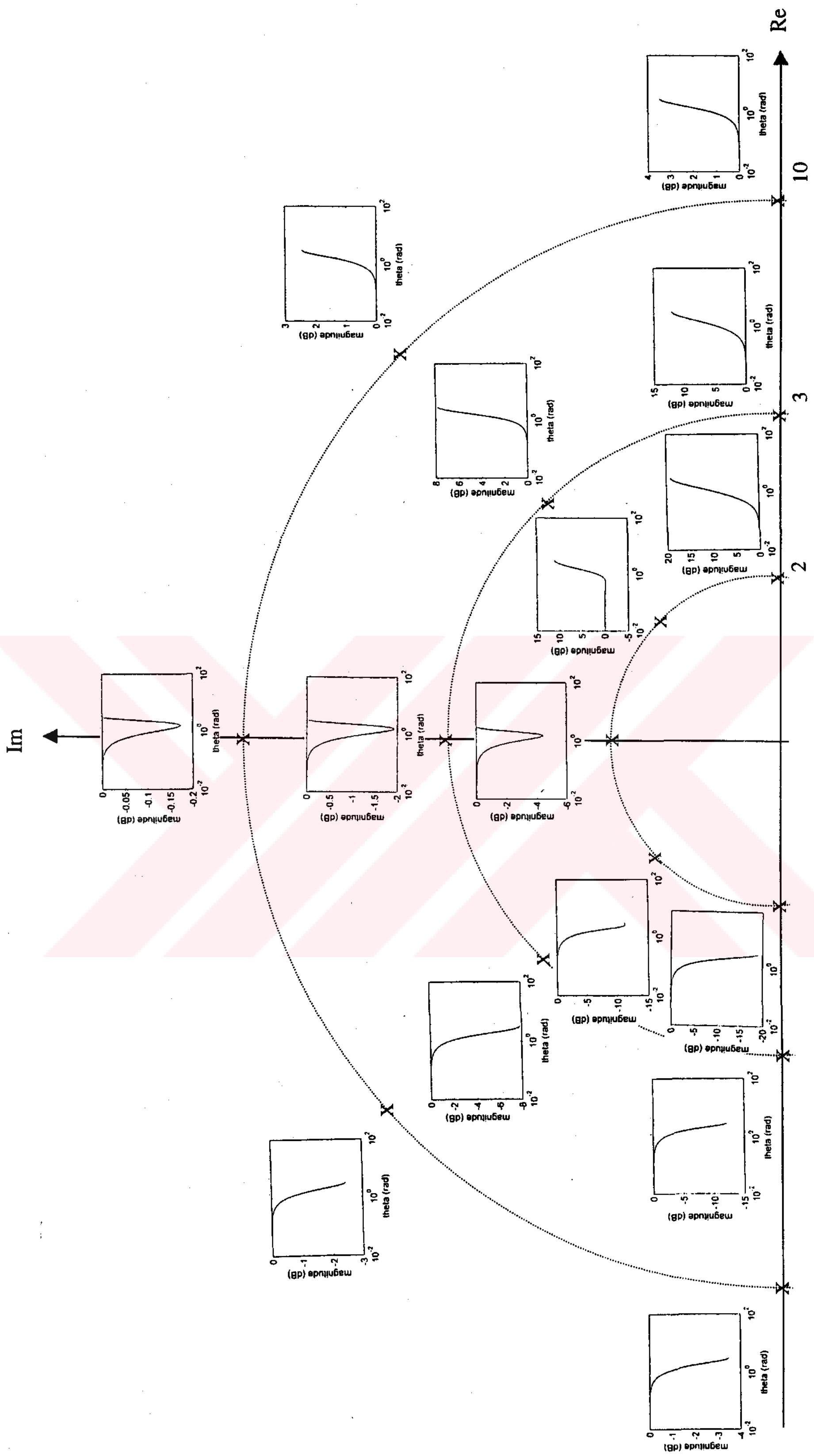

Figure. 2.7b Effect of zero location on magnitude frequency response (2.20) (not to scale)

Analysis of Figures 2.6 and 2.7 reveals that for right half plane NMP zero pairs close to the imaginary axis, the valley occurs at $\theta<\pi/2$ (B in Figure 2.6) and for similar left half plane NMP zero pairs the valley occurs at $\theta>\pi/2$. This effect becomes more pronounced as the NMP zero pair approaches the unit circle. Several observations follow.

Observation 1: In principle, one can still categorize NMP zeros as type 1 and type 2 based on whether the NMP zero (pair, if complex) lie(s) in the left half plane or right half plane as these generally have decreasing and increasing gain characteristics. The valleys that occur for complex NMP zero pairs close to the imaginary axis and to the unit circle create problems in this line of reasoning. This is due to the corresponding valley in their magnitude frequency response plots that changes the general trend at intermediate frequencies.

Observation 2: Purely imaginary NMP zero pairs are the hardest to compensate for if the desired tracking bandwidth is $\theta^*>\pi/2$.

Observation 3: The gain errors of complex NMP zero pairs z_1, $\bar{z}_1$ sufficiently far away from the unit circle and the imaginary axis can be compensated for by introducing z_2 and $\bar{z}_2$ where $z_2=-\mathrm{Re}(z_1)-j\mathrm{Im}(z_1)$ (opposite quadrant).

Observation 4: It is harder to compensate for gain errors of complex NMP zero pairs in comparison to real ones, this effect being more pronounced when the zeros are closer to the imaginary axis and the unit circle. Feedforward compensators therefore require more gain compensation zeros for systems with complex NMP zero pairs as compared to systems with real NMP zeros for comparable performance.

It is clear from the qualitative characterization above that compensating for gain errors is more involved for complex NMP zeros than it is for real NMP zeros. The extended PTC (EPTC) method which is an extension of the PTC method to systems with complex NMP zero pairs is given in the following section. The optimal PTC method of Aksun Güvenç and Güvenç (1999) given in section 2.2.5 can also handle systems with complex NMP zeros in addition to real ones.

2.2.4 Extended Precision Tracking Controller (EPTC)

In the EPTC method, complex conjugate zero pairs can also be used as gain compensating zeros for real NMP zeros, to satisfy requirements like achieving a flat frequency response in addition to achievement of the desired bandwidth (Güvenç et al, 1995).

Consider the discrete time transfer function

$$G(z) = \frac{n_{mp}(z) n_{nmp}(z)}{d(z)} \tag{2.21}$$

where $n_{mp}(z)$ and $n_{nmp}(z)$ are the minimum phase and nonminimum phase parts, respectively, of the numerator. The nonminimum phase part of the numerator can be factored into

$$n_{nmp}(z) = \prod_{k=1}^{m_r}(z - z_k)\prod_{l=1}^{m_c}(z - z_l)(z - \bar{z}_l) \tag{2.22}$$

and has m_r real and m_c complex conjugate pairs of NMP zeros. Thus, $n_{nmp}(z)$ in (2.21) has a total of m_r+2m_c NMP zeros. The EPTC approximate inverse filter for G(z) in (2.21) is given by

$$\tilde{G}^{-1}(z) = \frac{d(z)}{n_{mp}(z)}\prod_{k=1}^{m_r}\frac{(z^{-1} - z_k)}{(1 - z_k)^2}\frac{(z - z_{k1}^*)(z^{-1} - z_{k1}^*)}{(1 - z_{k1}^*)^2}\frac{(z - z_{k2}^*)(z^{-1} - z_{k2}^*)}{(1 - z_{k2}^*)^2} \cdot$$

$$\prod_{l=1}^{m_c}\frac{(z^{-1} - \bar{z}_l)(z^{-1} - z_l)}{(1 - \bar{z}_l)^2(1 - z_l)^2}\frac{(z - z_{l1}^*)(z^{-1} - z_{l1}^*)}{(1 - z_{l1}^*)^2}\frac{(z - z_{l2}^*)(z^{-1} - z_{l2}^*)}{(1 - z_{l2}^*)^2} \tag{2.23}$$

Note that the zero phase shift requirement is met by pairing up terms of the form $(z - z_l)$ with terms of the form $(z^{-1} - \bar{z}_l)$. The product of each such pair has zero phase shift on the unit circle $(z = e^{j\theta})$. The first part of (2.23), i.e. $d(z)/n_{mp}(z)$, is the invertible part of $G(z)$ in (2.21). The quantities in (2.23) with asterisks are the gain compensating zeros. z_{k1}^*, z_{k2}^* can be either both real or form a complex conjugate pair. Similarly z_{l1}^*, z_{l2}^* are either both real or form a complex conjugate pair. Thus five different combinations of NMP zeros and corresponding gain compensating zeros in $\widetilde{G}^{-1}(z)$ are possible. These combinations are:

(a) One real gain compensating zero corresponding to each real NMP zero z_k of $G(z)$ ($z_{k1}^* \in \boldsymbol{R}$, $z_{k2}^* = 0$. Same as PTC.)

(b) One complex conjugate gain compensating zero pair corresponding to each real NMP zero z_k of $G(z)$. ($z_{k1}^*, z_{k2}^* \in \boldsymbol{C}, \notin \boldsymbol{R}$. $z_{k1}^* = \bar{z}_{k2}^*$.)

(c) Two real gain compensating zeros corresponding to each real NMP zero z_k of $G(z)$. ($z_{k1}^*, z_{k2}^* \in \boldsymbol{R}$.)

(d) One complex conjugate gain compensating zero pair for each complex conjugate NMP zero pair $z_l, \bar{z}_l$ of $G(z)$. ($z_{l1}^*, z_{l2}^* \in \boldsymbol{C}, \notin \boldsymbol{R}$. $z_{l1}^* = \bar{z}_{l2}^*$.)

(e) Two real gain compensating zeros corresponding to each complex conjugate NMP zero pair $z_l, \bar{z}_l$ of $G(z)$. ($z_{l1}^*, z_{l2}^* \in \boldsymbol{R}$.)

Define

$$B(\theta, z_i, z_j) = \left. \frac{(z - z_i)(z^{-1} - \bar{z}_i)(z - z_j)(z^{-1} - \bar{z}_j)}{(1 - z_i)(1 - \bar{z}_i)(1 - z_j)(1 - \bar{z}_j)} \right|_{z = e^{j\theta}} \tag{2.24}$$

where z_i and z_j are either both real or a complex conjugate pair. The desired tracking bandwidth θ^* can be approximated by the gain cross-over frequency. This amounts to solving

$$\left| \widetilde{G}^{-1}(z) G(z) \right|_{z = e^{j\theta^*}} = \prod_{k=1}^{m_r} B(\theta^*, z_k, 0) B(\theta^*, z_{k1}^*, z_{k2}^*) \cdot \prod_{l=1}^{m_c} B(\theta^*, z_l, \bar{z}_l) B(\theta^*, z_{l1}^*, z_{l2}^*) = 1 \tag{2.25}$$

Order the m_r+2m_c NMP zeros of G(z) with the m_r real ones followed by the m_c complex conjugate pairs. Solving

$$B(\theta^*, z_k, 0) \cdot B(\theta^*, z_{k1}^*, z_{k2}^*) = 1; \qquad k = 1,2,\cdots,m_r \tag{2.26}$$

$$B(\theta^*, z_l, \bar{z}_l) \cdot B(\theta^*, z_{l1}^*, z_{l2}^*) = 1; \qquad l = m_r + 1,\cdots,m_r + m_c \tag{2.27}$$

for the gain compensating zeros will result in θ^* being the gain cross-over frequency. Equations (2.26) and (2.27) can be expanded into

$$(B_i - 1)\gamma_i^2 + \lfloor B_i(4\cos^2\theta^* - 2\alpha_i \cos\theta^* - 2) + 2\alpha_i \; - 2\rfloor \gamma_i +$$
$$\lfloor B_i(\alpha_i^2 - 2\alpha_i \cos\theta^* + 1) - \alpha_i^2 + 2\alpha_i - 1\rfloor = 0 \tag{2.28}$$

where

$$\alpha_i = \begin{cases} z_{k1}^* + z_{k2}^* & \text{cases b, c} \\ z_{l1}^* + z_{l2}^* & \text{cases d, e} \end{cases} \tag{2.29}$$

$$\gamma_i = \begin{cases} z_{k1}^* \, z_{k2}^* & \text{cases b, c} \\ z_{l1}^* \, z_{l2}^* & \text{cases d, e} \end{cases} \tag{2.30}$$

and

$$B_i = \begin{cases} B(\theta^*, z_k, 0) & \text{cases b, c} \\ B(\theta^*, z_l, \bar{z}_l) & \text{cases d, e} \end{cases} \tag{2.31}$$

Case a (PTC) was treated in detail earlier and hence is not included in (2.29)-(2.31). Note that B_i, α_i and γ_i are real for all the cases considered. Two design objectives are set for the determination of the gain compensating zeros as achieving the desired tracking bandwidth θ^* and making sure that the magnitude frequency response is sufficiently flat within that bandwidth. The design procedure is given in Güvenç et al (1995).

The disadvantage of relying on only the 0 dB crossover point for the desired bandwidth inherent in the PTC method is also present in the EPTC method. Therefore, an optimal method named OPTC that utilizes the precision tracking feedforward compensator but where the gain compensating zeros are determined so as to minimize a performance index is formulated next.

2.2.5 Optimal Precision Tracking Controller (OPTC)

In the OPTC method developed by Aksun Güvenç and Güvenç (1999), the performance index to be minimized is chosen as

$$\min_{z_k^*} \int_0^{\theta_{\max}} \left| 1 - \frac{(z-z_k)(z^{-1}-z_k)}{(1-z_k)^2} \frac{(z-z_k^*)(z^{-1}-z_k^*)}{(1-z_k^*)^2} \right|^2_{z=e^{j\theta}} d\theta, \mathrm{k}=1,2,....,\mathrm{m} \quad (2.32)$$

to determine the optimal PTC gain compensating zero z_k^* where the second expression within the absolute value sign is the transfer function $\widetilde{G}^{-1}(z)G(z)$ of the feedforward compensated system whose magnitude frequency response should be unity in the ideal case and a low pass filter of desired tracking bandwidth in practice. Here $[0,\theta_{\max}]$ with $\theta_{\max} \leq \pi$ is the frequency interval where the optimization is performed. The performance index is modified as

$$\min_{z_k^*} \int_0^{\pi} \left| W(e^{j\theta}) \right| \left| 1 - \frac{(z-z_k)(z^{-1}-z_k)}{(1-z_k)^2} \frac{(z-z_k^*)(z^{-1}-z_k^*)}{(1-z_k^*)^2} \right|^2_{z=e^{j\theta}} d\theta, \ \mathrm{k}=1,2,..,\mathrm{m} \qquad (2.33)$$

when the compensated transfer function is desired to be a low pass filter ($W(z)\big|_{z=e^{j\theta}}$).
Both problems are solved using available optimization routines.

To demonstrate its use, the OPTC method is applied to the model of a hydraulic positioning system used in noncircular turning (see Xia and Menq, 1990) whose transfer function is given by

$$G(z) = \frac{0.02127(z+0.1239)(z+1.3231)}{(z-0.952)\left[(z+0.0621)^2+(0.1677)^2\right]} = \frac{n_{mp(z)}n_{nmp(z)}}{d(z)}$$

$$n_{mp}(z) = 0.02127(z+0.1239)$$
$$n_{nmp}(z) = z+1.3231 \qquad (2.34)$$

where there is a real NMP zero at z_1= -1.3231

The OPTC optimal feedforward compensator for this system is determined using (2.32) with θ_{max}=0.589 rad as

$$\tilde{G}^{-1}_{OPTC}(z) = \frac{d(z)}{n_{mp}(z)} \frac{(z^{-1}+1.3231)}{(1+1.3231)^2} \frac{(z-5.6608)(z^{-1}-5.6608)}{(1-5.6608)^2} \qquad (2.35)$$

where z_1^*=5.6608 is the optimal gain compensating zero.

The ZPET feedforward compensator for this system is determined to be

$$\tilde{G}^{-1}_{ZPETC}(z) = \frac{d(z)}{n_{mp}(z)} \frac{(z^{-1}+1.3231)}{(1+1.3231)^2} \qquad (2.36)$$

A comparison of the magnitude frequency responses of the ZPET and OPTC compensated systems shown in Figure 2.8 demonstrates the larger tracking bandwidth achieved by the OPTC method. Accordingly, simulation results also show that the OPTC compensated system achieves much lower tracking errors.

Even though, the method and the example considered used real NMP zeros, it will not be very difficult to extend the method to cope with pairs of complex conjugate NMP zeros. Consider the discrete time transfer function $G(z)$ given previously in equation (2.21).The OPTC approximate inverse filter for this form of G(z) is given by

$$\tilde{G}^{-1}(z) = \left[\frac{d(z)}{n_{mp}(z)}\right]\cdot\left[\prod_{k=1}^{m_{r1}}\frac{(z^{-1}-z_k)}{(1-z_k)^2}\prod_{l=1}^{m_{c1}}\frac{(z^{-1}-\bar{z}_l)(z^{-1}-z_l)}{(1-\bar{z}_l)^2(1-z_l)^2}\right]\cdot$$

$$\left[\prod_{r=1}^{m_{r2}}\frac{(z-z_r)(z^{-1}-z_r)}{(1-z_r)^2}\right]\left[\prod_{c=1}^{m_{c2}}\frac{(z-z_c)(z^{-1}-\bar{z}_c)}{(1-z_c)^2}\frac{(z-\bar{z}_c)(z^{-1}-z_c)}{(1-\bar{z}_c)^2}\right] \tag{2.37}$$

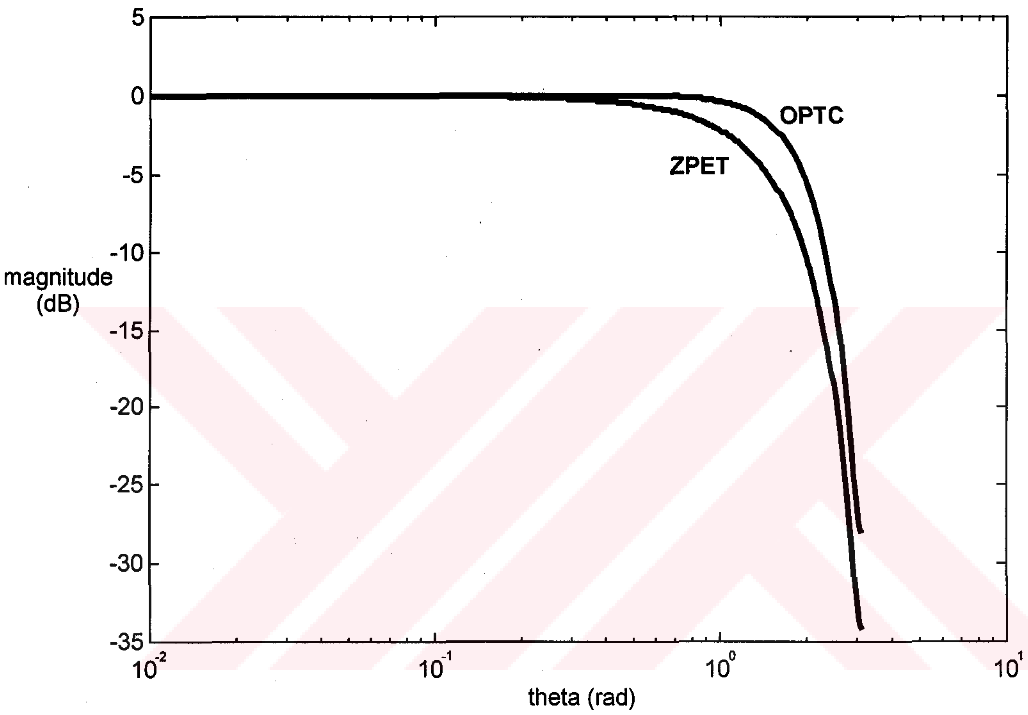

Figure 2.8 Comparison of gain frequency responses of ZPET and OPTC compensated systems

where $z_r \in \boldsymbol{R}$ and $z_c \in \boldsymbol{C}$. The first part of (2.37), $d(z)/n_{mp}(z)$, is the invertible part of G(z) as before. The second expression in (2.37) is for zero phase of $n_{nmp}(z)$ after compensation and the last two expressions are for gain error compensation with m_{r2} real (cases a, c and e of EPTC) and m_{c2} complex conjugate pairs (cases b and d of EPTC) of gain compensation zeros. The overall transfer function $\tilde{G}^{-1}(z)G(z)$, then, has, by construction, zero phase at all frequencies and the gain compensation zeros are chosen optimally by solving

$$\min_{\substack{z_r \in \mathbf{R}; r=1,2,\ldots,m_{r2} \\ z_c \in \mathbf{C}; c=1,2,\ldots,m_{c2}}} \int_0^{\pi} \left| W(\theta)\left(1-\tilde{G}^{-1}\left(e^{j\theta}\right)G\left(e^{j\theta}\right)\right) \right|^2 d\theta \tag{2.38}$$

W(θ) in (2.38) is a weighting function which is usually chosen as

$$W(\theta)=\begin{cases} 1, & \theta \le \theta^* \\ 0, & \theta > \theta^* \end{cases} \tag{2.39}$$

where θ^* is the desired bandwidth of feedforward compensation. As an alternative, the weight can also be selected to minimize the tracking error for a given input (Menq and Xia, 1995), if the desired input trajectory is known in advance. The formulation in (2.39) works well for real as well as for most complex conjugate NMP zero pairs but there are some problems when the complex conjugate NMP zero pair is close to the imaginary axis and the unit circle. The formulation that works better in such cases is given in the following in the context of a simulation study on an example system.

The closed loop position control system of a hydraulic linear actuating system, used for tool positioning in noncircular machining by Tsao and Tomizuka (1994) is chosen for the simulation study since its model has a complex conjugate NMP zero pair. The discrete time, reduced order model of the closed loop system is given by

$$G(z)=\frac{0.06z^2+0.034z+0.071}{z^7-0.606z^6-0.747z^5+0.519z^4}=0.06\frac{n_{nmp}(z)}{d_G(z)} \tag{2.40}$$

The complex NMP zeros are $z_1, \bar{z}_1 = -0.2833 \pm j1.0503$ This pair of complex conjugate NMP zeros is close to the imaginary axis and the unit circle and is thus hard to compensate for. The gain associated with it has a valley close to $\theta = \pi/2$ rad and then rises to about unity at $\theta = \pi$ rad. In order to compensate for these gain characteristics, the compensating zeros need to introduce sufficient gain amplification at intermediate frequencies and sufficient gain attenuation at high frequencies. Since the optimization formulation in (2.38) creates problems for these types of hard to compensate complex conjugate NMP zero pairs, it is replaced in this example by

$$\min_{\substack{z_r \in R; r=1,2,\ldots,m_{r2} \\ z_c \in C; c=1,2,\ldots,m_{c2}}} \int_0^{\pi} \left| 1 - W(\theta)\tilde{G}^{-1}\left(e^{j\theta}\right) G\left(e^{j\theta}\right) \right|^2 d\theta \tag{2.41}$$

where the weight W(θ) is chosen to have large gain at frequencies above θ^* and is chosen in this example as $3.61/|e^{j\theta}+0.9|^2$ to provide large weight at high frequencies and, thus, force the compensated magnitude frequency response to a sharp decrease with frequency. The weight should be selected by balancing the desired tracking bandwidth requirement (uniform weight up to θ^*) with the low gain requirement at high frequencies (large weight above θ^*) for robustness of performance. The OPTC computations, successively, with one real, two real and one complex conjugate gain compensation zero pair resulted in the best result being obtained by the two real zero case (m_{r2}=2 and m_{c2}=0 in (2.37)). The two real gain compensating zeros are z_1=-0.3947 and z_2=-0.9452. The magnitude frequency response plots in Figure 2.9 show the improvement over ZPET compensation.

The response of the compensated system is simulated using

$$r = 250 + 250\sin\left(\frac{2\pi}{0.05}t - \frac{\pi}{2}\right) \tag{2.42}$$

as the input. The sampling time used is 0.4 msec. The simulation results in Figure 2.10 show smaller tracking error using the OPTC method as compared to the ZPET method.

2.2.6 Truncated Series Approximation (TSA)

The truncated series approximation (TSA) method of Gross et al (1994) which is the only non-zero phase error algorithm considered here can be obtained either by polynomial long division or by solving the optimization problem

$$\min_{a_0, a_1, \ldots, a_p \in R} \int_0^{2\pi} \left| \frac{1}{z - z_1} - (a_0 + a_1 z + a_2 z^2 + \ldots + a_p z^p) \right|_{z=e^{j\theta}}^2 d\theta \tag{2.43}$$

where $\boldsymbol{R}$ is used to denote real numbers, z_1 is the NMP zero being compensated and the series expression in parentheses is the part of the feedforward compensator to be cascaded with the invertible part of the plant in forming the feedforward controller. Similar to the other methods, the TSA method can make the tracking degradation effect of NMP zeros arbitrarily small when more compensation terms are used. The method may be an alternative to ZPET when a system, having NMP zeros, requires better gain characteristics, but it cannot be applied to zeros occuring on the unit circle.

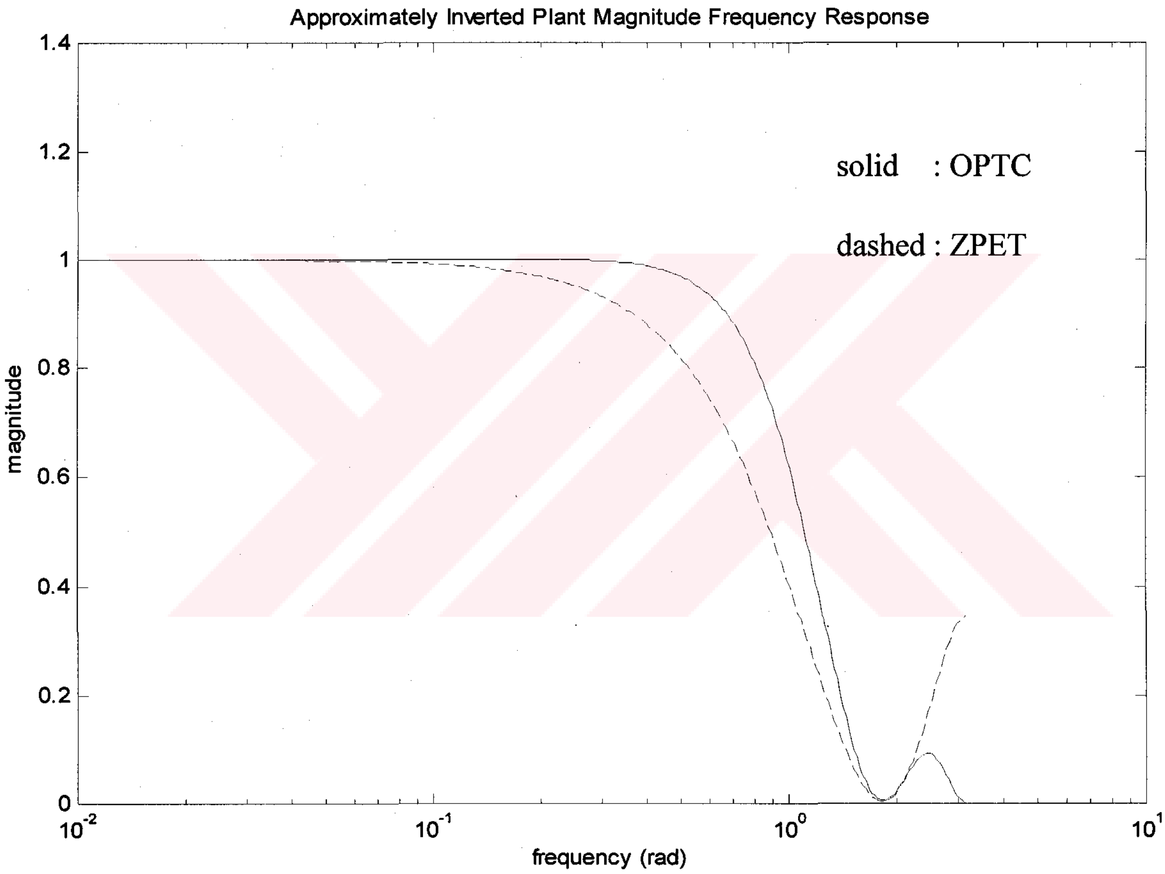

Figure 2.9 Magnitude frequency responses of OPTC and ZPET compensated systems

The number of required preview steps is dependent on the distance the NMP zero is from the unit circle.

2.3 Robustness Analysis

Reference feedforward controllers cannot affect either the stability or the stability robustness of the loop being compensated. Robustness of performance of the feedforward compensated system is, thus, addressed here when the location of the zeros of G(z) is uncertain. A robustness analysis similar to the one used by Gross et al (1994) is given here to address this issue. Only a complex NMP zero pair in the discrete time plant is considered since the corresponding result for a real NMP zero is its special case. If a complex conjugate NMP zero pair, believed to be at z_n and $\bar{z}_n$ is actually at $z_n + \delta$ and $\bar{z}_n + \bar{\delta}$, respectively, the compensated transfer function becomes

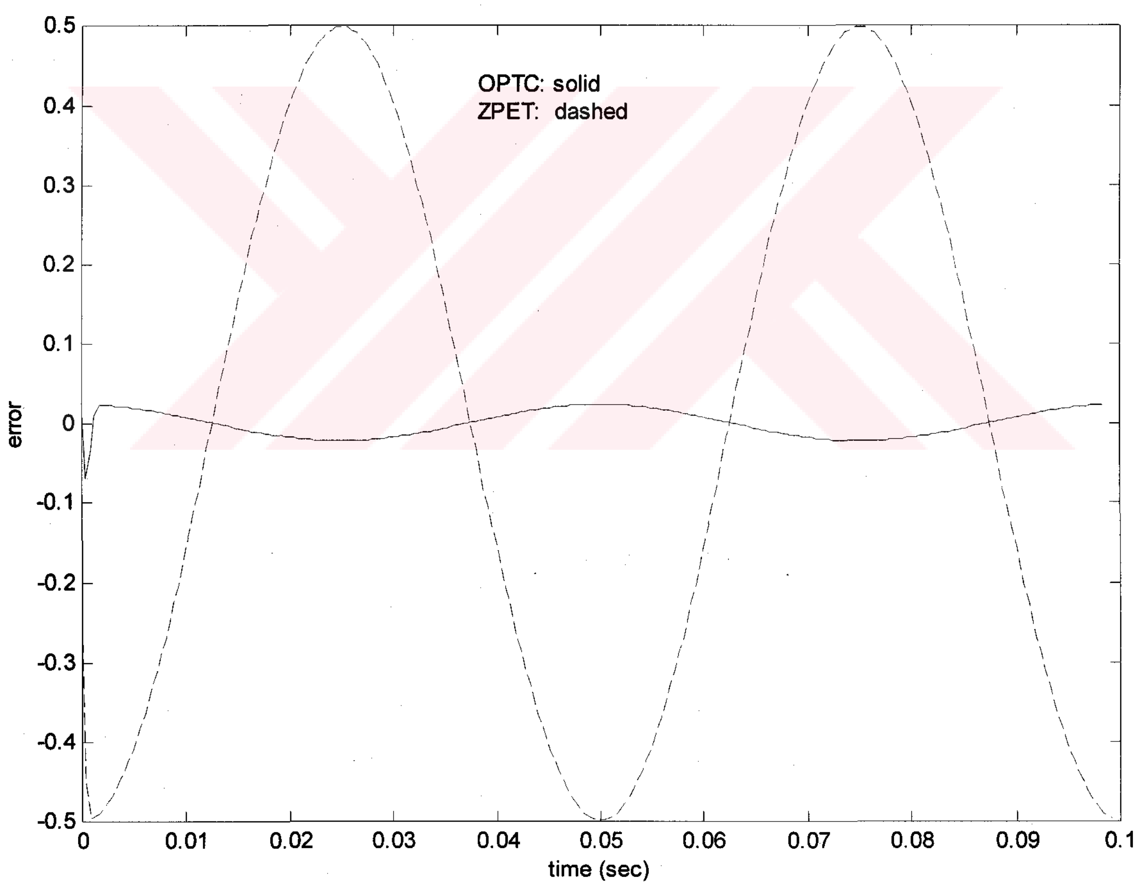

Figure 2.10 Simulated tracking errors

$$\tilde{G}^{-1}(z)G(z) = \frac{\tilde{G}_n^{-1}(z)G_n(z)}{(z - z_n)(z - \bar{z}_n)}\big(z - (z_n + \delta)\big)\big(z - (\bar{z}_n + \bar{\delta})\big) \tag{2.44}$$

where $G_n(z)$ is the nominal (unperturbed) system and $\widetilde{G}_n^{-1}(z)$ is the approximate inverse filter designed for it. Algebraic manipulations on (2.44) result in

$$\widetilde{G}^{-1}(z)G(z) = \widetilde{G}_n^{-1}(z)G_n(z) + \varepsilon(\delta, z) \tag{2.45}$$

where the additive term is

$$\varepsilon(\delta, z) = \frac{\widetilde{G}_n^{-1}(z)G_n(z)}{(z - z_n)(z - \bar{z}_n)}\left(-\delta(z - \bar{z}_n) - \bar{\delta}(z - z_n) + \delta\bar{\delta}\right) \tag{2.46}$$

A conservative bound for this error is

$$|\varepsilon(\delta, z)| < \left|\frac{\widetilde{G}_n^{-1}(z)G_n(z)}{(z - z_n)(z - \bar{z}_n)}\right|\left[\left(|z - \bar{z}_n| + |z - z_n|\right)|\delta| + |\delta|^2\right] \tag{2.47}$$

It is clear that as z_n comes closer to the unit circle and as the uncertainty δ decreases, the robustness of the magnitude frequency response will be better as a result of a smaller bound on $|\varepsilon(\delta, z)|$ in (2.47).

3. ROBUSTNESS OF REFERENCE FEEDFORWARD CONTROL USING SSV ANALYSIS

The robustness of a control system can be expressed as not being sensitive to differences between the actual plant and the model of the plant for which the controller was designed. Control designs are based on the use of a design model which can be a mathematical model constructed using governing physical laws or an experimentally determined one. The quality of a model, be it purely mathematically or experimentally determined, depends on how closely its responses match those of the true plant. Since no single fixed model can respond exactly like the true plant, it would be desirable to construct a set of models that contains the true plant. Since a model set which includes the exact physical plant can never be constructed, an engineer should base his/her control design taking into account this inadequacy of models. A good model should be simple enough to facilitate design, yet complex enough to give the engineer confidence that designs based on the model will work on the true plant. The term model uncertainty refers to the differences or errors between models and actual system and whatever mechanism is used to express these errors is called a representation of uncertainty.

The approach taken in robust control is:

1. Finding a mathematical representation of the model uncertainty and determination of the uncertainty set.

2. Checking robustness of stability (RS) by determining whether the system remains stable for all plants in the uncertainty set.

3. Checking robustness of performance (RP) by determining whether in addition to robustness of stability the performance specifications are also met for all plants in the uncertainty set.

To account for model uncertainty, it will be assumed that the dynamic behaviour of a plant is described not by a single linear time invariant model but by a set of possible linear time invariant models, denoted as the uncertainty set.

3.1 Representation of Uncertainty

Uncertainty in the plant model may have several origins:

1. There are always parameters in the linear model which are only known approximately or are simply in error.
2. The parameters in the linear model may vary due to nonlinearities or changes in the operating conditions (a linear parameter varying model).
3. Imperfections of measurement devices may give rise to inaccuracies in experimental plant model determination.
4. At high frequencies, even the structure and the order of the model are unknown. This type of uncertainty is called high frequency unmodeled dynamics.
5. One may choose to work with a simpler (low-order) nominal model and represent the neglected dynamics as uncertainty even when a very detailed model is available.

The various sources of model uncertainty mentioned above may be grouped into two main classes:

1. Parametric Uncertainty
2. Unmodeled Dynamics Uncertainty

It is also possible to use a combination of the two different groups of uncertainty listed above.

3.1.1 Parametric Uncertainty

In this kind of uncertainty, the structure of the model (including the order) is known, but some of the parameters are uncertain. This is illustrated using a simple example. Suppose that, there is a process $G(s)$ which is represented by a first-order lag with uncertain time constant τ, $\tau \in \boldsymbol{R}$ given by

$$G(s) = \frac{1}{\tau s + 1}; \quad \tau_{\min} \le \tau \le \tau_{\max} \tag{3.1}$$

where it is assumed that τ lies in the interval $\tau \in [\tau_{\min}, \tau_{\max}]$.

The time constant parametric uncertainty can be written as

$$\tau = \bar{\tau} + \Delta_{\max}\delta, \quad \Delta_{\max} \equiv \frac{\tau_{\max} - \tau_{\min}}{2}, \quad \bar{\tau} \equiv \frac{\tau_{\min} + \tau_{\max}}{2} \tag{3.2}$$

where $\Delta_{\max}$ is the maximum deviation of the time constant from its nominal value. $\bar{\tau}$ is the nominal (average) time constant and δ is any real scalar perturbation satisfying $|\delta| \leq 1$. This kind of uncertainty is called parametric uncertainty. Its main advantage is that the corresponding uncertainty structure is easily and naturally derived from the mathematical model of the plant. Parametric uncertainty representation also has the following disadvantages:

1. It usually requires a large effort to model parametric uncertainty for more complicated plant models and unmodelled dynamics cannot be dealt with in robustness studies

2. A parametric uncertainty model is somewhat deceiving in the sense that it provides a very detailed and accurate description even though the underlying assumptions about the model and the parameters may be much less exact.

3. Real perturbations are mathematically and numerically more difficult to deal with.

Parametric uncertainty is sometimes represented by complex perturbations to avoid the mathematical and computational problems. For example, it may be desired to replace the real perturbation, $-1 \leq \delta \leq 1$ by a complex perturbation with $|\delta(j\omega)| \leq 1$. This is of course conservative as it introduces the possibility of plants that are not present in the original set.

3.1.2 Unmodeled Dynamics Uncertainty

Models of uncertainty are not limited to parametric uncertainty. Often, a low order nominal model, which suitably describes the low to mid frequency plant behaviour is available but the high-frequency plant behaviour is uncertain. In this situation, even the dynamic order of the actual plant is not known and a characterization that is richer than parametric uncertainty is needed to represent this kind of uncertainty. An additive or multiplicative uncertainty block is used for this purpose, to capture phase uncertainty also. Consider the multiplicative uncertainty case with nominal model

$G(s)$ and a multiplicative uncertainty weighting function $W(s)$. The multiplicative uncertainty set is

$$S(G,W) \equiv \left\{ \widetilde{G} : \left| \frac{\widetilde{G}(j\omega) - G(j\omega)}{G(j\omega)} \right| \leq |W(j\omega)| \right\} \tag{3.3}$$

or

$$\Delta \equiv \frac{\widetilde{G} - G}{GW}, \quad \max_{\omega} |\Delta(j\omega)| \leq 1 \tag{3.4}$$

with the additional restriction that the number of right-half plane (RHP) poles of $\widetilde{G}$ is equal to the number of RHP poles of G. The multiplicative uncertainty can also be written in its conventional form as

$$\widetilde{G} = G(I + W\Delta); \quad |\Delta(j\omega)| \leq 1 \ \forall \omega \tag{3.5}$$

The structure of the multiplicative uncertainty can be seen in Figure 3.1 $|W(j\omega)|$ represents the maximum potential percentage difference between all of the plants represented by $S(G,W)$ and the nominal plant model G. Usually, a simple multiplicative weight of the form (Skogestad, 1996)

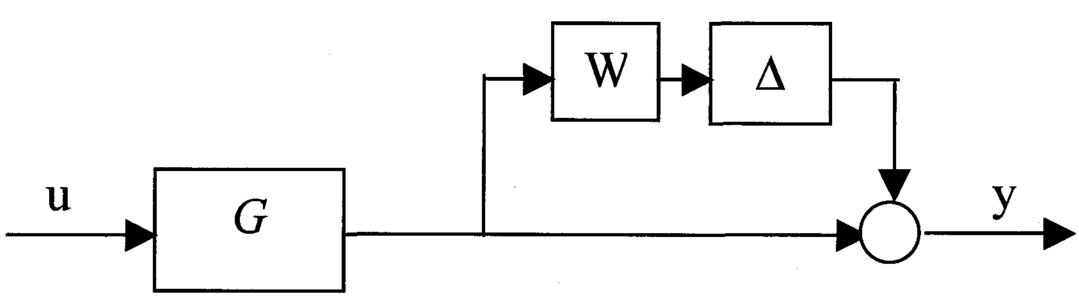

Figure 3.1 Structure of multiplicative uncertainty

$$W(j\omega) = \frac{\tau s + r_0}{(\tau / r_\infty)s + 1} \tag{3.6}$$

is used. In (3.6), r_0 is the relative uncertainty at low frequency, $1/\tau$ is (approximately) the frequency at which the relative uncertainty reaches 100% and r_∞ is the magnitude of the weight at higher frequencies. Typically, the uncertainty $|W|$, associated with each input, is at least 10% at steady state ($r_0 \geq 0.1$) and it increases at higher frequencies to account for uncertain dynamics (typically $r_\infty \geq 2$).

The uncertainty can also be represented by additive uncertainty of the form

$$\widetilde{G}(s) = G(s) + W(s)\Delta(s); \qquad |\Delta(j\omega)| \leq 1 \; \forall\omega \tag{3.7}$$

where $\Delta(s)$ is any stable transfer function which is at most one in magnitude at each frequency.

3.2 Linear Fractional Transformations (LFTs)

The basic idea in modeling an uncertain system is to separate what is known from what is unknown in a feedback-like connection and bound the possible values of the unknown elements. This is a direct generalization of the notion of a state-space realization where a linear dynamical system is written as a feedback interconnection of a constant matrix and a very simple dynamical element made up of a diagonal matrix of delays or integrators. This realization greatly facilitates manipulation and computation of linear systems and linear fractional transformations (LFTs) provide the same capability for uncertain systems. LFTs were introduced by Doyle (1984) into the control literature. Their use provides a powerful and flexible approach to represent uncertainty in matrices and systems (Balas et al, 1995). Relevant properties of LFTs are repeated below. More detailed information can be found in Skogestad (1996).

Consider a matrix P of dimension $(n_1 + n_2) \times (m_1 + m_2)$ and partition it as follows:

$$P = \begin{bmatrix} P_{11} & P_{12} \\ P_{21} & P_{22} \end{bmatrix} \tag{3.8}$$

Let the matrices Δ and K have dimensions $m_1 \times n_1$ and $m_2 \times n_2$, respectively (compatible with the upper and lower partitions of P, respectively). The following lower and upper linear fractional transformations of P w.r.t. K and Δ, respectively, are

$$F_l(P, K) \equiv P_{11} + P_{12}K(I - P_{22}K)^{-1}P_{21} \tag{3.9}$$

$$F_u(P,\Delta) \equiv P_{22} + P_{21}\Delta(I - P_{11}\Delta)^{-1}P_{12} \tag{3.10}$$

where the subscript l denotes lower and the subscript u upper. In the following, let R denote a matrix function resulting from an LFT (see Figure 3.2).

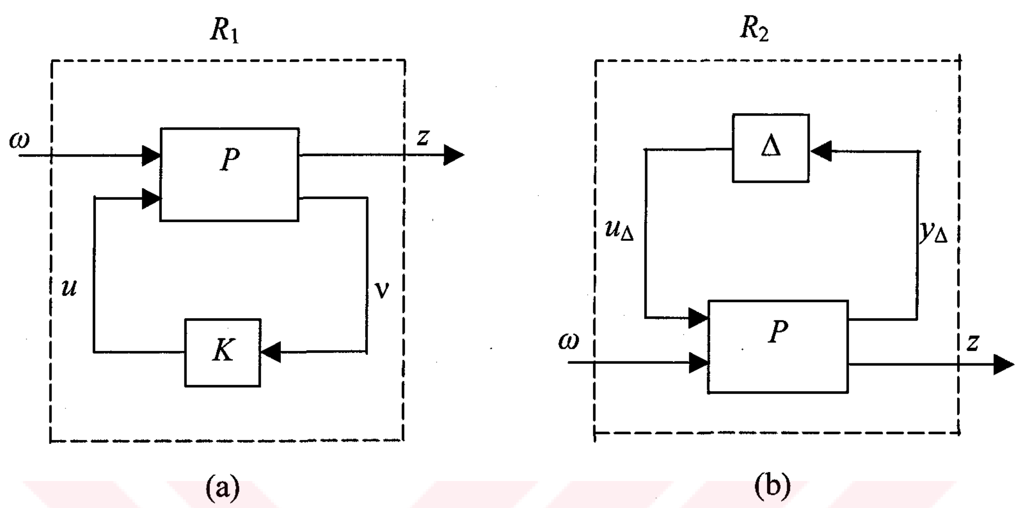

Figure 3.2 (a) R_1 as lower LFT in terms of K (b) R_2 as upper LFT in terms of Δ

The lower linear fractional transformation $F_l(P,K)$ is the transfer function R_1 resulting from positive feedback of K around the lower part of P as is shown in Figure 3.2a. To see this, note that the block diagram in Figure 3.2a may be written as

$$z = P_{11}\omega + P_{12}u, \quad v = P_{21}\omega + P_{22}u, \quad u = Kv \tag{3.11}$$

Upon elimination of v and u from these equations,

$$z = R_1\omega = F_l(P,K)\omega = [P_{11} + P_{12}K(I - P_{22}K)^{-1}P_{21}\}\omega \tag{3.12}$$

is obtained. In other words, R_1 is written as a lower LFT of P in terms of the parameter K. Similarly, in Figure 3.2b the upper LFT, $R_2 = F_u(P,\Delta)$ is obtained by positive feedback of Δ around the upper part of P.

An important property of LFTs is that any interconnection of LFTs is again an LFT. Typical algebric operations such as frequency response, cascade connections, parallel connections and feedback connections preserve the LFT structure. This means that normal interconnections of LFTs are still in the form of an LFT. Hence LFT is an excellent choice for a general hierarchial representation of uncertainty. Consider

Figure 3.3 where R is written in terms of a lower LFT of $K^{'}$ which again is a lower LFT of K and R is desired to be expressed directly as an LFT of K. As it is seen from Figure 3.3, it can be written as

$$R = F_l(Q, K^{'}) \quad \text{where} \quad K^{'} = F_l(M, K) \tag{3.13}$$

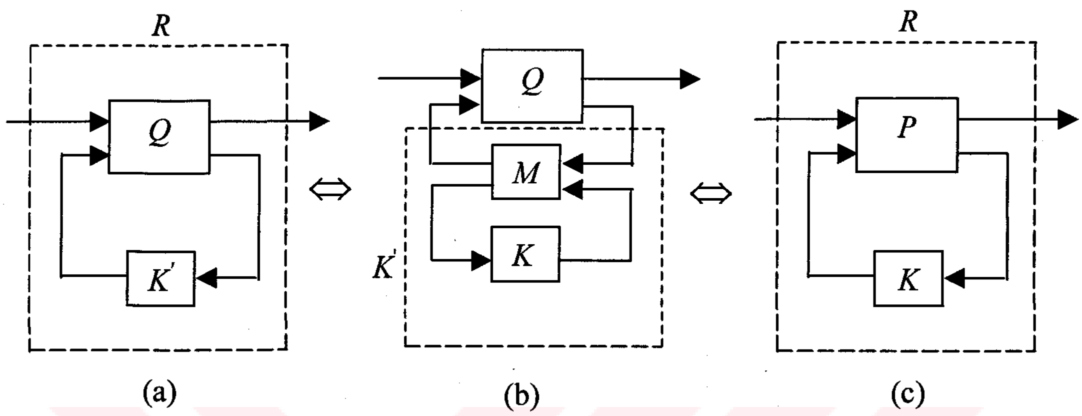

Figure 3.3 An interconnection of LFTs yields an LFT

P is desired to be obtained (in terms of Q and M) such that $R = F_l(P, K)$. The following is obtained

$$P = \begin{bmatrix} P_{11} & P_{12} \\ P_{21} & P_{22} \end{bmatrix} = \begin{bmatrix} Q_{11} + Q_{12}M_{11}(I - Q_{22}M_{11})^{-1}Q_{21} & Q_{12}(I - M_{11}Q_{22})^{-1}M_{12} \\ M_{21}(I - Q_{22}M_{11})^{-1}Q_{21} & M_{22} + M_{21}Q_{22}(I - M_{11}Q_{22})^{-1}M_{12} \end{bmatrix} \tag{3.14}$$

Similar expressions apply when upper LFTs are used. Consider

$$R = F_u(M, \Delta^{'}) \quad \text{where} \quad \Delta^{'} = F_u(Q, \Delta) \tag{3.15}$$

$R = F_u(P, \Delta)$ is obtained where P is given in terms of Q and M by equation (3.14).

Another important property is the close relationship between F_l and F_u. If $R = F_l(M, K)$ is known then R is directly obtained in terms of an upper transformation of K by reordering M. That is

$$F_u(\widetilde{M}, K) = F_l(M, K) \tag{3.16}$$

where

$$\widetilde{M} = \begin{bmatrix} 0 & I \\ I & 0 \end{bmatrix} M \begin{bmatrix} 0 & I \\ I & 0 \end{bmatrix} \tag{3.17}$$

On the assumption that all the relevant inverses exist,

$$(F_l(M,K))^{-1} = F_l(\overline{M},K) \tag{3.18}$$

where $\overline{M}$ is given by

$$\overline{M} = \begin{bmatrix} M_{11}^{-1} & -M_{11}^{-1}M_{12} \\ M_{21}M_{11}^{-1} & M_{22} - M_{21}M_{11}^{-1}M_{12} \end{bmatrix} \tag{3.19}$$

is obtained.

Given an LFT in terms of K, it is possible to derive an equivalent LFT in terms of K^{-1}. Assuming that all the relevant inverses exist,

$$F_l(M,K) = F_l(\hat{M},K^{-1}) \tag{3.20}$$

where $\hat{M}$ is given by

$$\hat{M} = \begin{bmatrix} M_{11} - M_{12}M_{22}^{-1}M_{21} & -M_{12}M_{22}^{-1} \\ M_{22}^{-1}M_{21} & M_{22}^{-1} \end{bmatrix} \tag{3.21}$$

is obtained. A generalization of the upper and lower LFTs is provided by Redheffer's star product. As it is seen from Figure 3.4, Q and M are interconnected such that the last n_u outputs from Q are the first n_u inputs of M, and the first n_l outputs from M are the last n_l inputs of Q. The corresponding partitioned matrices are

$$Q = \begin{bmatrix} Q_{11} & Q_{12} \\ Q_{21} & Q_{22} \end{bmatrix}, \quad M = \begin{bmatrix} M_{11} & M_{12} \\ M_{21} & M_{22} \end{bmatrix} \tag{3.22}$$

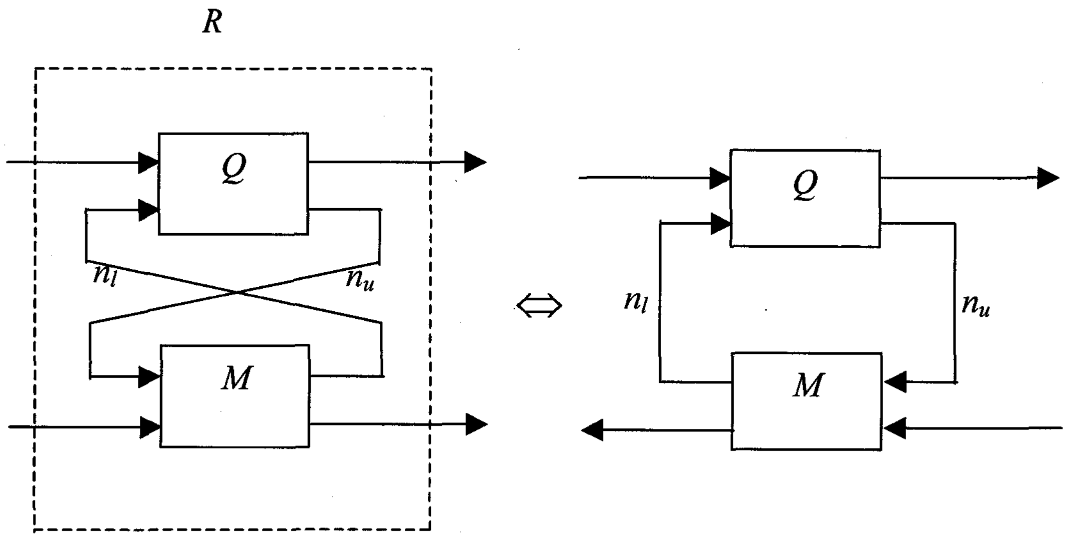

Figure 3.4 Star product of Q and M, R=$S(Q,M)$

As it is seen from Figure 3.4, the overall matrix R with these interconnections closed is called the star product, $S(Q,M)$, between Q and M. R is obtained as

$$R = S(Q,M) = \begin{bmatrix} Q_{11} + Q_{12}M_{11}(I - Q_{22}M_{11})^{-1}Q_{21} & Q_{12}(I - M_{11}Q_{22})^{-1}M_{12} \\ M_{21}(I - Q_{22}M_{11})^{-1}Q_{21} & M_{22} + M_{21}Q_{22}(I - M_{11}Q_{22})^{-1}M_{12} \end{bmatrix} \quad (3.23)$$

Note that $S(Q,M)$ depends on the chosen partitioning of the matrices Q and M. If one of the matrices is not partitioned then this means that this matrix has no external inputs and outputs and $S(Q,M)$ then gives the maximum interconnection. The following two LFTs can be given as an example.

$$F_l(P,K) = S(P,K) \quad (3.24)$$

$$F_u(P,\Delta) = S(\Delta,P) \quad (3.25)$$

The order in the last equation is not a misprint. Of course, this assumes that the dimensions of K and Δ are smaller than those of P.

3.3 Robustness Using SSV Analysis

The feedforward controlled system P(s) with uncertainty block Δ is shown in Figure 3.5. Δ in this section is used to model the block diagonal parametric and nonparametric uncertainty matrix whose structure is given by

$$\Delta_G \equiv \{diag(\delta_1, \delta_2, ..., \delta_r, \Delta_1, \Delta_2 ..., \Delta_f) : \delta_i \in \Re, 1 < i < r;\ \Delta_j \in C^{m_j x m_j}; 1 < j < f\} \quad (3.26)$$

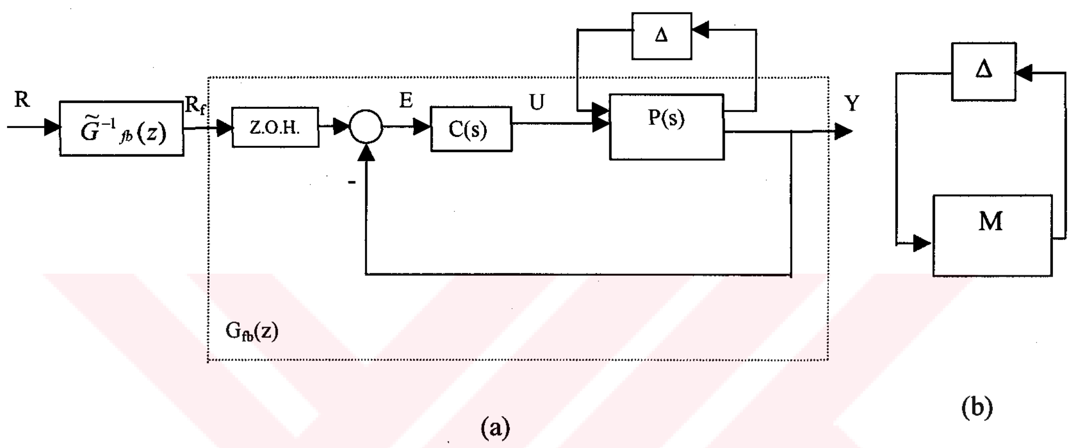

Figure 3.5 Feedforward controlled system with uncertainty and its equivalent LFT

where the real parametric uncertainty is captured in the δ_i and nonparametric or complex uncertainty is captured in the Δ_j blocks. The structured singular value (abbreviated as SSV) is a function which provides a generalization of the singular value, σ, and the spectral radius ρ (the magnitude of the largest eigenvalue of a matrix). The structured singular value μ is then defined as the inverse of the magnitude of the minimum sized destabilizing uncertainty matrix Δ (measured in terms of $\bar{\sigma}(\Delta)$) of chosen structure at each frequency. Mathematically,

$$\mu(M)^{-1} \equiv \min_{\Delta}\{\bar{\sigma}(\Delta) | \det(I - M\Delta) = 0 \text{ for structured } \Delta\} \quad (3.27)$$

Clearly $\mu(M)$ depends not only on M but also on the allowed structure for Δ. This is sometimes shown explicitly by using the notation $\mu_\Delta(M)$. Also μ depends on whether the perturbation is real or complex.

A value of $\mu = 1$ means that there exists a perturbation with $\bar{\sigma}(\Delta) = 1$ which is just large enough to make $I - M\Delta$ singular. A larger value of μ is undesirable as it means that a smaller perturbation makes $I - M\Delta$ singular whereas a smaller value of μ is desirable. More information about the properties of SSV can be found in Appendix A and more detailed information on SSV can be found in Packard and Doyle (1993), Doyle (1984) and Zhou et al (1996).

The robustness of stability of the feedback system within the dashed rectangle in Figure 3.5a, redrawn in its equivalent, more suitable linear fractional transformation (LFT) form in Figure 3.5b can be analyzed by SSV analysis using the robust stability theorem of Doyle (1984). According to this theorem, the feedback control system in Figure 3.5 with plant model uncertainty Δ is robustly stable for $\forall\Delta \in \Delta_G$ with $\|\Delta\|_\infty \leq 1$ if and only if

$$\sup_{\omega} \mu_{\Delta}\left(F_u\left(M(j\omega)\right)\right) < 1 \tag{3.28}$$

where $F_u(..)$ denotes the upper LFT of the argument. This theorem is based on the multivariable Nyquist stability criterion.

Since the feedforward controller $\tilde{G}_{fb}^{-1}(z)$ in Figure 3.5 is outside the feedback loop, it cannot affect stability. Hence, it is only possible to study the stability robustness of the feedback loop alone. Regarding the overall feedforward controlled system, how its performance changes in the presence of modeling error Δ is an important problem since the feedforward controller design is based only on the nominal plant model. Moreover, no information about changes in the plant is fed back to the feedforward controller during operation. It is, thus, necessary to assess the robustness of performance of feedforward controlled systems in the presence of plant modeling error and to develop suitable measures of performance to be used in connection. SSV analysis is chosen here as the method of performance robustness analysis as it allows the treatment of mixed problems with a combination of real parametric and high frequency unmodeled dynamics type plant modeling errors.

Performance criteria are incorporated into SSV analysis by the addition of a fictitious, complex uncertainty block Δ_F as shown in Figure 3.6 between the input and output signals of interest. According to the robust performance theorem of Doyle (1984), the performance criterion of $\left\|M_{P_{Nf}}\right\|_\infty < 1$ and robustness of stability of the feedback loop exist for $\forall\Delta \in \Delta_G$ and $\forall\Delta_F \in C^{Nf\mathrm{x}Nf}$ with $\|\Delta\|_\infty \leq 1$ and $\|\Delta_F\|_\infty \leq 1$ if and only if

$$\sup_{\omega} \mu_{\Delta,\Delta_F}\left(F_u\left(M_P(j\omega)\right)\right) < 1. \tag{3.29}$$

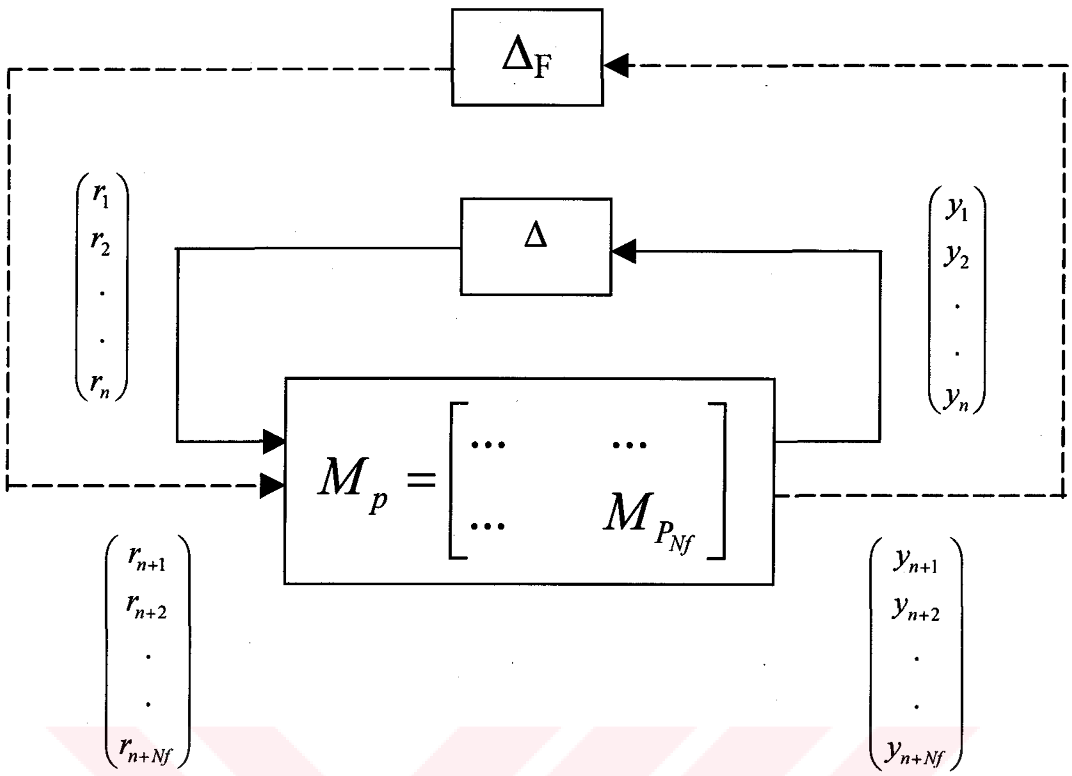

Figure 3.6 Robust performance

3.4 Performance Measures

Possible performance measures for feedforward tracking control systems are introduced and evaluated in this section.

3.4.1 Sensitivity Minimization

Sensitivity minimization from input R to error E (see Figure 3.5) seems to be the most obvious choice of measuring performance of a control system. The structure to be used in SSV analysis of robust performance for this choice of performance criterion is shown in Figure 3.7. Considering only the nominal case Δ=0, the sensitivity transfer function is given by

$$S = \tilde{G}_{fb}^{-1}(z)Z\left(\frac{1}{1+C(s)P(s)}\right) \tag{3.30}$$

where Z denotes the zero order hold method of transforming the s-domain argument to the z-domain. The reliability of this performance criterion is checked by

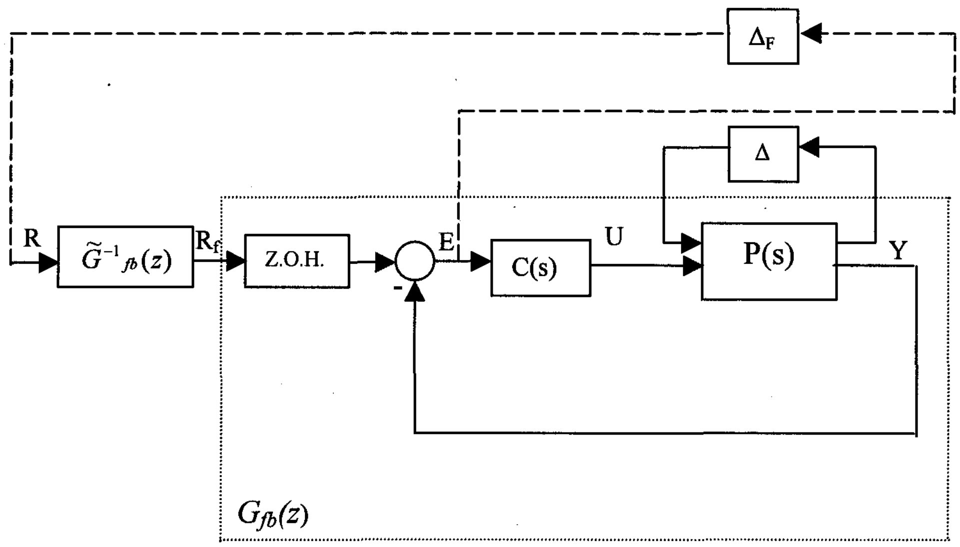

Figure 3.7 SSV analysis framework for sensitivity minimization

comparing the magnitude frequency responses of S for the cases of no feedforward controller and with different feedforward controllers as shown in Figure 3.8 for the example system considered in the next section.

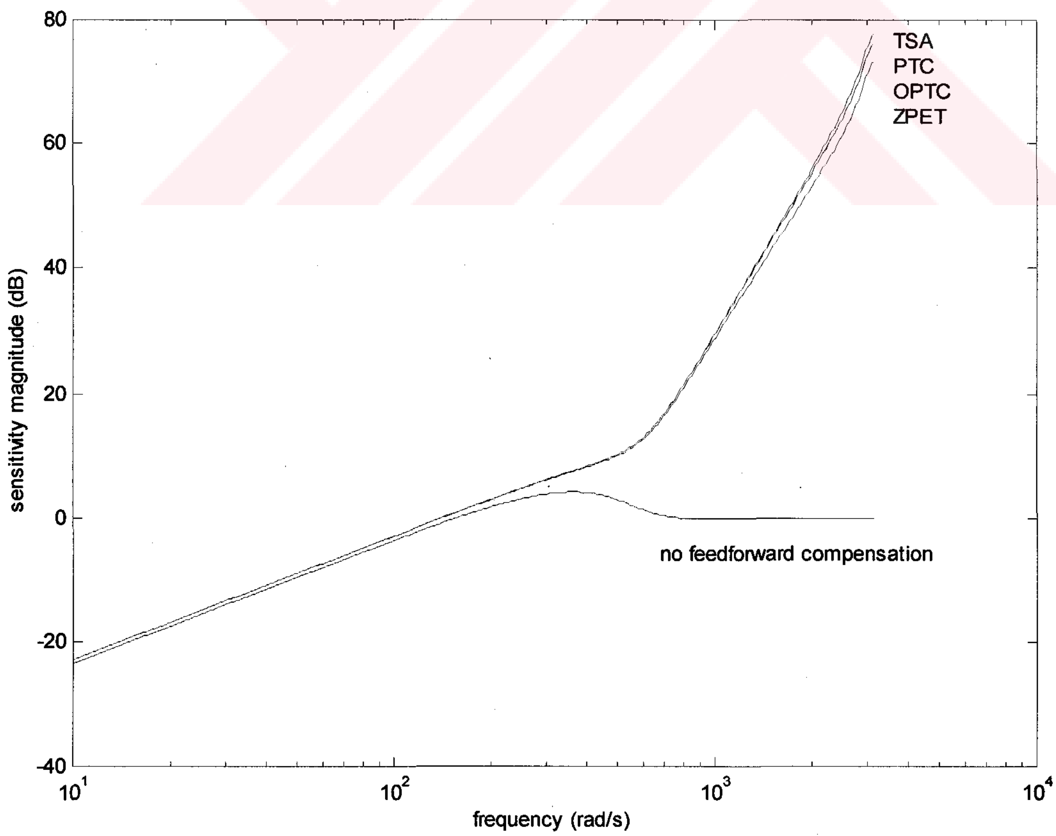

Figure 3.8 Sensitivity magnitude comparison

It is obvious from Figure 3.8 that sensitivity magnitude minimization is not a good measure of performance for reference feedforward tracking control as the incorporation of feedforward control increases sensitivity magnitude of the nominal system rather than decreasing it. This result makes sense since feedforward tracking control works by minimizing the tracking error

$$E_{tr} = R - Y \tag{3.31}$$

between system output and the actual reference trajectory. Since R_f (see Figure 3.5a) is a filtered version of the reference trajectory, it is not meaningful to try to minimize

$$E = R_f - Y \tag{3.32}$$

as is done in sensitivity magnitude minimization.

A more suitable measure of performance in reference feedforward tracking control is thus minimizing the magnitude of the tracking sensitivity given by

$$S_{tr} = \frac{E_{tr}}{R} = \frac{R-Y}{R} = 1 - \frac{Y}{R} \tag{3.33}$$

The tracking sensitivity magnitude plot for the same example system, shown in Figure 3.9, validates this assertion since $|S_{tr}|$ is much lower when feedforward control is added to the nominal plant. It is seen in this figure that different methods of feedforward controller design result in varying levels of nominal performance when tracking sensitivity magnitude minimization is used as the performance criterion with the OPTC and PTC methods resulting in the best performance up to a certain frequency. After this frequency, the series method has better nominal performance for the example considered here (given in section 3.5.1).

3.4.2 Model Matching

Minimization of S_{tr} is equivalent to the model matching measure given by

$$\left\| W\left(1 - \frac{Y}{R}\right) \right\|_\infty = \left\| W\left(1 - \tilde{G}_{fb}^{-1}(z) Z\left(\frac{C(s)P(s)}{1 + C(s)P(s)}\right)\right) \right\|_\infty < 1 \tag{3.34}$$

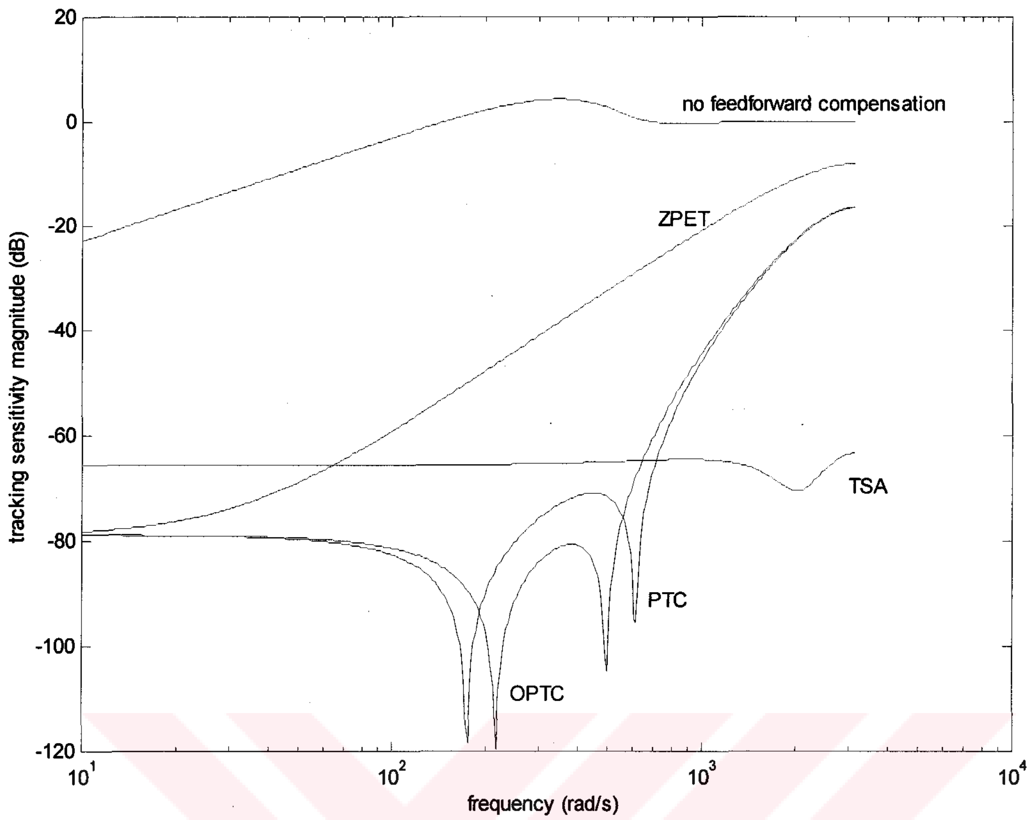

Figure 3.9 Tracking sensitivity magnitude comparison

where W is a low pass filter introduced to specify the frequency range of model matching. Model matching or equivalently tracking sensitivity minimization is thus used here as the performance measure in SSV analysis with the corresponding structure shown in Figure 3.10.

3.4.3 Phase Error

Reference feedforward tracking control schemes like the ZPET and PTC methods achieve zero phase error between reference input and system output by using a noncausal filter $\tilde{G}_{fb}^{-1}(z)$ with several preview steps. This zero phase error property is a very important measure of performance since tracking error is reduced considerably even by ZPET control alone. All the reference feedforward control techniques considered here except for the series method have this zero phase property. The corresponding phase in the series method turns out to be extremely small for a good design and also benefits from this zero phase effect[1]. So, it would be desirable to analyze the robustness of this zero phase property in the presence of plant modeling

[1] or near zero phase effect in this case

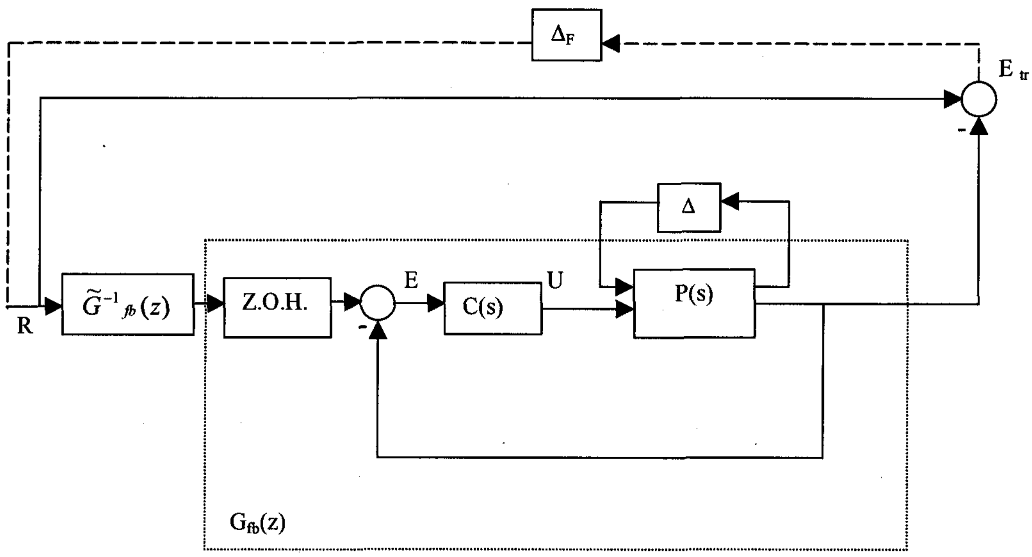

Figure 3.10 SSV analysis framework for tracking sensitivity minimization or model matching

error. Unfortunately, it is not possible to directly formulate the zero phase error property as a performance criterion in the SSV analysis framework. However, as a complement to the SSV analysis results, it is worthwhile to at least determine the effect of several selected parametric plant uncertainties on the zero phase property while checking for robustness of performance.

3.5 SSV Analysis Example

Use of SSV performance robustness analysis is demonstrated in this section using an electrohydraulic material testing machine model available in the literature.

3.5.1 Nominal System and Uncertainty Model

The example system considered here is an electrohydraulic material testing machine model given in Srinivasan and Shaw (1991). The nominal model of this system under proportional feedback control K_p is

$$C(s)(P(s))_{nominal} = \left(\frac{KK_p}{s(\tau_{sv}s+1)\left(\frac{s^2}{\omega_h^2}+\frac{2\zeta_h s}{\omega_h}+1\right)} \right)_{nominal} \tag{3.35}$$

where KK_p=150, $\bar{\tau}_{sv}$=0.00187 sec, $\bar{\zeta}_h$=0.4 and $\bar{\omega}_h$=618 rad/sec are the nominal parameter values. Real parametric uncertainty in the time constant τ_{sv}, the damping ratio ζ_h and hydraulic resonant frequency ω_h given by

$$\begin{aligned} \tau_{sv} &= \bar{\tau}_{sv} + (\Delta\tau_{sv})_{\max}\delta_{\tau},\ \delta_{\tau} \in \boldsymbol{R},\ |\delta_{\tau}| < 1 \\ \zeta_h &= \bar{\zeta}_h + (\Delta\zeta_h)_{\max}\delta_{\zeta}, \delta_{\zeta} \in \boldsymbol{R},\ |\delta_{\zeta}| < 1 \\ \omega_h &= \bar{\omega}_h + (\Delta\omega_h)_{\max}\delta_{\omega},\ \delta_{\omega} \in \boldsymbol{R},\ |\delta_{\omega}| < 1 \end{aligned} \tag{3.36}$$

with $(\Delta\tau_{sv})_{\max}$=0.0000935 sec, $(\Delta\zeta_h)_{\max}$=0.05 and $(\Delta\omega_h)_{\max}$=30.9 rad/sec were used. Unstructured multiplicative uncertainty with a high frequency selective weight was also used to model high frequency unmodeled dynamics.

In order to better visualize the effect of the real parametric uncertainty on the closed loop plant $G_{fb}(z)$, the abovementioned parameters were varied within their allowed ranges and the corresponding gain changes in Figures 3.11 were obtained. The gain changes in $G_{fb}(z)$ shown in Figure 3.11 illustrate that the presence of the feedback loop reduces the effect of open loop plant parameter variations. The effect of the plant parameter variations on the magnitude and phase plots of the overall feedforward compensated system was observed to be quite similar for the four different feedforward controllers used here. This is not surprising as they all approximately invert the same nominal closed loop system. The phase plot in Figure 3.12 for the OPTC design, for example, shows phase angle errors of –12° to +17° at high frequencies.

The extraction of the real parametric uncertainty blocks in

$$C(s)P(s) = \left(\frac{KK_p}{s((\tau_{sv}+\Delta\tau_{sv})s+1)\left(\frac{s^2}{(\omega_h+\Delta\omega_h)^2}+\frac{2(\zeta_h+\Delta\zeta_h)s}{(\omega_h+\Delta\omega_h)}+1\right)} \right) \tag{3.37}$$

for use in SSV analysis is illustrated in the block diagrams of Figure 3.13.

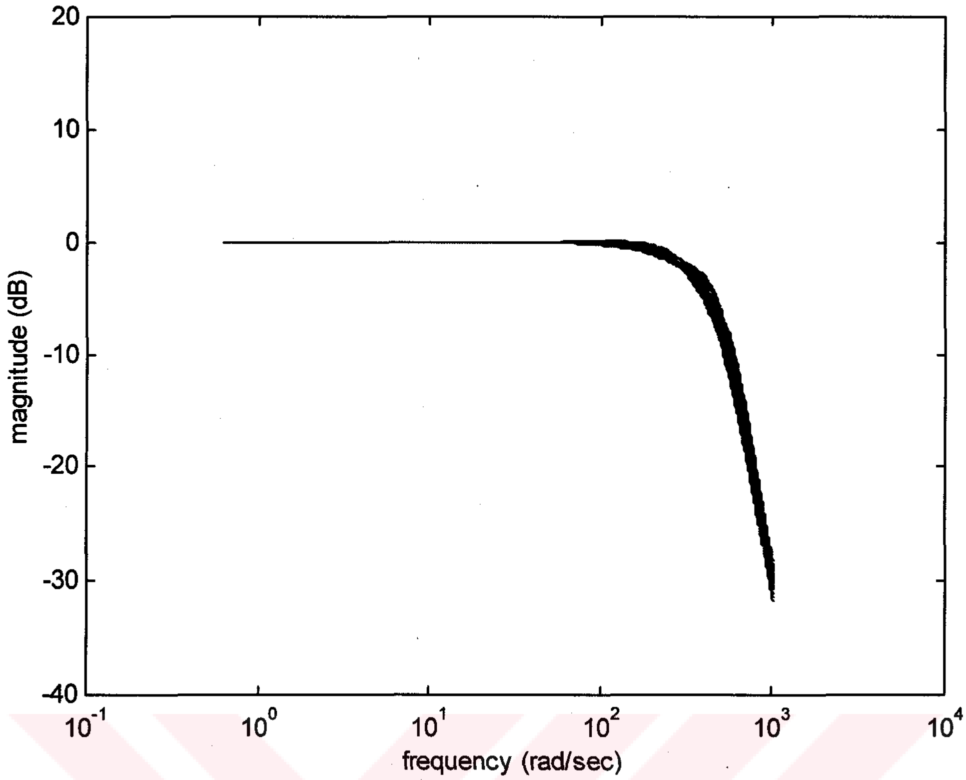

Figure 3.11 Effect of real parametric plant variations on magnitude of $G_{fb}(z)$

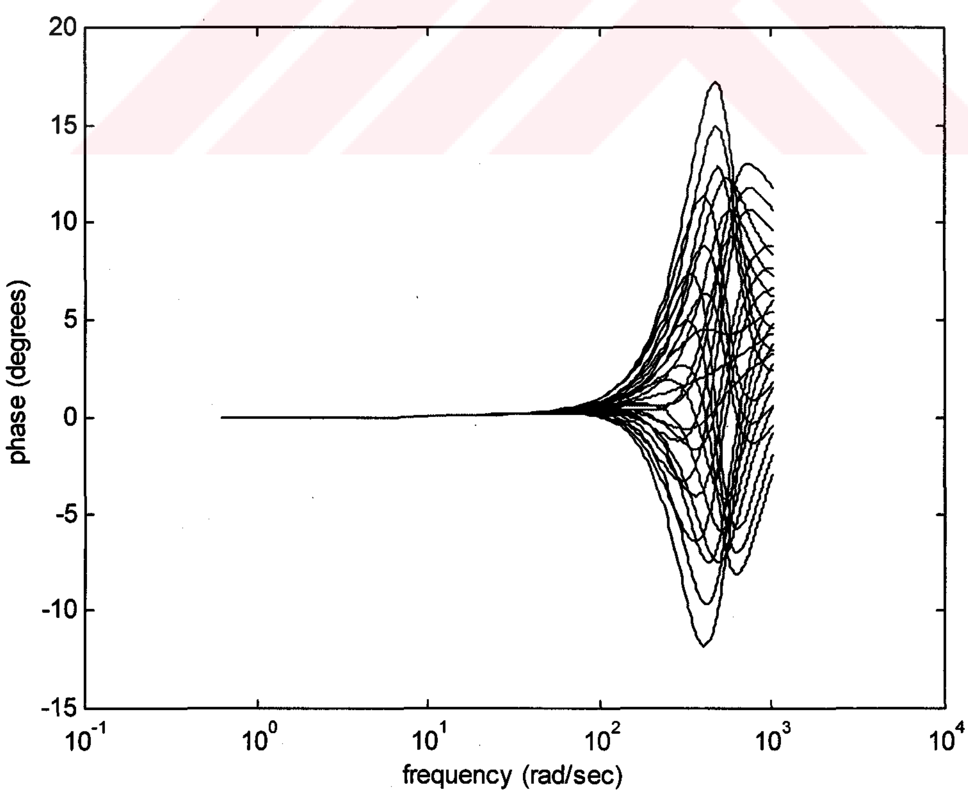

Figure 3.12 Effect of real parametric plant variations on phase of $\widetilde{G}_{OPTC}^{-1}(z)G_{fb}(z)$

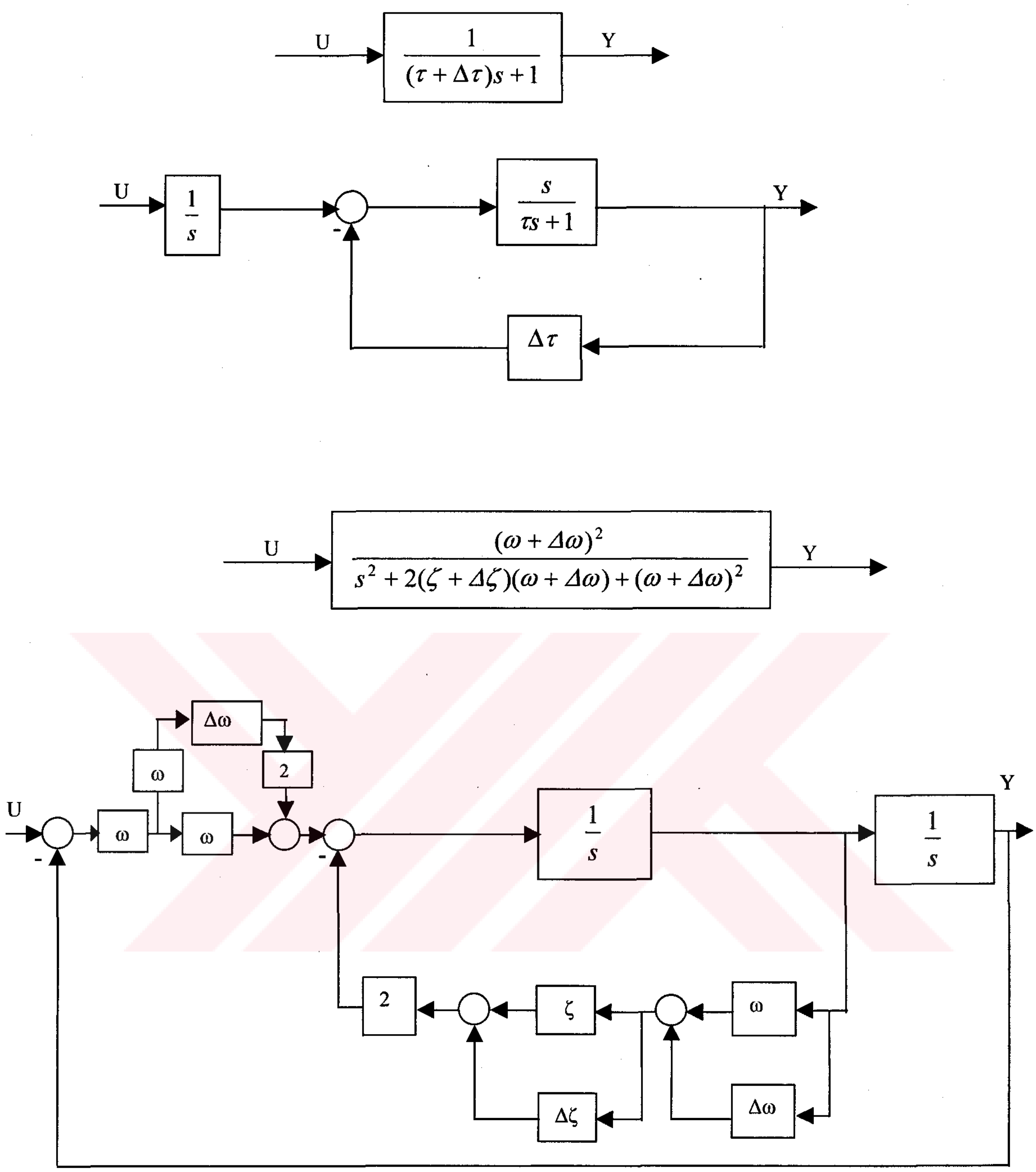

Figure 3.13 Extraction of real parametric uncertainty

3.5.2 Feedforward Controller Design and Nominal Performance

The feedback loop in Figure 3.5a with the nominal plant model (3.35) is discretized using the zero order hold method with a sampling time of 0.001 sec. This results in a system nonminimum phase zero at z_1=-7.9488. The corresponding ZPET, PTC, OPTC and TSA feedforward tracking filters for this system are then

$$
\begin{aligned}
\widetilde{G}_{ZPET}^{-1}(z) &= \frac{d(z)}{n_{mp}(z)}\frac{0.0993z+0.0125}{z} \\
\widetilde{G}_{PTC}^{-1}(z) &= \frac{d(z)}{n_{mp}(z)}\frac{-0.0102z^3+0.118z^2+0.00482z-0.00129}{z^2} \\
\widetilde{G}_{OPTC}^{-1}(z) &= \frac{d(z)}{n_{mp}(z)}\frac{-0.0101z^3+0.118z^2+0.00491z-0.00127}{z^2} \\
\widetilde{G}_{TSA}^{-1}(z) &= \frac{d(z)}{n_{mp}(z)}\left(-0.000203z^3+0.00201z^2-0.0158z+0.126\right)
\end{aligned}
\tag{3.38}
$$

where $\theta=\pi/5$ rad was specified as the desired bandwidth in the PTC and OPTC methods and a third order truncated series was used in the TSA approach. As a measure of nominal performance, the complementary sensitivity Y/R and the tracking sensitivity E_{tr}/R achieved by the feedforward tracking controllers (3.38) are shown in Figures 3.14 and 3.9, respectively. It is seen that the chosen ZPET, OPTC, PTC and TSA resulted in successively better nominal performance for the example system considered here based on the complementary sensitivity magnitude.

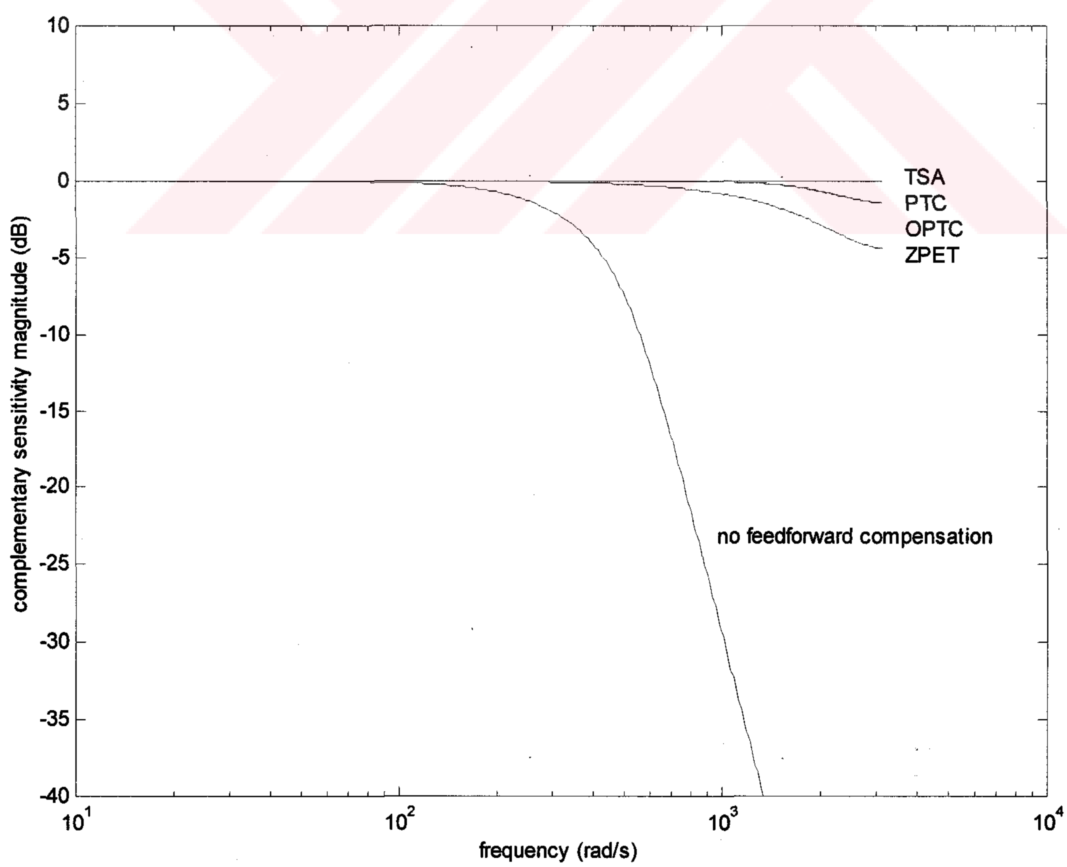

Figure 3.14 Complementary sensitivity magnitude comparison

3.5.3 SSV Analysis Results

Real parametric uncertainty given by (3.37) and illustrated in Figure 3.13, combined with multiplicative high frequency unstructured uncertainty and the fictitious robust performance block corresponding to the model matching criterion in (3.34) with W=1 results in a mixed (real and complex) SSV analysis problem (Fan et al, 1991). This problem is readily solved by commercially available robust control software (Balas et al, 1995). The resulting SSV plots for the feedforward controllers in (3.38) are shown in Figure 3.15. Analysis of this figure reveals that robustness of performance is not achieved in this example in the absence of feedforward control, as the maximum SSV value is greater than unity in this case. In comparison, all the feedforward controllers considered here achieve robustness of performance with relatively small differences in SSV at higher frequencies for the example system.

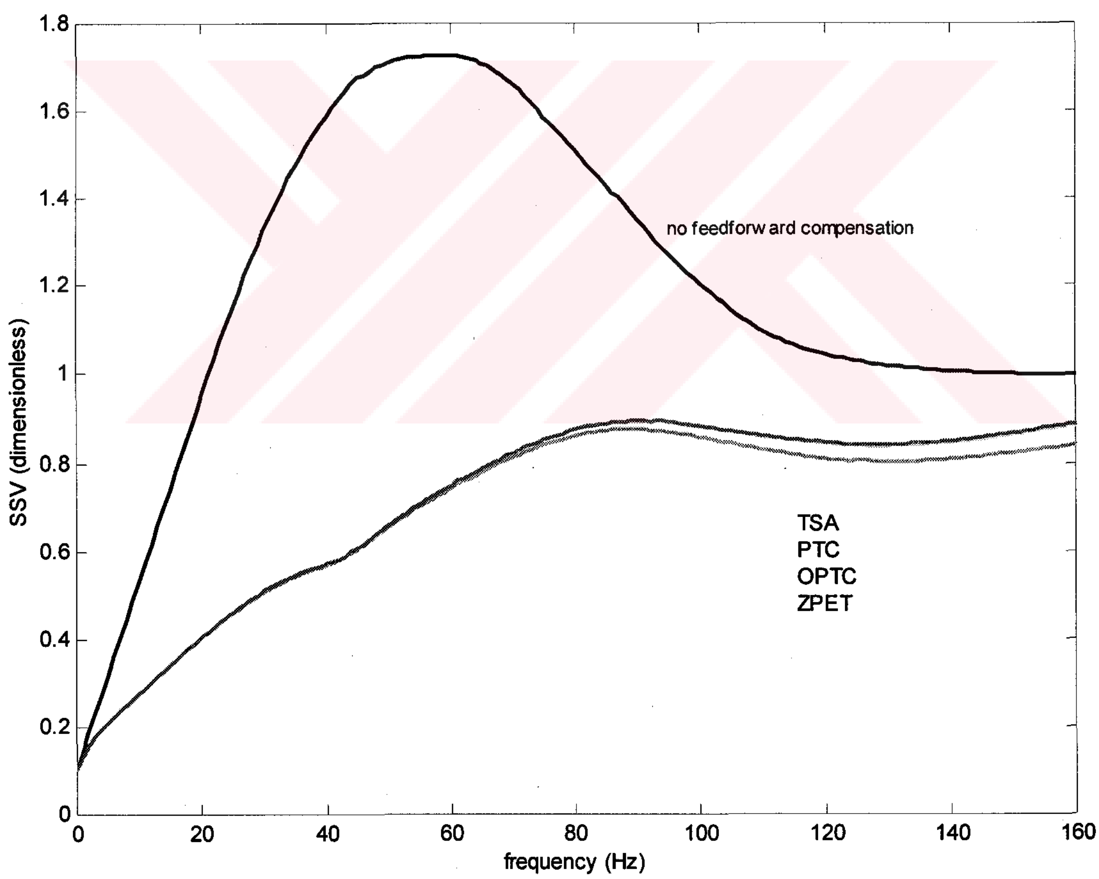

Figure 3.15 Structured singular value plots

As a result, the use of SSV analysis along with a suitably chosen measure of performance has been demonstrated here to result in a useful tool for evaluating performance robustness of discrete time reference feedforward control systems.

Tracking sensitivity magnitude minimization or equivalently model matching has been chosen here and shown to be a good measure of performance for feedforward control systems. While actual results will be dependent on the plant and associated model uncertainty, it has been seen at least for the example considered here that the incorporation of reference feedforward control does not deteriorate performance beyond acceptable limits. It was also seen that tracking performance was improved in a robust manner for the example plant with structured model uncertainty, by the incorporation of feedforward compensation.

Determination of changes in the zero phase error property of reference feedforward control systems for the plant parameter variations has also been proposed here as an added measure of performance. This zero phase error check, complemented with the SSV-based performance robustness analysis was seen to be a useful tool for checking robustness of feedforward control systems or for comparing different feedforward controller designs.

4. TWO DEGREE OF FREEDOM ROBUST CONTROL, THE MODEL REGULATOR

A two degree of freedom controller that provides very good disturbance rejection along with a high level of robustness to unmodeled dynamics is presented in this chapter. The application of this control architecture to vehicle steering control and vehicle lateral control in automated path following are treated in Chapters 5 and 6, respectively. Early work on this control architecture can be found in Ohnishi (1987) and Umeno and Hori (1991). Even though some authors have called this control architecture a disturbance observer, this name will not be used here as this control architecture, although somewhat similar in its disturbance cancellation objective, is not an implementation of a state estimator for disturbances as in Mita et al (1998), and Liu and Peng (2000). Out of the other names like model regulator and disturbance estimating/canceling filter, the name *model regulator* will be used here. This is a logical choice since the aim of this control method is to force the input-output behaviour of the actual system to follow that of a chosen model in the presence of external disturbances and model uncertainty. The term two degree of freedom controller is also used frequently to describe the model regulator since it is a specific method of implementing/designing a two degree of freedom controller. The model regulator has been used successfully in a variety of motion control applications including high speed direct drive positioning (Kempf and Kobayashi, 1999) and friction compensation (Güvenç and Srinivasan, 1994). It can also be used to achieve dynamics similar to those obtained by the use of inner feedback loops through control (Güvenç, 1999). The augmentation of the plant G with the model regulator as seen in Figure 4.1 forces it to behave like its nominal (or desired) model within the bandwidth of the model regulator. The feedback controller C for this augmented plant is then designed simply based on the nominal plant model G_n which can also be chosen as a desired model.

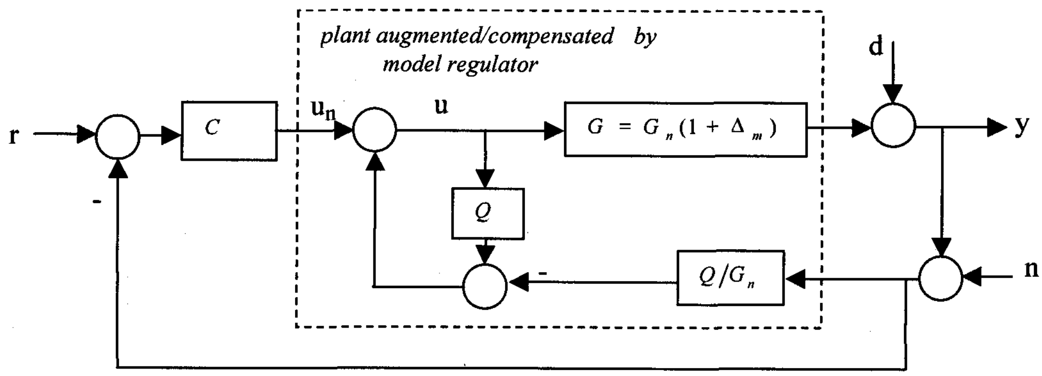

Figure 4.1 System with model regulator

The model regulation is achieved by first comparing the actual input u to the plant with the input that should have been applied to obtain the measured output y based on the nominal (or desired) knowledge of the plant and then by passing the difference through a positive feedback loop. The model regulator is introduced and analyzed in detail in the following sections.

Along with its desirable model regulation and disturbance rejection properties, the model regulator also introduces stability and stability robustness problems due to its use of feedback. It is standard practice to use an unstructured description of model uncertainty and low pass filter the model regulator output to avoid stability robustness problems at high frequencies corresponding to unmodeled dynamics. Many problems (see for example Bünte et al, 2001) involve well defined real parametric uncertainty in our knowledge of the plant. The conventional stability robustness analysis based on unstructured uncertainty becomes conservative in such cases. Real structured singular value (abbreviated henceforth as real SSV) analysis is therefore used in the last two sections of this chapter to investigate the effect of real parametric uncertainty on stability and performance robustness of model regulator compensated systems.

4.1 The Structure of the Model Regulator

Consider plant G with multiplicative model error Δ_m and external disturbance d. Its input-output relation can be expressed as

$$y = Gu + d = \left(G_n(1+\Delta_m)\right)u + d \tag{4.1}$$

where G_n is the nominal model of the plant. The aim in model regulator design is to obtain

$$y = G_n u_n \tag{4.2}$$

as the input – output relation in the presence of model uncertainty and external disturbance. u_n in (4.2) is a new input signal to be defined below. This aim is achieved in model regulator design by treating the external disturbance and model uncertainty as an extended disturbance e and solving for it as

$$y = G_n u + (G_n \Delta_m u + d) = G_n u + e \tag{4.3}$$

$$e = y - G_n u \tag{4.4}$$

and using the new control signal u_n given by

$$u = u_n - \frac{e}{G_n} = u_n - \frac{1}{G_n} y + u \tag{4.5}$$

to approximately cancel its effect in (4.3). With the aim of trying to limit the compensation to a pre-selected low frequency range (in an effort not to overcompensate at high frequencies and to avoid stability robustness problems), the feedback signals in (4.5) are multiplied by the low pass filter Q. In this case, the implementation equation becomes

$$u = u_n - \frac{Q}{G_n}(y + n) + Qu \tag{4.6}$$

where y+n with n representing the sensor noise is used as this is the actual output signal that is available. This is illustrated in the block diagram of Figure 4.1. The relative degree of the unity d.c. gain low pass filter Q is chosen to be at least equal to the relative degree of G_n for causality of Q/G_n. The loop gain of the model regulator compensated plant is

$$L = \frac{GQ}{G_n(1-Q)} \tag{4.7}$$

with the model regulation, disturbance rejection and sensor noise rejection transfer functions given by

$$\begin{aligned}
\frac{y}{u_n} &= \frac{G_n G}{G_n(1-Q)+GQ} \\
\frac{y}{d} &= \frac{1}{1+L} = \frac{G_n(1-Q)}{G_n(1-Q)+GQ} \\
\frac{y}{n} &= \frac{-L}{1+L} = \frac{-GQ}{G_n(1-Q)+GQ}
\end{aligned} \tag{4.8}$$

from which it is obvious that Q must be a unity gain low pass filter. As is desired, this choice will result in $y/u_n \to G_n$, $y/d \to 0$ at low frequencies where $Q \to 1$ and $y/n \to 0$ at high frequencies where $Q \to 0$.

Regarding the design of the Q filter, it makes no sense to increase the bandwidth of the Q filter above the actuator bandwidth in model regulator design. Another bandwidth limitation for the Q filter and hence the model regulator comes from the stability robustness requirement. First of all let's look at the case of plant with only model regulator (C=0).

Rewrite the characteristic equation in (4.8) given by

$$G_n(1-Q)+G_n(1+\Delta_m)Q=0 \tag{4.9}$$

as

$$G_n(1+\Delta_m Q)=0 \;\rightarrow\; Q=-\frac{1}{\Delta_m} \tag{4.10}$$

and noting that when the presence of Δ_m does not change the number of unstable poles and zeros of G in comparison to those of G_n, the application of the Nyquist stability criterion results in equation (4.11) as the necessary and sufficient condition for stability.

$$|Q| < \left|\frac{1}{\Delta_m}\right|, \; for\ \forall\omega \tag{4.11}$$

The model regulator design requirements specified in terms of the filter Q are summarized in Figure 4.2.

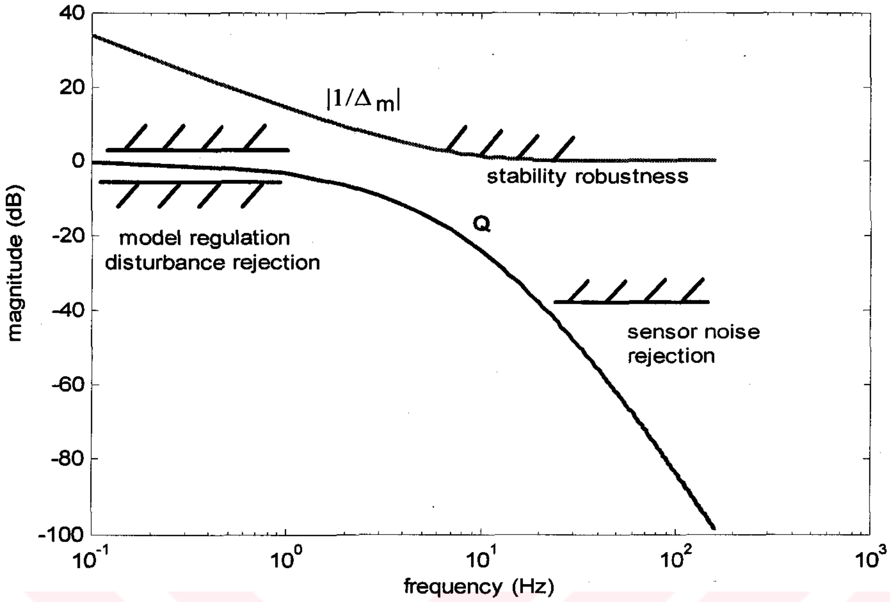

Figure 4.2 Model regulator design requirements

4.2 Integral Action

For specific choices of Q(s), the model regulator introduces integrators into the loop, resulting in reduced steady state error for reference and disturbance inputs. To see how the integrators are introduced, consider the equivalent form of the model regulator in Figure 4.3 and consider Q(s) of the form

$$Q(s) = \frac{a_m s^m + a_{m-1}s^{m-1} + \ldots + a_2 s^2 + a_1 s + 1}{a_n s^n + a_{n-1}s^{n-1} + \ldots + a_2 s^2 + a_1 s + 1},\ m < n \tag{4.12}$$

Evaluate $Q/(1-Q)$ in the loop gain of (4.7) to obtain

$$\frac{Q}{1-Q} = \frac{a_m s^m + a_{m-1}s^{m-1} + \ldots + a_2 s^2 + a_1 s + 1}{s^{m+1}(a_n s^{n-m-1} + a_{n-1}s^{n-m-2} + \ldots + a_{m+1})} \tag{4.13}$$

which shows that m+1 integrators are incorporated into the loop for the choice of Q in (4.12).

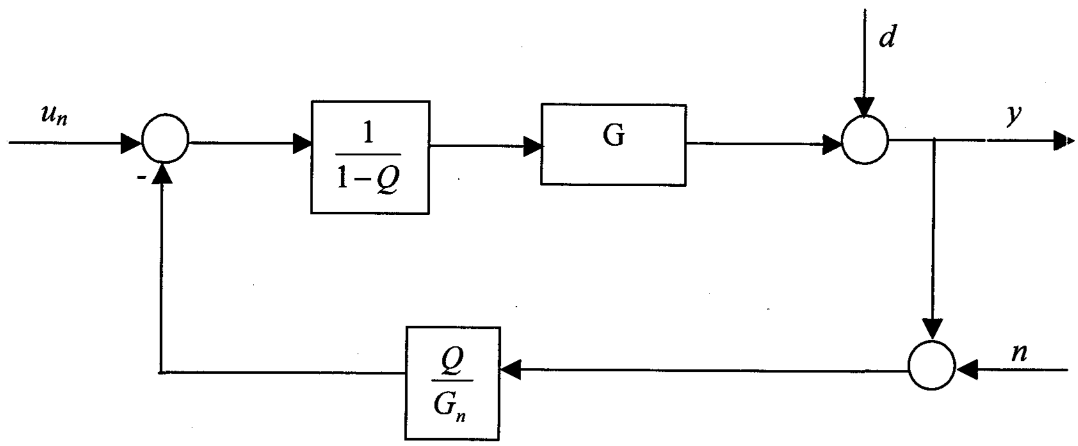

Figure 4.3 Equivalent form of model regulator

Note that several commonly used forms for Q(s) are of the form (4.12) and hence provide integral action. $Q(s) = 1/(\tau s+1)^k$ (m=0, n=1) for example introduces one integrator into the loop. Similarly $Q(s) = 1/((s/\omega)^2 + (2\zeta/\omega)s+1)$ (m=0, n=2) also introduces one integrator into the loop. $Q(s) = (3\tau s+1)/(\tau^3 s^3 + 3\tau^2 s^2 + 3\tau s + 1)$ (m=1, n=3) used by Kempf and Kobayashi (1999) introduces two integrators into the loop. It should also be noted that while the presence of integral action is useful for reducing steady state error, the model regulator is not simply an alternative design of an integral controller as suggested by Mita et al (1998). An analysis of Figure 4.1 and 4.2 reveals that there is more to the model regulator than integral action. Moreover, not all forms of the low pass filter Q(s) will result in integral action. Certainly, the ideal situation of Q=1 does not result in integral action in the loop, but rather infinite gain at all frequencies.

4.3 State Estimator Formulation

Note that although not equivalent to the model regulator, a state estimator formulation can also be used to estimate and cancel the effect of the disturbance. Consider a state space representation of the plant given by

$$\begin{aligned} \dot{x}_0 &= A_0 x_0 + b_0 u \\ y &= c_0 x_0 \end{aligned} \tag{4.14}$$

Let (A_0,b_0) be controllable and let (A_0,c_0) be observable. Assuming that the disturbance d satisfies

$$\dot{d} = 0 \tag{4.15}$$

i.e. a step disturbance, the state space model of the plant can be extended as

$$\begin{aligned} \dot{x} &= \begin{bmatrix} \dot{x}_0 \\ \dot{d} \end{bmatrix} = \begin{bmatrix} A_0 & b_0 \\ 0 & 0 \end{bmatrix} \begin{bmatrix} x_0 \\ d \end{bmatrix} + \begin{bmatrix} b_0 \\ 0 \end{bmatrix} u = Ax + Bu \\ y &= \begin{bmatrix} c_0 & 0 \end{bmatrix} \begin{bmatrix} x_0 \\ d \end{bmatrix} = Cx \end{aligned} \tag{4.16}$$

where d has been used as an additional state variable. Design the state observer

$$\dot{\hat{x}} = A\hat{x} + Bu + L(y - C\hat{x}) \tag{4.17}$$

for the system in (4.16). Then,

$$\hat{d}(t) = [0...0 \;\; 1]\hat{x}(t) = C_d \hat{x} \tag{4.18}$$

is an estimate of the external disturbance. The control law

$$u = u_n - \hat{d} \tag{4.19}$$

can be used to cancel the effect of the disturbance in (4.14) provided that $\hat{d} \to d$.

Using transfer functions, one obtains

$$\hat{d}(s) = (C_d (sI - A + LC)^{-1} Bu(s) + C_d (sI - A + LC)^{-1} L) y(s) \tag{4.20}$$

The state estimator for disturbance estimation is shown in Figure 4.4.

4.4 Open Loop Unstable Plant

A lot of control applications like the inverted pendulum or fighter aircraft have open loop unstable plants. Note that for an unstable plant G, $1/G_n$ will be non minimum phase if G_n has the same poles as G. This is not a problem but the right half plane pole cancellation in forming the loop gain in (4.7) in that case will lead to internal

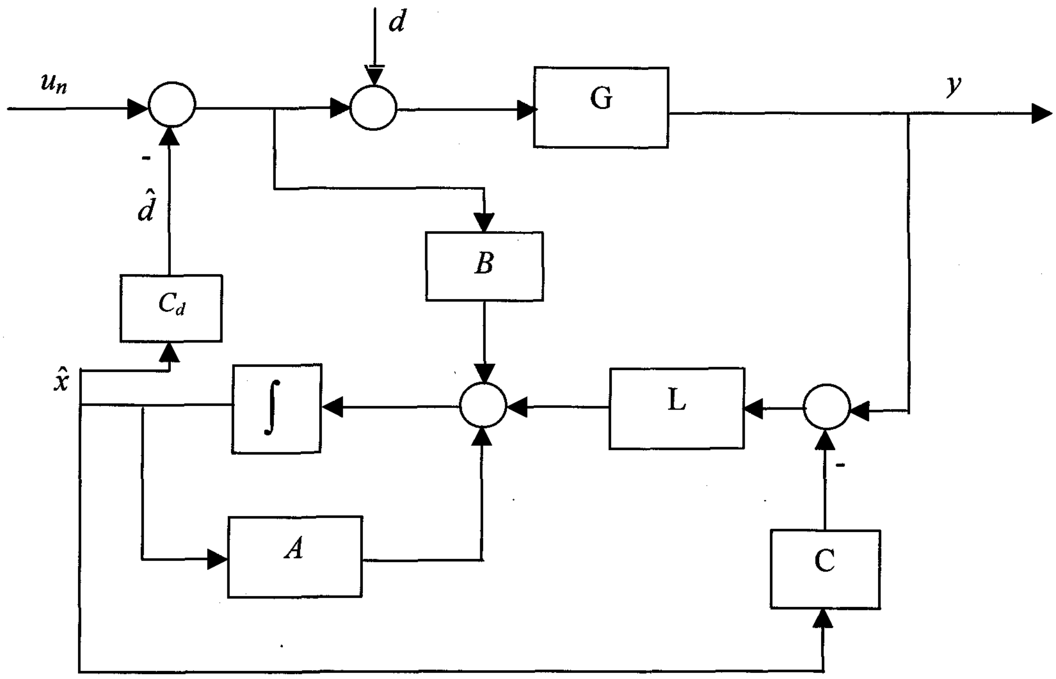

Figure 4.4 Disturbance estimator

instability. Therefore, G_n should be chosen as a stable (and minimum phase) system. This makes sense as no one would want their plant to follow the behaviour of an unstable system. In this case, $Q/(G_n(1-Q))$ should stabilize the plant G. If this is not possible, a filter F_s can be used to stabilize the plant G before application of the model regulator. This concept is illustrated in Figure 4.5.

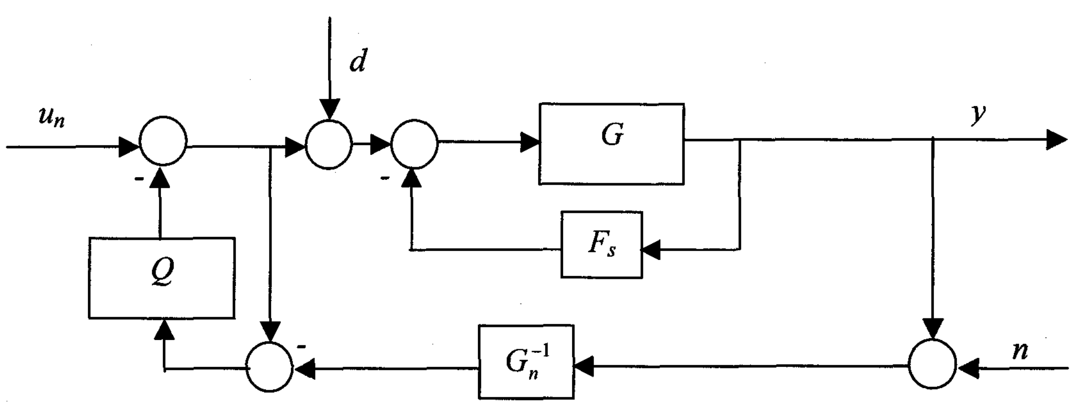

Figure 4.5 Unstable plant

A simple example that can be used to illustrate model regulation of an unstable system is given next. Consider the unstable plant

$$G(s) = \frac{1}{s-a}, \quad a \in \boldsymbol{R},\ a > 0 \tag{4.21}$$

where the desired model is chosen as

$$G_n(s) = \frac{1}{\tau_n s + 1} \tag{4.22}$$

and the Q filter is chosen as

$$Q = \frac{1}{\tau_Q s + 1} \tag{4.23}$$

There is no internal stability problem, as no RHP pole-zero cancellation occurs in forming the loop gain L. The characteristic equation is

$$\tau_Q s^2 + (\tau_n - a\tau_Q)s + 1 = 0 \tag{4.24}$$

which indicates stability for $\tau_n > a\tau_Q$. This simple example shows that it is possible to construct a stable model regulator loop for an open loop unstable plant. Note that the use of a stabilizing filter F_s may, nevertheless, help with robustness of stability and performance.

4.5 Treatment of Parametric Uncertainty

Robustness of the model regulator in the presence of real parametric uncertainty is treated in this section using the model of an electrohydraulic positioning system as an example.

4.5.1 Electrohydraulic system model

The model of an electrohydraulic system given by

$$G(s) = \frac{1}{s(\tau s + 1)\left(\frac{s^2}{\omega^2} + \frac{2\zeta s}{\omega} + 1\right)} \tag{4.25}$$

with nominal parameter values of $\bar{\tau}$=0.00187 sec, $\bar{\zeta}$=0.4 and $\bar{\omega}$=618 rad/sec is used here to illustrate the concept. The desired model is chosen to be of the same form as G in (4.25) but with real parametric uncertainty in the time constant τ, the damping ratio ζ and hydraulic resonant frequency ω given by

$$\begin{aligned} \tau &= \bar{\tau} + (\Delta\tau)_{\max}\delta_\tau, \quad \delta_\tau \in \boldsymbol{R}, \ |\delta_\tau| < 1 \\ \zeta &= \bar{\zeta} + (\Delta\zeta)_{\max}\delta_\zeta, \quad \delta_\zeta \in \boldsymbol{R}, \ |\delta_\zeta| < 1 \\ \omega &= \bar{\omega} + (\Delta\omega)_{\max}\delta_\omega, \quad \delta_\omega \in \boldsymbol{R}, \ |\delta_\omega| < 1 \end{aligned} \tag{4.26}$$

with $(\Delta\tau)_{\max}$=0.000187 sec (10 %), $(\Delta\zeta)_{\max}$=0.1 (25 %) and $(\Delta\omega)_{\max}$=61.8 rad/sec (10 %). This uncertain model was used in a frequency grid of computations for combinations of the variations in (4.26) covering all of the extreme points and several points in between to convert this real parametric variation to an approximate unstructured multiplicative uncertainty Δ_m. The corresponding $|1/\Delta_m|$ plot is displayed in Figure 4.2 where Q taken to be of the form

$$Q = \frac{1}{(\tau_Q s + 1)^k} \tag{4.27}$$

with k=3 and τ=0.00318 sec does not violate the stability robustness condition (4.11).

4.5.2 Real SSV Analysis

Real SSV (see deGaston and Safonov, 1988) is defined as (see Figure 4.6)

$$\mu_{\Delta_r}(N) = \frac{1}{\min\limits_{\delta_i \in \boldsymbol{R}; i=1,2,\ldots,n} \{(\max|\delta_i|) : \det(I - N \cdot diag(\delta_1, \delta_2, \cdots, \delta_n)) = 0\}} \tag{4.28}$$

and is one over the size of the smallest destabilizing perturbation among the real parametric model uncertainty (Doyle et al, 1992; Packard and Doyle, 1993; Zhou et al, 1996). N in (4.28) is the generalized plant in linear fractional transformation (LFT) form and $\Delta_r = diag(\delta_1, \delta_2, \cdots, \delta_n)$ is the diagonal matrix of real parametric uncertainty $\delta_i \in \boldsymbol{R}$. Real SSV can either be calculated using results from the parametric approach to robust control (Elgersma et al, 1996) or lower and upper bounds for it can be computed in the frequency domain approach to robust control (Doyle et al, 1992; Packard and Doyle, 1993). The latter approach is taken here as it

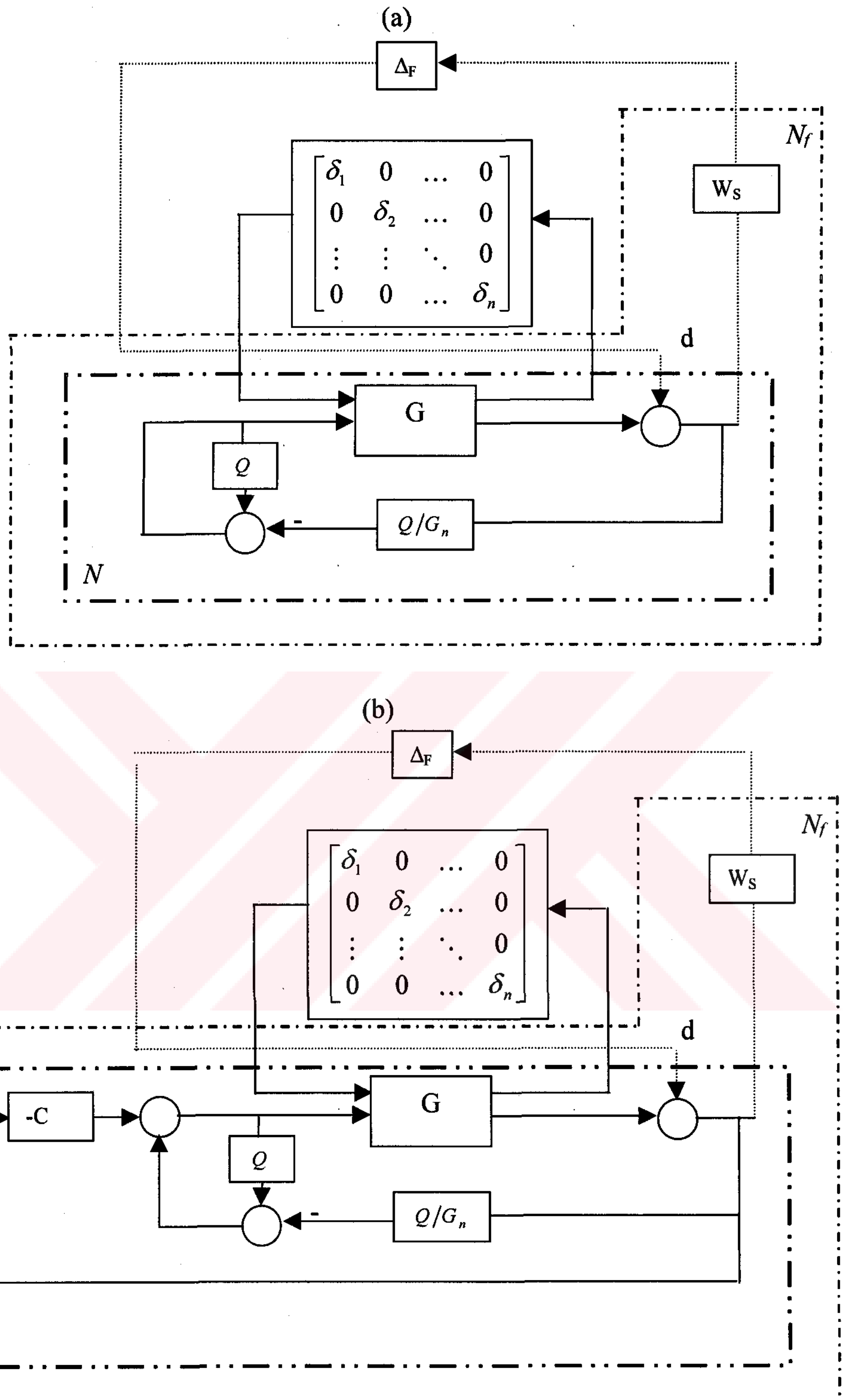

Figure 4.6 System with model regulator and structured uncertainty for a) no feedback and b) with feedback controller

is implemented in commercially available software (Balas et al, 1995; Chiang and Safonov, 1992). In the SSV setting, robustness of stability for a feedback system with $\|\Delta_r\|_\infty \leq 1$ is equivalent to satisfying

$$\sup_{\omega \in \mathbf{R}} \mu_{\Delta_r}(N(j\omega)) < 1. \tag{4.29}$$

The SSV-analysis technique is easily extended to handle robustness of performance by treating the performance criterion as a fictitious, extra uncertainty block (see Δ_F in Figure 4.6). How the real parametric uncertainty in (4.25) is pulled out was illustrated in Figure 3.13.

Real SSV, in contrast to complex SSV, is plagued by its discontinuous nature as a function of frequency (Barmish et al, 1989; Packard and Pandey, 1991). It is, therefore, possible to miss isolated real SSV peaks in a frequency sweep during computations. The robust performance formulation requires the use of a fictitious complex uncertainty block, resulting in what is known as the the mixed SSV problem that combines at least one complex uncertainty block with the remaining real parametric uncertainty blocks.

Mixed SSV is continuous with frequency, however, tall and narrow peaks that exist for mixed SSV may still be missed in a frequency sweep. Thus, real SSV and mixed SSV plots are complemented by the complex SSV plot of corresponding Δ structure (displayed as a dashed line in the plots to follow in this chapter) in all of the SSV plots reported here. By superimposing this latter, conservative upper bound in the SSV plots, the risk of missing isolated peaks is reduced.

The stability robustness real SSV plot for the example system in (4.25) shown in Figure 4.7 exhibits two peaks. The first peak frequency of approximately 20 Hz is close to the –3 dB bandwidth of the Q filter used (bandwidth of model regulation), illustrating the presence of stability robustness problems at this intermediate frequency. Note that conventional model regulator design concentrates on the low and high frequency asymptotic behaviour of Q without paying enough attention on what happens in the intermediate frequency range where Q is neither 0 nor 1 and where the phase of Q also plays an important role. The second, less pronounced peak frequency in Figure 4.7 is close to the resonant peak in the second order part of plant (4.25) with large uncertainty in the damping ratio. It is clear that the Q filter cutoff frequency should not coincide with such critical peak frequencies in order not to aggravate the stability robustness problem.

As was mentioned before, the discontinuities in real SSV can cause problems in the convergence of the lower bound power algorithm. For problems with purely real uncertainty, the lower bound algorithm may converge to a value which is significantly lower than the SSV itself, or may not even converge at all. While the

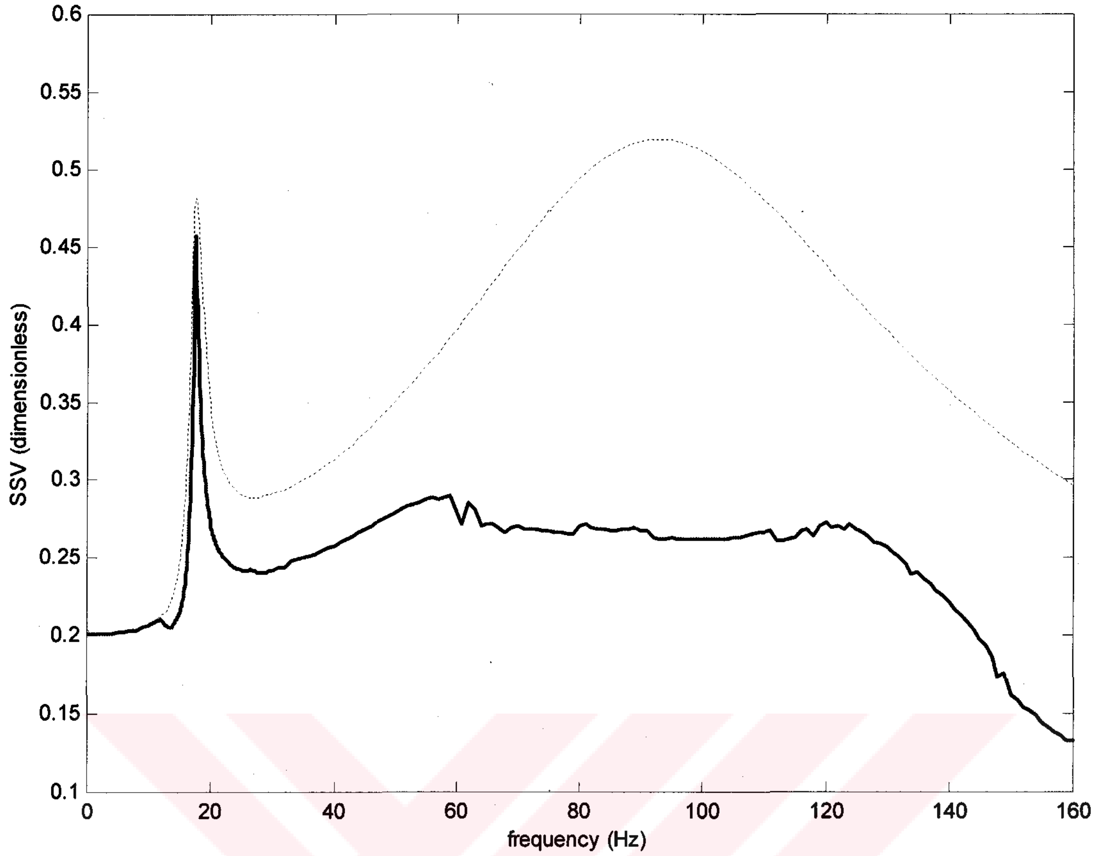

Figure 4.7 SSV for robust stability of model regulator compensated plant (C=0)

upper bound SSV computation will be effective, the lower bound will potentially have convergence problems, yielding little information in terms of bad perturbations. This could have been a serious problem if almost all problems had not had a full complex block associated with a robust performance specification. It turns out that if an SSV problem has a complex block then its SSV will be continuous at the problem data.

In the case of real uncertainty only, a fix, which has both engineering and mathematical justification, is available (Balas et al, 1995). The block structure can be expanded (to twice the original size) by including complex blocks which are exactly the same dimension as the original real blocks as is seen in Figure 4.8. The matrix of real uncertainty Δ_R can be expanded by the addition of a fictitious, complex uncertainty matrix Δ_C of the same structure. α is a user adjustable small real number. The SSV calculation determines upper and lower bounds for robust stability in the uncertain system shown in Figure 4.8. In this process, each real parameter δ_R within Δ_R has been replaced by a real parameter plus a smaller complex parameter $(\alpha^2\delta_c)$.

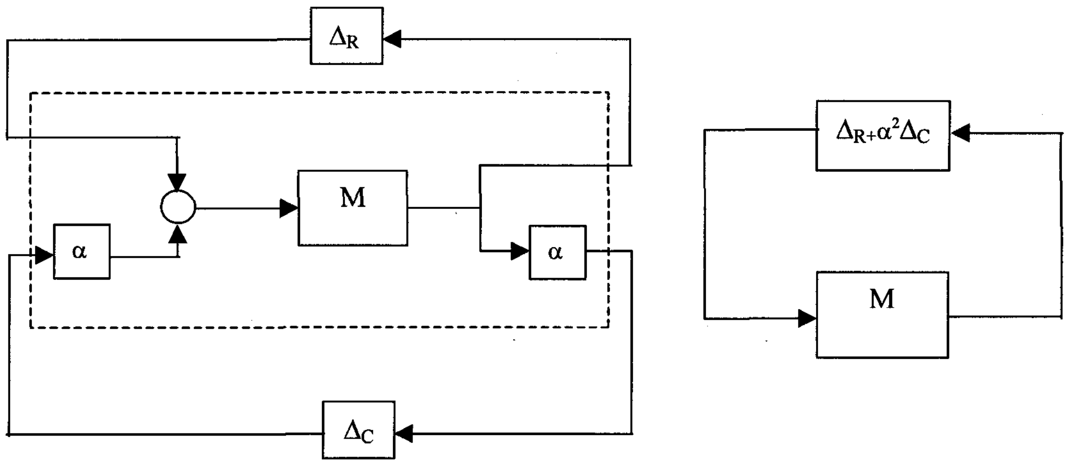

Figure 4.8 Replacing real uncertainty with real and complex uncertainty

Rather than computing robustness margins to purely real parameters, the modified problem determines the robust stability characteristics of the system with respect to predominantly real uncertainties, where each uncertainty is allowed to have a very small complex part. This slight variation is easy to accept in engineering problems, since models of uncertainty are rarely fixed and small amounts of phase uncertainty in coefficients of physical models can usually be explained by some underlying dynamics that have been ignored. Moreover, as the parameter α converges to zero, the calculated robustness margin associated with just the original real parameters is obtained. As a result, SSV with respect to this structure has guaranteed continuity properties and the lower bound generally has better convergence behaviour.

4.5.3 The Effect of the Feedback Controller

Noting that the feedback controller C also has an effect on stability (and on performance) robustness, the conventional stability robustness result in the presence of unstructured plant modeling error is extended to this case here. The feedback controller is a proportional controller with gain C=150 in the example system treated here. First, note that with the feedback controller C in place (see Figure 4.1) the model regulation, disturbance rejection and sensor noise rejection closed loop transfer functions become

$$\frac{y}{u_n}=\frac{CG_nG}{G_n(1-Q)+G(CG_n+Q)}$$
$$\frac{y}{d}=\frac{G_n(1-Q)}{G_n(1-Q)+G(CG_n+Q)} \qquad (4.30)$$
$$\frac{y}{n}=\frac{-G(CG_n+Q)}{G_n(1-Q)+G(CG_n+Q)}$$

Based on (4.30), ideal model regulator operation at low frequencies with $Q \to 1$ results in the model regulator augmented plant behaving as its nominal model G_n in the block diagram of Figure 4.1.

In order to obtain the robust stability requirement in the case of a plant with model regulator and feedback ($C \neq 0$), rewrite the characteristic equation in (4.30) given by

$$G_n(1-Q)+G_n(1+\Delta_m)(CG_n+Q)=0 \qquad (4.31)$$

as

$$G_n[1+CG_n+\Delta_m(CG_n+Q)]=0 \to \frac{Q+CG_n}{1+CG_n}=-\frac{1}{\Delta_m} \qquad (4.32)$$

Application of the Nyquist stability criterion results in

$$\left|\frac{Q+CG_n}{1+CG_n}\right|=\left\{\begin{matrix} 1 & for\ small\ \omega\ with\ \ Q\approx 1 \\ T_n & for\ l\arg er\ \omega\ with\ \ Q\approx 0 \end{matrix}\right\}<\left|\frac{1}{\Delta_m}\right| \quad for\ \forall\omega \qquad (4.33)$$

as the necessary and sufficient condition for stability. (4.33) should be satisfied for stability robustness in the presence of unstructured multiplicative uncertainty Δ_m. T_n in (4.33) is the complementary sensitivity y/u_n in the absence of the model regulator and with the plant behaving as its nominal model G_n. The plot of the left hand side of (4.33) and the $|1/\Delta_m|$ plot displayed in Figure 4.9 intersect at higher frequencies meaning that the stability robustness requirement is not satisfied.

Real SSV analysis, on the other hand, is less conservative and predicts robustness of stability as the maximum SSV value in Figure 4.10a is below unity. It is interesting to note in Figure 4.10b that the second peak is more pronounced for the feedback controlled system without the model regulator as compared to that in in Figure 4.7.

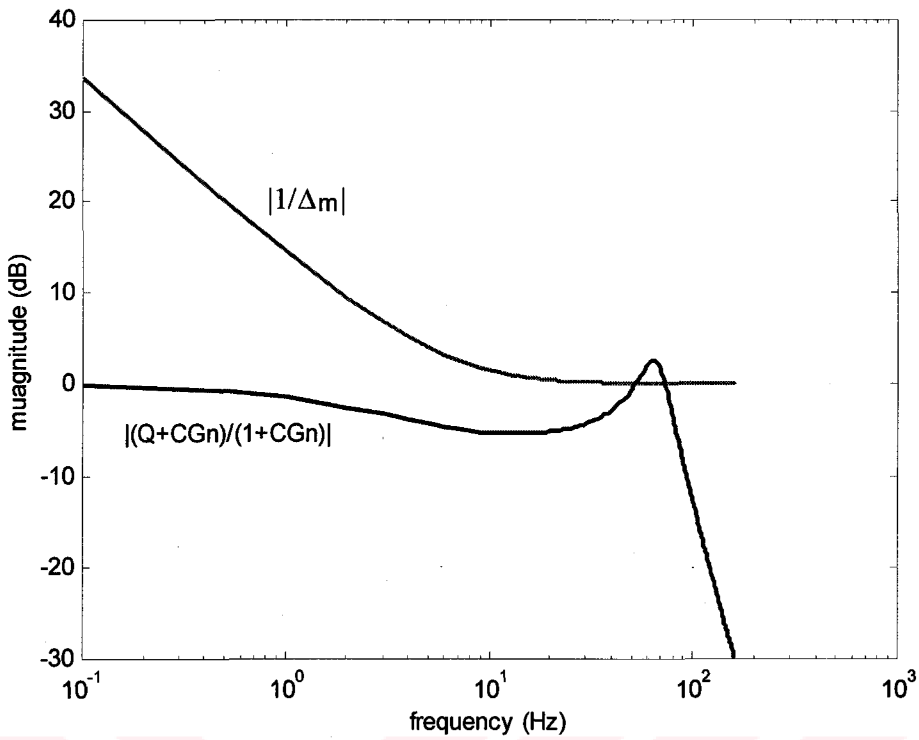

Figure 4.9 Stability robustness for unstructured uncertainty and with feedback control

In the presence of the model regulator, the peak close to 20 Hz (see Figure 4.10a) is observed in this case also even though the peak magnitude is slightly larger than that in the absence of the feedback controller as was displayed in Figure 4.7. On the contrary, the second peak magnitude is increased in the presence of the feedback loop. Also note that treating each real parametric uncertainty as a 1x1 complex block in SSV analysis (see dashed lines in Figure 4.7 and Figure 4.10) results in conservative results as the overall peak magnitude is greater and the associated frequency is different as compared to the real SSV results on the same plots. Even then, the analysis is not as conservative as in the case of one unstructured (thus complex) multiplicative modeling error (see Figure 4.9) as the complex SSV plot in Figure 4.10 is also always below unity.

4.6 Performance robustness

The sensitivity function is a very good indicator of closed-loop performance. The main advantage of considering S is that it is sufficient to consider just the magnitude, $|S|$, because S is ideally desired to be small. That is, there is no need to worry about the phase of S. The typical specifications in terms of S include:

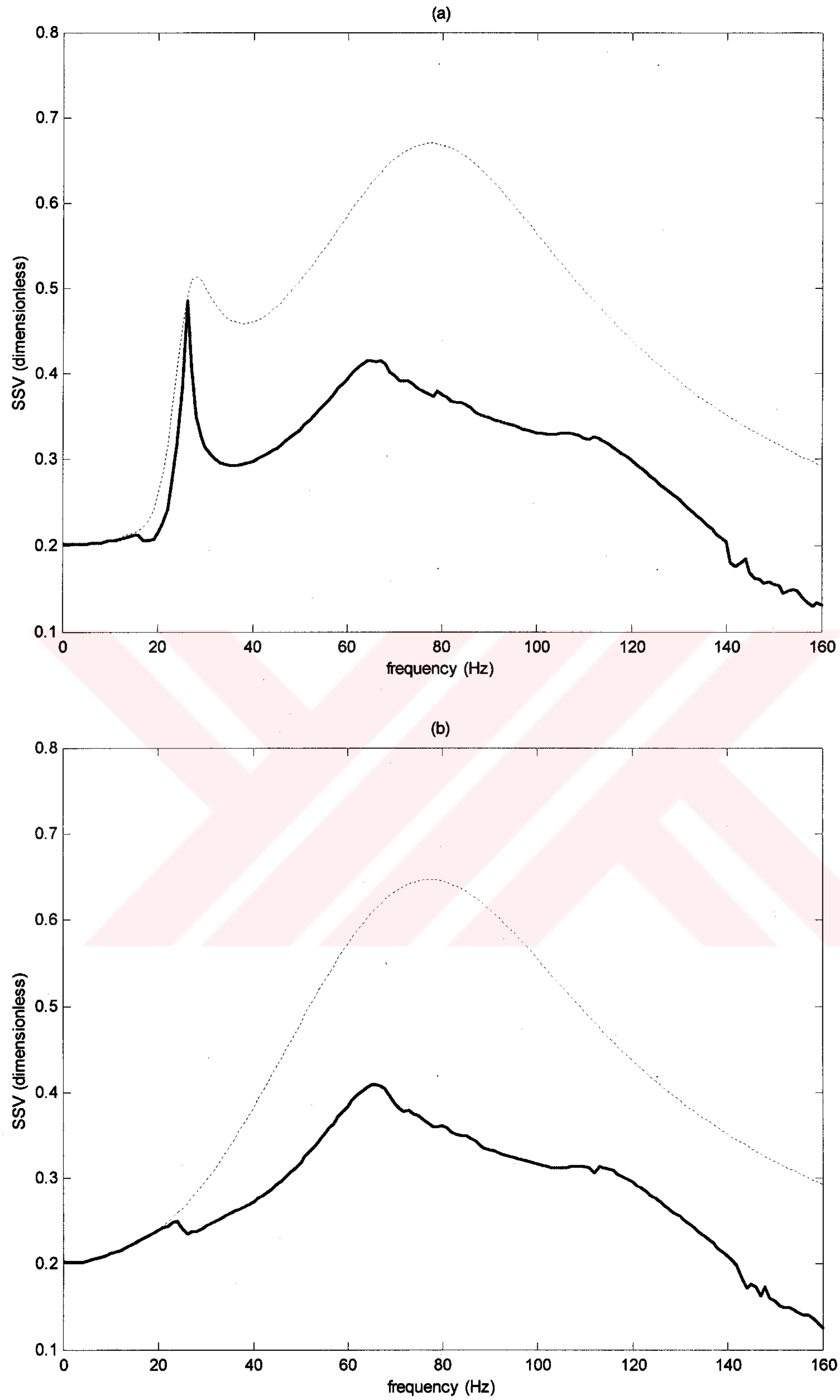

Figure 4.10 SSV for robust stability of plant with feedback control (a) with and (b) without model regulator

- Minimum bandwidth frequency ω_B^* (defined as the frequency where $|S(j\omega)|$ crosses 0.707 from below).

- Maximum tracking error at selected frequencies.

- System type or alternatively the maximum steady-state tracking error, A.

- Shape of S over selected frequency ranges.

- Maximum peak magnitude of S, $\|S(j\omega)\|_\infty \le M$.

The peak specification prevents amplification of noise at high frequencies and also introduces a margin of robustness. M=2 is typically used. Mathematically, these specifications may be captured by an upper bound, $1/|W_S|$, on the magnitude of S, where $W_S(s)$ is a weight selected by the designer. The performance requirement of weighted sensitivity minimization is

$$\begin{aligned} &|S(j\omega)| < 1/|W_S(j\omega)|, \forall\omega \\ \Leftrightarrow\ &|W_S S| < 1, \forall\omega \ \Leftrightarrow\ \|W_S S\|_\infty < 1 \end{aligned} \tag{4.34}$$

An asymptotic plot of a typical upper bound, $1/|W_S|$, is shown in Figure 4.11.

The weight illustrated may be represented by

$$W_S(s) = \frac{s/M + \omega_B^*}{s + \omega_B^* A} \tag{4.35}$$

It is seen that $1/|W_S(j\omega)|$ is equal to $A \le 1$ at low frequencies and $M \ge 1$ at high frequencies. The high frequency asymptote crosses 1 at the frequency ω_B^*, which is approximately the bandwidth requirement. In some cases, a steeper slope for the loop gain L (and S) may be desired below the bandwidth in order to improve performance. In this case, a higher-order weight may be selected (Skogestad and Postlethwaite, 1996).

It is possible to extend the SSV analysis to investigation of robustness of performance by treating the weighted sensitivity minimization performance constraint

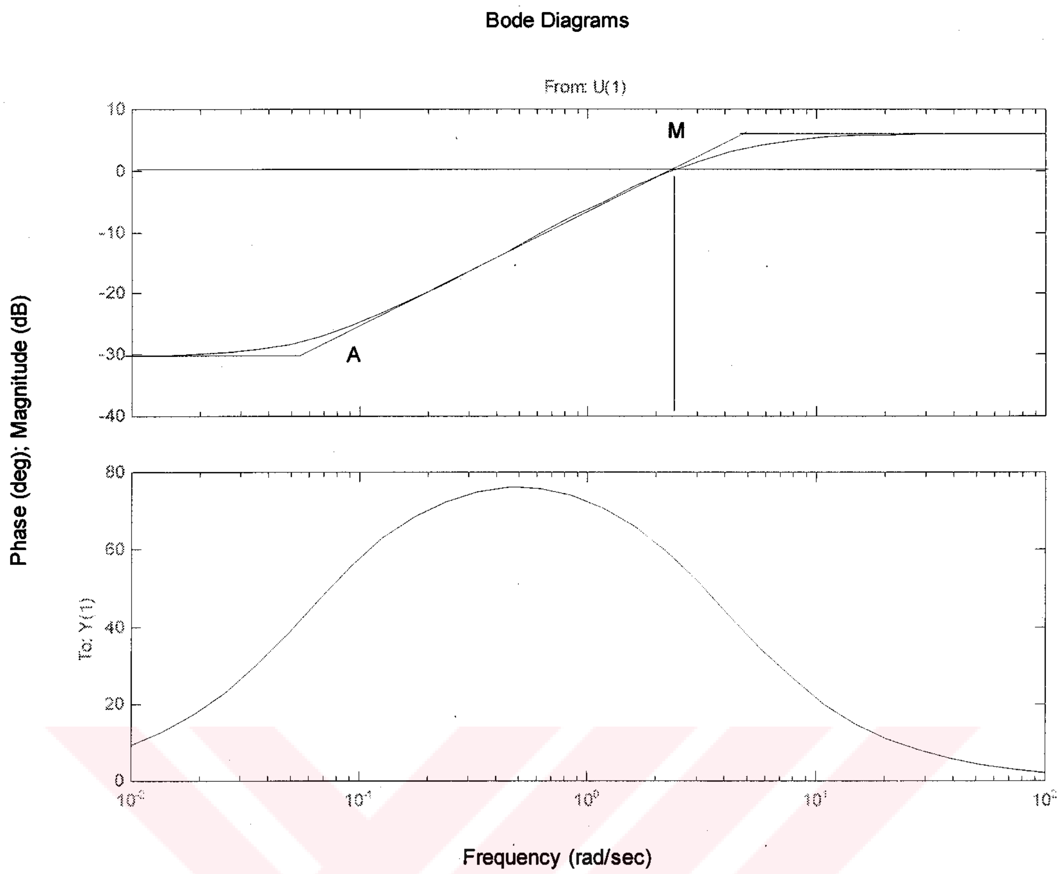

Figure 4.11 Inverse of performance weight

$$|W_S(\omega)S(j\omega)| < 1 \tag{4.36}$$

where

$$W_S(\omega) = \left| \left(10 \frac{s/80+1}{s+1} \right)_{s=j\omega} \right| \tag{4.37}$$

in the SSV framework by introducing the 1x1 fictitious, complex performance uncertainty block Δ_F in Figure 4.6. Performance constraint (4.37) corresponds to robust disturbance rejection with a specified level of -20 dB at low frequencies. The corresponding mixed SSV is defined as

$$\mu_{\Delta_r,\Delta_F}(N_F) = \frac{1}{\min\limits_{\delta_i \in \boldsymbol{R}; i=1,2,\ldots,n; \Delta_F \in C} \{(\max(|\delta_1|,|\delta_2|,\ldots,|\delta_n|,|\Delta_F|)) : \det(I - N_F \cdot diag(\delta_1,\delta_2,\cdots,\delta_n,\Delta_F)) = 0\}} \tag{4.38}$$

The corresponding mixed SSV plot of Figure 4.12 where robustness of performance for the plant augmented by the model regulator (Figure 4.6a) was investigated, demonstrates that the disturbance rejection requirement (4.36) is not met at the peak frequency of approximately 20 Hz as SSV is greater than unity there. It is interesting to note that the most problematic frequency range corresponds once again to those frequencies close to the -3 dB bandwidth of the Q filter used. Possible remedies are to re-design the Q filter and if this cannot be done due to other constraints (like sensor noise rejection), to relax the performance specification in (4.36). Luckily, however, the situation is not so bad when the main feedback loop is also closed. The presence of the feedback loop ($C \neq 0$) alleviates the problems as the overall robust disturbance rejection requirement (4.33) is satisfied at the peak frequency also as seen in Figure 4.13.

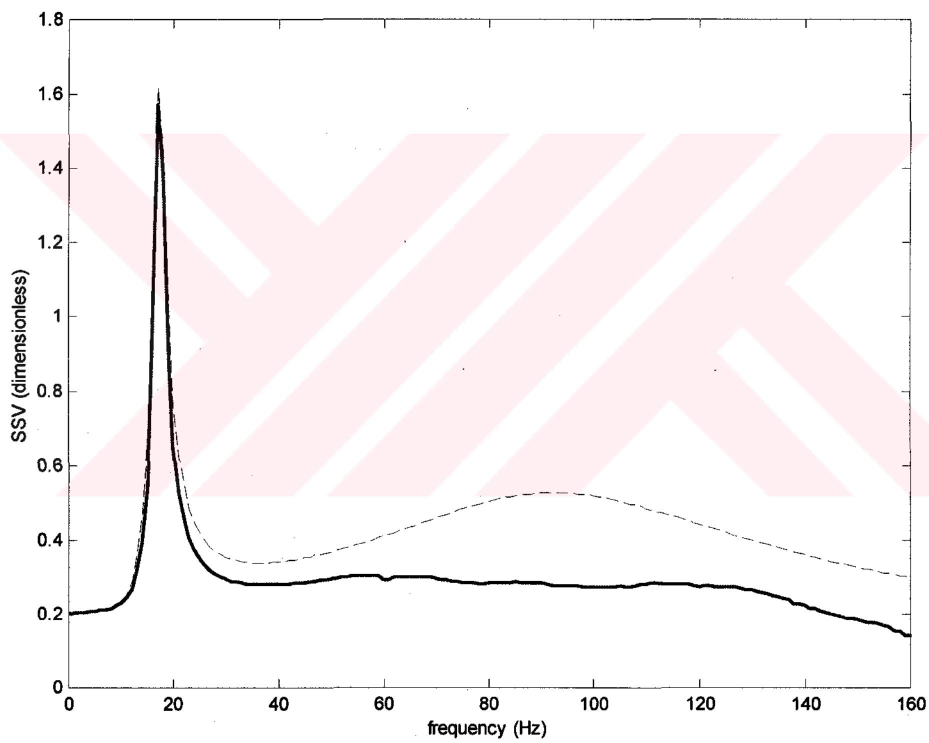

Figure 4.12 SSV for robust performance of plant with model regulator (C=0)

Real SSV analysis for stability robustness was applied to model regulator compensated systems with well known real parametric uncertainty in the plant model. In such cases, the conventional stability robustness analysis for model regulator compensated systems based on lumping all uncertainty into one complex block of multiplicative uncertainty was seen to be unnecessarily conservative with more reliable results being obtained by real SSV analysis. An additional advantage of the SSV analysis method was seen to be the capability of analyzing robustness of

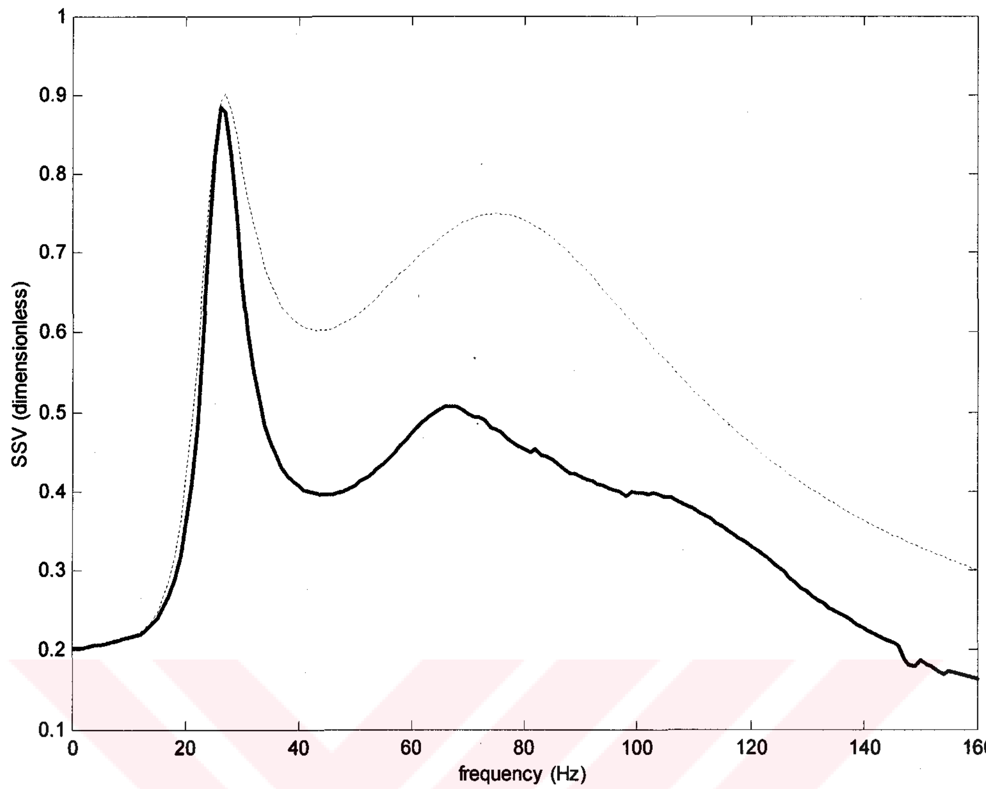

Figure 4.13 SSV for robust performance of plant with model regulator under feedback control

performance within the same framework and mixed SSV analysis was used here to obtain the associated result. Finally, in both the stability and performance robustness analyses, the frequencies close to the -3 dB bandwidth frequency of the Q filter were seen to be critical. Thus, for reasons of robustness, special care should be used around this frequency during Q filter design.

5. ROBUST VEHICLE STEERING CONTROL

Dangerous yaw motions of an automobile may result from unexpected yaw disturbances caused by unsymmetrical car dynamics perturbations like unilateral loss of tire pressure or braking on unilaterally icy road (μ-split braking). Safe driving requires the driver to react extremely quickly in such dangerous situations. This is not possible as the driver who can be modeled as a high gain control system with dead time overreacts, resulting in instability. Consequently, improvement of automobile yaw dynamics by active control to avoid such catastrophic situations has been and is continuing to be a subject of active research. The model regulator that was introduced in the previous chapter is used as a steering controller to improve vehicle yaw dynamics in this chapter.

As far as hardware implementation is concerned, two possibilities exist. The first is the steer-by-wire approach where the steering wheel is no longer mechanically connected to the tires. This approach which is expected to be a standard in the automotive industry in the future allows the easiest implementation. Only the steer-by-wire controller code has to be properly modified in that case. In the absence of steer-by-wire, an additional actuator has to be used to add the auxiliary steering command from the steering controller to the driver supplied steering command. Both steer-by-wire and auxiliary steering input implementations are considered here.

5.1 Vehicle Model and Yaw Dynamics

The vehicle model which is used for the investigations in this chapter is the classical single track model, also called the bicycle model, which is shown in Figure 5.1. The major variables and geometric parameters of the single track model are

F_f (F_r) : Lateral wheel force at front (rear) wheel

F_x, F_y : Forces in the x and y directions

M_z : Moment about the vertical axis z through the center of gravity (CG)

r : Yaw rate

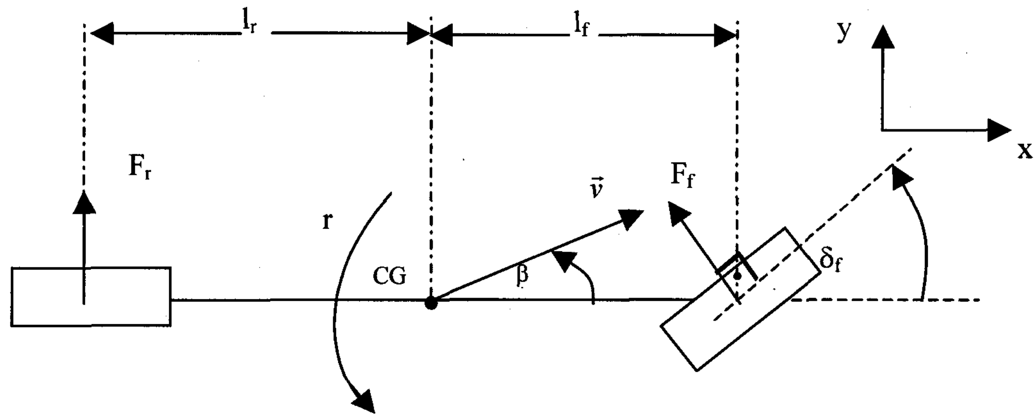

Figure 5.1 Single track model for car steering

β	: Chassis side slip angle at vehicle CG
$\alpha_f\,(\alpha_r)$	: Front (rear) tire side slip angle
v	: Magnitude of velocity vector at CG ($v > 0, \dot{v} = 0$)
$l_f\,(l_r)$	: Distance from front (rear) axle to CG
δ_f	: Front wheel steering angle
δ_r	: Rear wheel steering angle
m	: The mass of the vehicle
J	: The moment of inertia w.r.t. a vertical axis through the CG

The nonlinear single track model is characterized by the steering angle projection (also called the force coordinate transformation)

$$\begin{bmatrix} F_x \\ F_y \\ M_z \end{bmatrix} = \begin{bmatrix} -\sin\delta_f & -\sin\delta_r \\ \cos\delta_f & \cos\delta_r \\ l_f\cos\delta_f & -l_r\cos\delta_r \end{bmatrix} \begin{bmatrix} F_f \\ F_r \end{bmatrix}, \tag{5.1}$$

the dynamics equations

$$\begin{bmatrix} mv(\dot{\beta}+r) \\ m\dot{v} \\ J\dot{r} \end{bmatrix} = \begin{bmatrix} -\sin\beta & \cos\beta & 0 \\ \cos\beta & \sin\beta & 0 \\ 0 & 0 & 1 \end{bmatrix} \begin{bmatrix} F_x \\ F_y \\ M_z \end{bmatrix}, \tag{5.2}$$

and the equations of kinematics/geometry

$$\tan\beta_f = \tan\beta + \frac{l_f r}{v\cos\beta}, \tag{5.3}$$

$$\tan\beta_r = \tan\beta - \frac{l_r r}{v\cos\beta}. \tag{5.4}$$

The tire forces F_f and F_r are nonlinear functions of the corresponding side slip angles α_f and α_r. F_f and F_r also depend on the friction characteristics between the road and the tires. The nonlinear single track model is shown in the block diagram of Figure 5.2.

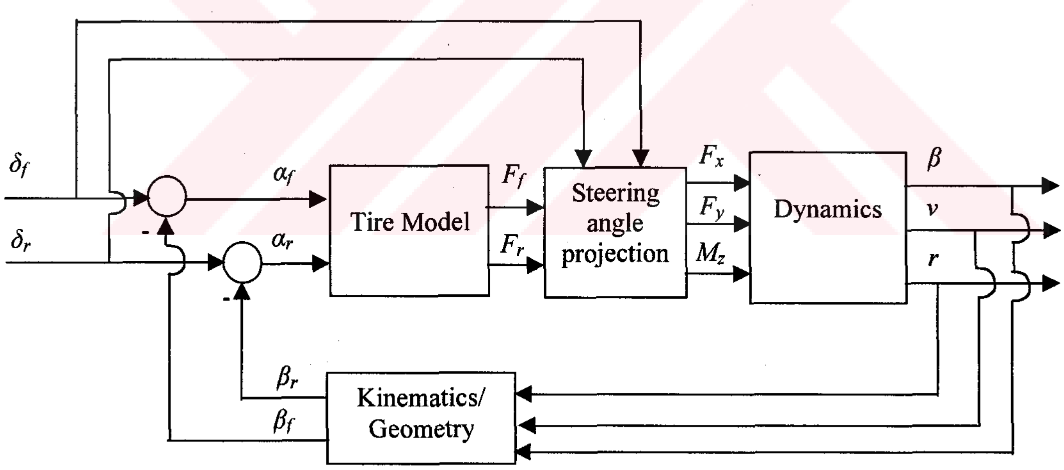

Figure 5.2 The nonlinear single track model

The variable exhibiting the largest variation in the single track model is the longitudinal velocity v. It is customary to linearize the single track model while keeping v as a variable parameter. The resulting model is a linear parameter varying model whose operating condition depends on the velocity of operation. It is also customary to design controllers for several velocity values and use a gain scheduling controller. This approach is used here as well.

The nonlinear single track model is linearized assuming small steering angles δ_f and δ_r and small side slip angle β. The tire force characteristics are linearized as

$$F_f(\alpha_f) = \mu c_{f0}\alpha_f = c_f\alpha_f, \quad F_r(\alpha_r) = \mu c_{r0}\alpha_r = c_r\alpha_r \tag{5.5}$$

with the tire cornering stiffnesses c_f, c_r, the road adhesion factor μ and the tire side slip angles given by

$$\alpha_f = \delta_f - \left(\beta + \frac{l_f}{v}r\right), \tag{5.6}$$

$$\alpha_r = \delta_r - \left(\beta - \frac{l_r}{v}r\right). \tag{5.7}$$

Note that c_{f0} and c_{r0} in (5.5) are the nominal values (μ=1) of the tire cornering stiffnesses. Assuming front wheel steering (δ_r = 0), the transfer function from the front wheel steering angle δ_f to the yaw rate r is given by

$$G_{r\delta_f}(s) = \frac{r(s)}{\delta_f(s)} = \frac{b_1 s + b_0}{a_2 s^2 + a_1 s + a_0} \tag{5.8}$$

with

$$\begin{aligned}
b_0 &= c_f c_r (l_f + l_r) v \\
b_1 &= c_f l_f m v^2 \\
a_0 &= c_f c_r (l_f + l_r)^2 + (c_r l_r - c_f l_f) m v^2 \\
a_1 &= (c_f (J + l_f^2 m) + c_r (J + l_r^2 m)) v \\
a_2 &= J m v^2
\end{aligned}$$

$G_{r\delta_f}(s)$ in (5.8) is also called the steering wheel input response transfer function here. The d.c. gain of the nominal single track model is

$$K_n(v) = \lim_{s\to 0} G_{r\delta_f}(s)\Big|_{\mu=\mu_n} \tag{5.9}$$

at the chosen longitudinal speed v and at nominal friction coefficient $\mu = \mu_n$ (taken as unity here).

The yaw disturbance input response is given by

$$G_{rM_z}(s) = \frac{r(s)}{M_z(s)} = \frac{mv^2 s + (c_f + c_r)v}{a_2 s^2 + a_1 s + a_0} \tag{5.10}$$

Another important variable of interest in vehicle lateral control is the lateral acceleration a_{fl} at the front axle given by

$$a_{fl} = v(r + \dot{\beta}) + \dot{r} l_f \tag{5.11}$$

The block diagram of the linearized single track model is shown in Figure 5.3. The reader is referred to references (see Ackermann et al, 1993 for example) for more detailed information on the single track model.

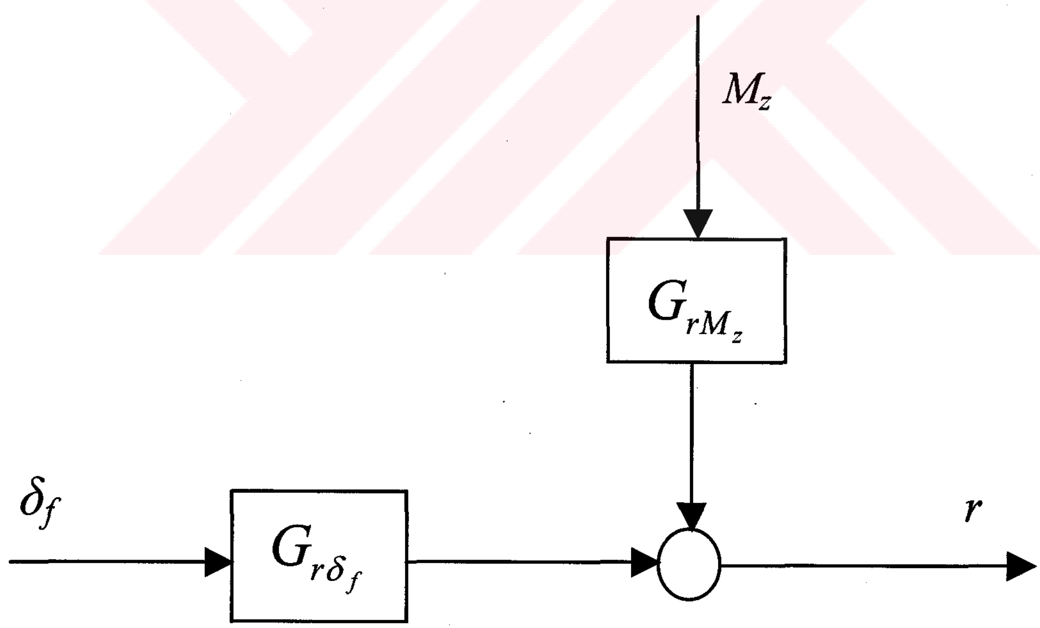

Figure 5.3 Linearized single track model

5.2 Problem Specifications

The vehicle model data used here corresponds to a mid-sized passanger car that is available in the literature. The nominal values of the variables in the linearized single track model of the previous section are l_f=1.25 m, l_r=1.32 m, m=1296 kg, J=1750 kgm^2, c_{f0}=84243 N/rad and c_{r0}=95707 N/rad. The nominal friction coefficient is $\mu_n = 1$ which corresponds to dry road. The two variables exhibiting the largest variation during operation are the longitudinal speed v and the mass m of the vehicle. The tire cornering stiffnesses c_f and c_r can also exhibit large variations due to variations in friction coefficient μ between the road and the tires. This effect is captured in the formulation of the new variables $\tilde{m} = m/\mu$ and $\tilde{J} = J/\mu$, called virtual mass and virtual moment of inertia, respectively.

The additional uncertainty in the cornering stiffnesses due to uncertain parameters like normal force, longitudinal acceleration, tire pressure and temperature are captured in uncertainty in c_{f0} and c_{r0} here. In addition to the single track model dynamics, there is also the steer-by-wire or auxiliary steering actuator whose dynamics should be considered.

The transfer function of the linearized steering actuator model is taken as

$$G_{sa} = \frac{\delta_f}{\delta_{ref}} = \frac{\omega_a^2}{s^2 + 2\zeta_a \omega_a s + \omega_a^2} \tag{5.12}$$

The steering actuator (5.12) is assumed to be under closed loop position control and is modeled as a second order system with a bandwidth of $\omega_a = 2\pi 5\,\text{Hz}$ and a damping ratio of $\zeta_a = 0.7$.

The uncertain parameters and their uncertainty ranges will first be given before the design specification. The longitudinal speed v is assumed to vary between a minimum value of 10 m/s and a maximum value of 50 m/s during operation. The yaw dynamics compensator is assumed to be shut off at speeds below 10 m/s since the driver is easily able to reject yaw disturbances at these speeds without the need for steering controller assistance. The friction coefficient μ is assumed to exhibit the characteristics displayed in Figure 5.4 with velocity. The maximum value of μ is unity at all speeds in this figure while its minimum possible value varies linearly between 0.2 at low speeds and 0.8 at high speeds. The mass $m \in [1296:1696]$ kg and moment of inertia $J \in [1750:2100]\,\text{kgm}^2$ are not totally unrelated and are assumed to be linearly related according to $J = 616\,\text{kgm}^2 + (0.875\,\text{m}^2)m$ as shown in Figure 5.5. A possible maximum uncertainty of ±0.1% in c_{f0} and c_{r0} is also assumed.

In this study, the operating regions for the vehicle are based on values of vehicle longitudinal speed between 10 and 50 m/s. The aim in steering compensator design is

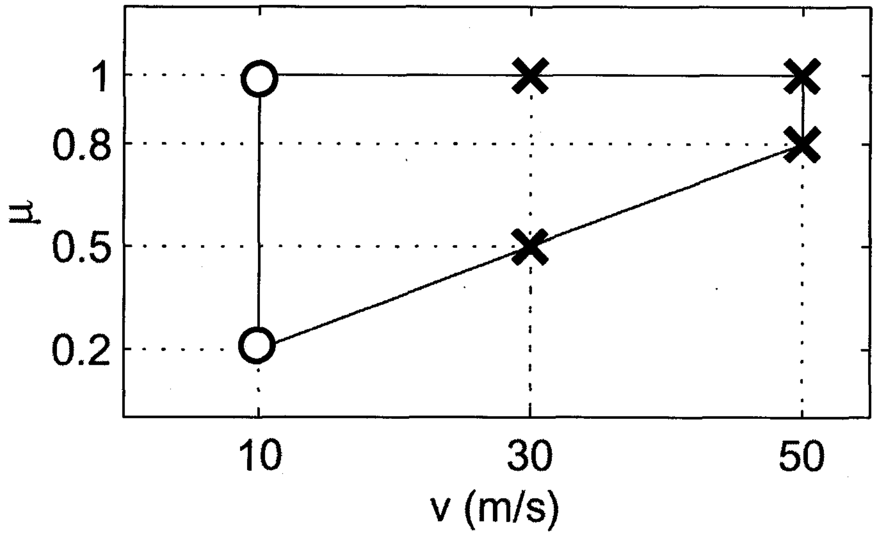

Figure 5.4 Operating domain

to make sure that, first stable operation, and then, improved yaw dynamics is achieved for all operating regions and all possible values of the uncertain parameters. The improved yaw dynamics corresponds to good disturbance rejection properties where the possible disturbances include the effect of side wind forces, tire rupture, unsymmetrical brake wear and μ-split braking. The steering wheel input response in the absence of disturbances should also be well damped regardless of the speed of operation. A model regulator based steering controller is designed and shown to effectively achieve the desired aims in the following sections.

5.3 Model Regulator Design

5.3.1 The Model Regulator

The model regulator knowledge of the previous chapter is partially repeated here in the context of vehicle steering. Referring to Figure 5.6, the vehicle model can also be expressed

$$r = G_a \delta_f + d = \left(G_n (1 + \Delta_m)\right) \delta_f + d \tag{5.13}$$

where G_a is the actual input-output relation between δ_f and r, Δ_m is the multiplicative model uncertainty in our knowledge of the nominal model G_n and d is the external disturbance. The location of the steering actuator transfer function G_{sa} in Figure 5.6 corresponds to a steer-by-wire system. The aim in model regulator design is to approximately obtain

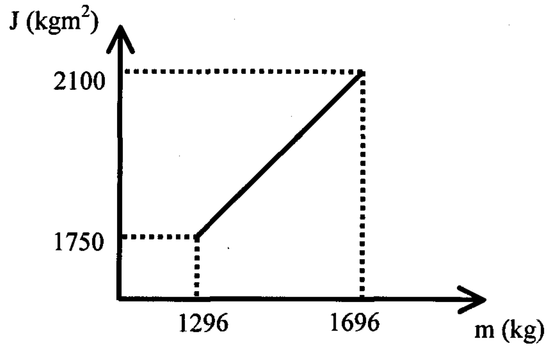

Figure 5.5 Relation of mass and moment of inertia

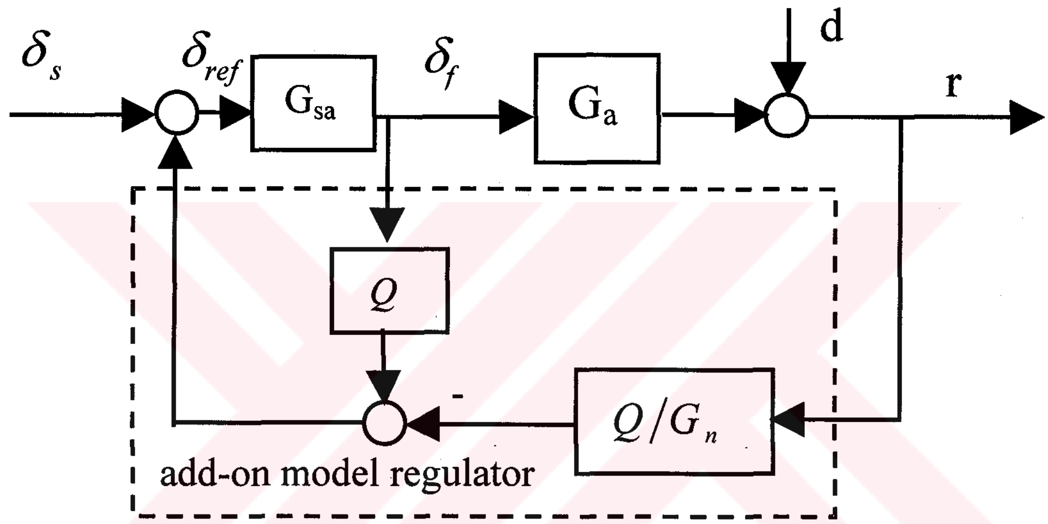

Figure 5.6 Steer-by-wire system with model regulator

$$\frac{r}{\delta_s} = G_n G_{sa} \tag{5.14}$$

as the input – output relation (steering transfer function) despite the presence of model uncertainty Δ_m and external disturbance d (δ_s is the new input i.e. the steering wheel angle). This aim is achieved by treating the external disturbance and model uncertainty as an extended disturbance e in model regulator design and solving for it as

$$r = G_n \delta_f + (G_n \Delta_m \delta_f + d) = G_n \delta_f + e \tag{5.15}$$

$$e = r - G_n \delta_f \tag{5.16}$$

and using the new control signal δ_s given by

$$\delta_f = G_{sa}\left(\delta_s - \frac{e}{G_n}\right) = G_{sa}\left(\delta_s - \frac{1}{G_n}r + \delta_f\right) \tag{5.17}$$

to approximately cancel its effect in (5.15). Substitution of (5.17) into (5.15) shows that the desired steering transfer function (5.14) is achieved if a good actuator ($G_{sa} \to 1$) is used. The front wheel steering angle δ_f is assumed to be the output of the steering actuator G_{sa}. With the aim of trying to limit the compensation to a preselected low frequency range (in an effort not to overcompensate at high frequencies), the feedback signals in (5.17) are multiplied by the low pass filter Q to obtain the implementation equation

$$\delta_f = G_{sa}\left(\delta_s + Q\delta_f - \frac{Q}{G_n}r\right) \tag{5.18}$$

which can also be seen in the block diagram of Figure 5.6. Incorporation of G_{sa} in the inner feedback loop with positive feedback around Q in Figure 5.6 helps in reducing the effect of actuator saturation on model regulator performance. The relative degree of the unity d.c. gain low pass filter Q is chosen to be at least equal to the relative degree of G_n for causality of Q/G_n. In this section, the structure of Q is assumed to be

$$Q = \frac{1}{\tau_Q s + 1} \tag{5.19}$$

Note that this choice will result in an integrator within the loop in Figure 5.6 (see Section 4.2) and hence zero steady state error in reponse to step steering commands and yaw torque disturbances.

The nominal (or desired) yaw dynamic model is chosen as a first order system here given by

$$G_n(s) = \frac{K_n(v)}{\tau_n s + 1} \tag{5.20}$$

where τ_n=0.165 sec is used and $K_n(v)$ is the d.c. gain of the nominal single track model at the chosen longitudinal speed v.

The open loop gain of the model regulator compensated yaw dynamics model shown in the equivalent block diagram of Figure 5.7 is

$$L = \frac{G_a G_{sa} Q}{G_n (1 - G_{sa} Q)} \tag{5.21}$$

with the model regulation, disturbance rejection and sensor noise rejection transfer functions given by

$$\begin{aligned} \frac{r}{\delta_s} &= \frac{G_n G_{sa} G_a}{G_n (1 - G_{sa} Q) + G_{sa} G_a Q} \\ S : \frac{r}{d} &= \frac{1}{1+L} = \frac{G_n (1 - G_{sa} Q)}{G_n (1 - G_{sa} Q) + G_{sa} G_a Q} \\ T : -\frac{r}{n} &= \frac{L}{1+L} = \frac{G_{sa} G_a Q}{G_n (1 - G_{sa} Q) + G_{sa} G_a Q} \end{aligned} \tag{5.22}$$

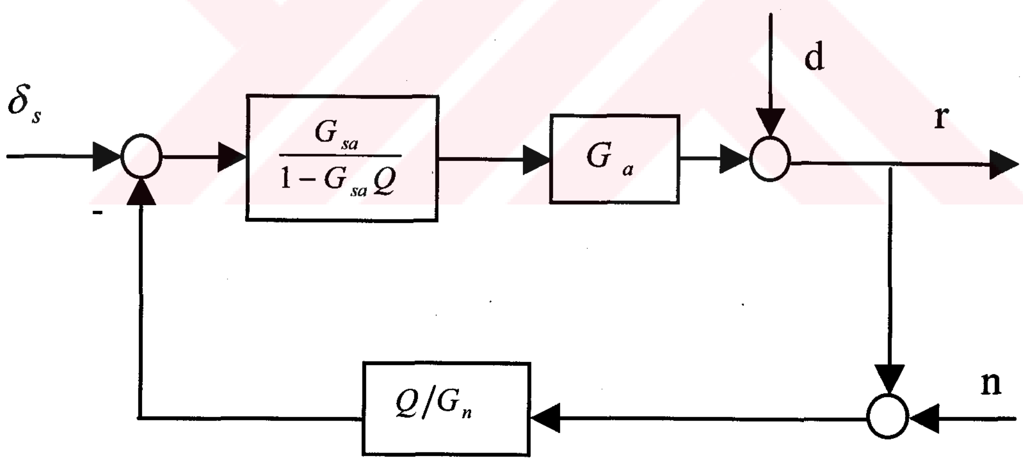

Figure 5.7 The equivalent block diagram

from which it is obvious that for good performance, Q must be a unity gain low pass filter (G_{sa} is a unity gain low pass filter as well). This choice will result in $r/\delta_s \to G_n$, $r/d \to 0$ at low frequencies where $Q \to 1$ and $r/n \to 0$ at high frequencies where $Q \to 0$, as is desired. Model regulator design is thus shaping the filter Q to satisfy the design objectives. The first limitation on the bandwidth of Q comes from the sensor noise rejection at sensor noise frequencies. The second limitation is that the bandwidth of Q should not be larger than the bandwidth of the actuator used as it makes no sense to command what cannot be achieved. Another bandwidth limitation for the Q filter comes from the stability robustness requirement

$$|Q| < \left|\frac{1}{\Delta}\right| \equiv \left|\frac{1}{G_{sa}\Delta_m}\right|, \quad for\ \forall\omega \tag{5.23}$$

in the presence of unstructured multiplicative model uncertainty Δ_m. The model regulator design requirements specified in terms of the filter Q are summarized in Figure 5.8.

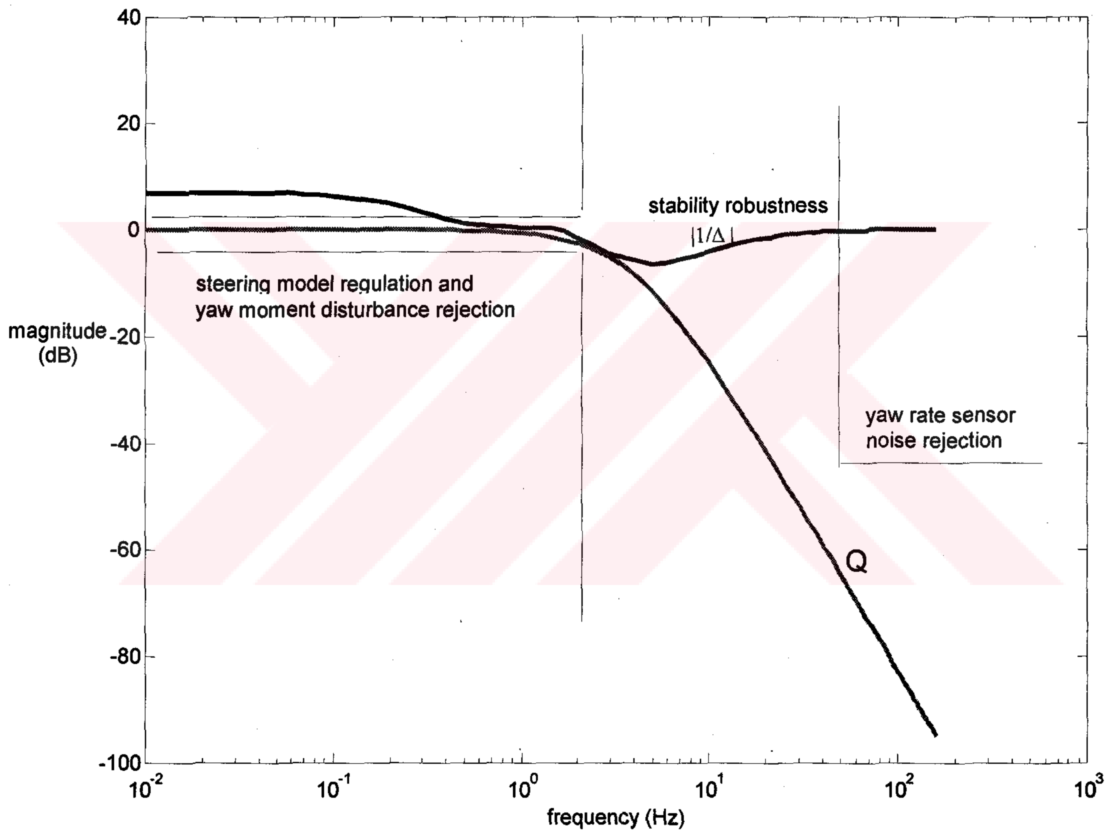

Figure 5.8 The steering model regulator design requirements

For the mass, moment of inertia and c_{f0}, c_{r0} uncertainty presented in Section 5.2, the corresponding $|1/\Delta|$ profiles were calculated at several different values of the longitudinal speed $v \in [10{:}50]$ m/s where $\tau_n = 0.165$ s was used. The composite lower bound obtained from this calculation is displayed as the upper robust stability boundary in Figure 5.8 from which a maximum allowable bandwidth value for Q can be determined.

5.3.2 Design In Parameter Space

Γ-stability can be defined as the poles of the closed loop system lying in a selected region of the left half complex plane. The Γ-stability region was chosen here to ensure a settling time of less than 2 seconds, a minimum damping ratio of 0.5 and a maximum natural frequency of 10 Hz.

The open loop single-input-single-output transfer function *L*, sensitivity function *S* and complementary sensitivity function *T* were given previously in (5.21)-(5.22). The nominal performance criterion can be expressed as the weighted sensitivity minimization

$$|W_S(j\omega)S(j\omega)| < 1, \quad \forall\omega \tag{5.24}$$

and the robust stability criterion in the presence of multiplicative uncertainty is

$$|W_T(j\omega)T(j\omega)| < 1, \quad \forall\omega \tag{5.25}$$

According to (5.24), for the system illustrated in Figure 5.6, $W_S(s)$ was chosen as

$$W_S(s) = 0.5556\,\frac{s+12.6}{s+0.7} \tag{5.26}$$

Two magnitude bounds on *T*, i.e. the magnitudes of $W_{T1}(s)$ and $W_{T2}(s)$, are selected to capture robustness w.r.t. unstructured uncertainty. They are

$$W_{T1}(s) = \frac{0.12804(s+43.98)(s+0.4833)}{(s+6.124)(s+2.882)}$$
$$W_{T2}(s) = 5\,\frac{s+3.77}{s+188.5} \tag{5.27}$$

While $W_{T1}(s)$ works at low frequencies, $W_{T2}(s)$ works at high frequencies. The first bound on *T*, i.e. $W_{T1}(s)$, is used to cover the model regulator stability specifications subject to model uncertainty in *m* and *J* as outlined in section 5.3.1 and is a curve fit of the $|1/\Delta|$ plot in Figure 5.8. The second bound on *T*, i.e. $W_{T2}(s)$, is for high frequency unmodeled dynamics. Recall that *Q* was chosen as a unity d.c. gain first order low pass filter with time constant τ_Q and that τ_n was the time constant of the nominal yaw dynamic model G_n in (5.20). τ_n and τ_Q are chosen as the controller parameters that have to be determined. These time constants are tuned such that the feedback provides the Γ-stability specifications, the nominal performance criterion and the robust stability criterion that were given above, for all of the points marked with crosses in the operating domain in Figure 5.4. These specifications mentioned above are mapped into the parameter plane of (τ_n, τ_Q), the procedure used being given in section 5.3.4 (see also Bünte et al, 2001). The design point τ_n=0.165 sec and τ_Q=0.0318 sec that satisfies all specifications is chosen and used in the simulations that follow.

5.3.3 Simulation Results

The conventional car and the controlled car are compared in this section by means of linear simulation. For the sake of comparability, the conventional car is assumed to be a steer-by-wire vehicle being equipped with the same steering actuator as the controlled car. The steering transfer function of the conventional car is

$$G_{conv} = \frac{r}{\delta_s} = G_{sa} G_a \tag{5.28}$$

with δ_s denoting the steering wheel angle and G_{sa} being the actuator dynamics. The steering transfer function of the controlled car is given in (5.22). The controller parameters were chosen in Section 5.3.2 as $\tau_Q = 0.0318$ sec and $\tau_n = 0.165$ sec. The two maneuvers of steering wheel step input and yaw disturbance torque step input are investigated here.

The steering wheel step input is normalized by the gain $K_n(v)$ for dry road (μ=1) in the simulations for easier comparison of the results. The maneuvers are performed at the four operating points marked with crosses in Figure 5.4. The results are shown in Figure 5.9 and Figure 5.10. The simulations show that the controller provides excellent disturbance rejection and good steering command following at all of the investigated operating points.

5.3.4 Mixed Sensitivity Design in Parameter Space

Let us extend the design in Section 5.3.2 to the mixed sensitivity case which is more restrictive since the nominal performance (NP) and the robust stability (RS) were

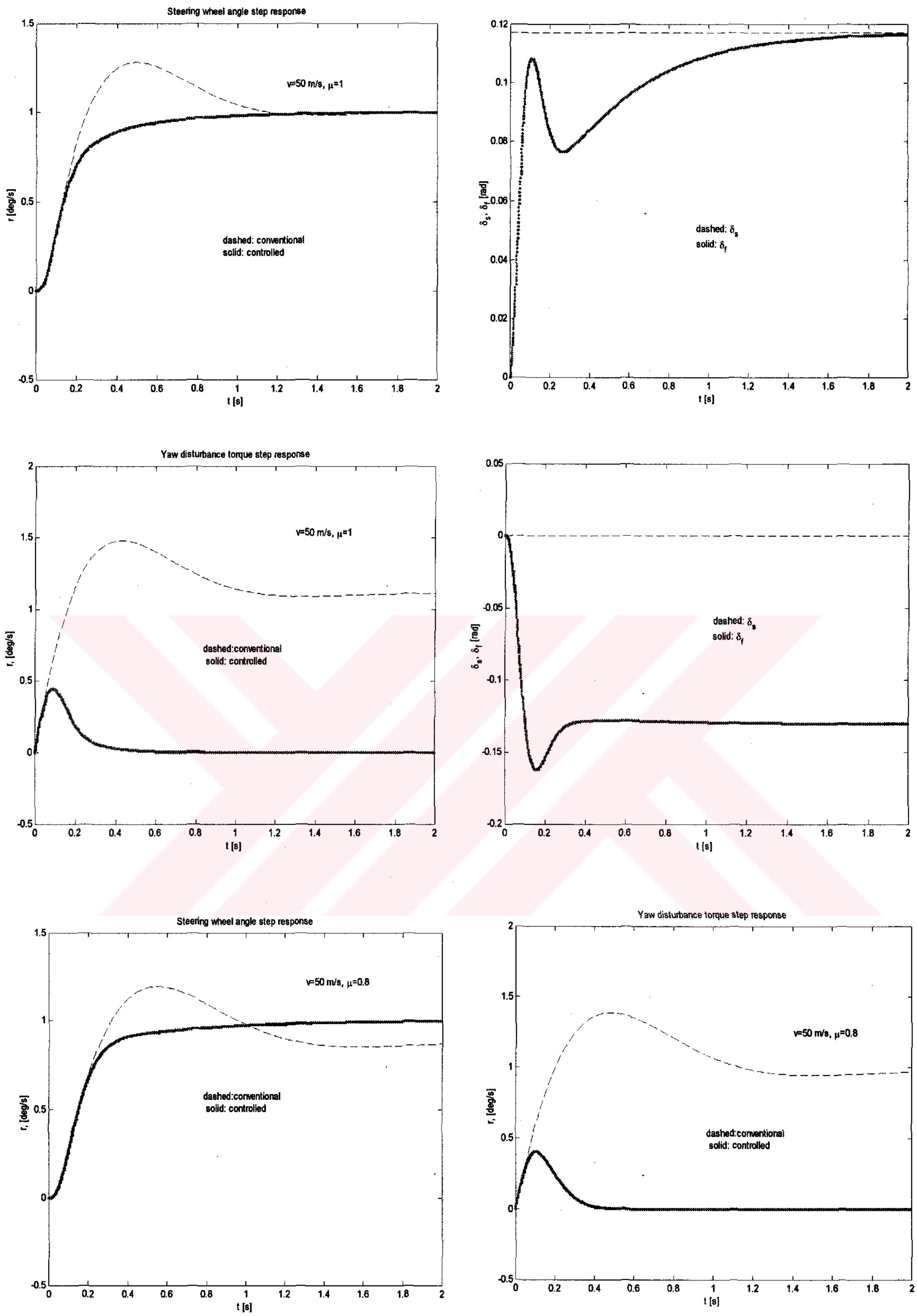

Figure 5.9 The results of linear simulations at the operating points

treated separately in the design of Section 5.3.2. Assuming a fast actuator, let us disregard the steering actuator (G_{sa}=1) and also look at low-speed operation at v=10 m/sec in the design (see the two new operating conditions marked with circles in Figure 5.4).

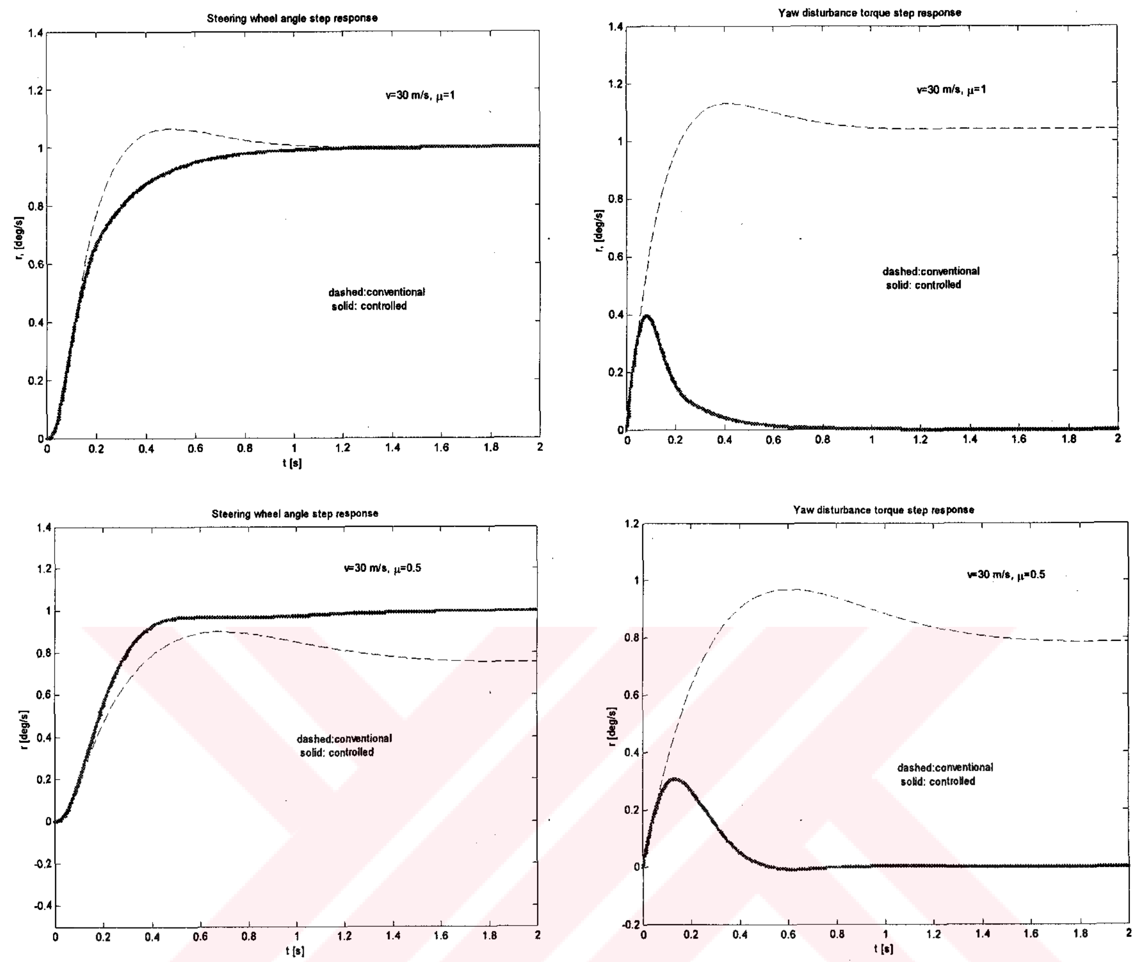

Figure 5.10 The results of linear simulations at the operating points

The two free controller parameters τ_n and τ_Q are tuned in the design effort to meet the mixed sensitivity requirement

$$|W_S S| + |W_T T| < 1 \ \ for \ \forall \omega \tag{5.29}$$

The sensitivity function weight W_S and the complementary sensitivity function weight W_T are chosen as in Section 5.3.2 where the nominal performance (weighted sensitivity minimization) and robust stability (weighted complementary sensitivity minimization) problems were treated separately. This, of course, leads to a conservative design when the aim is meeting the robust performance criterion of

(5.29), also called the nonstandard problem in H_∞ optimization[2]. The original weights in section 5.3.2 were scaled down by a factor of 1.5 to make problem (5.29) solvable for the combination of all six operating conditions considered here. Note that even after this down-scaling, problem (5.29) here is more restrictive than the separate minimizations treated in the abovementioned section. It is also well known that the solutions of the nonstandard problem $|W_S S|+|W_T T|<1$, the standard problem $|W_S S|^2+|W_T T|^2<1/2$ and the separate simultaneous minimization $|W_S S|<1 \cup |W_T T|<1$ can be significantly apart from each other (Owen and Zames, 1993).

The scaled weights used in the design are

$$W_S(s)=\frac{0.6667s+8.4}{1.8s+1.26} \tag{5.30}$$

$$W_T(\omega)=\max\left\{\left|\frac{3.333s+12.5667}{s+188.5}\right|_{s=j\omega},\left|\frac{0.0854s^2+3.7954s+1.8144}{s^2+9.006s+17.6494}\right|_{s=j\omega}\right\} \tag{5.31}$$

The complementary sensitivity weight in (5.31) is designed to penalize parametric uncertainty at low frequencies and unmodeled dynamics uncertainty at high frequencies.

The design approach is based on mapping the frequency domain constraint (5.29) with weights given in (5.30) and (5.31) into the plane of controller parameters τ_n and τ_Q. The solution procedure used is explained first, before presenting the results. The mixed sensitivity problem (5.29) can also be expressed in the limit as the equality

$$|W_S|+|W_T L|=|1+L| \quad \text{for} \ \forall\omega \tag{5.32}$$

which is called the point condition at each frequency. The idea is to solve (5.32) frequency at a time for a sufficient number of frequencies to determine regions of τ_n and τ_Q values in the τ_n-τ_Q plane that satisfy it. The point condition is illustrated graphically in Figure 5.11. A graphical solution for $|L|$ using the cosine rule in Figure 5.11 results in

---

[2] one distinction is that a controller that satisfies (5.29) is searched for here rather than a controller that minimizes the left hand side of (5.29) as in the conventional H_∞ approach

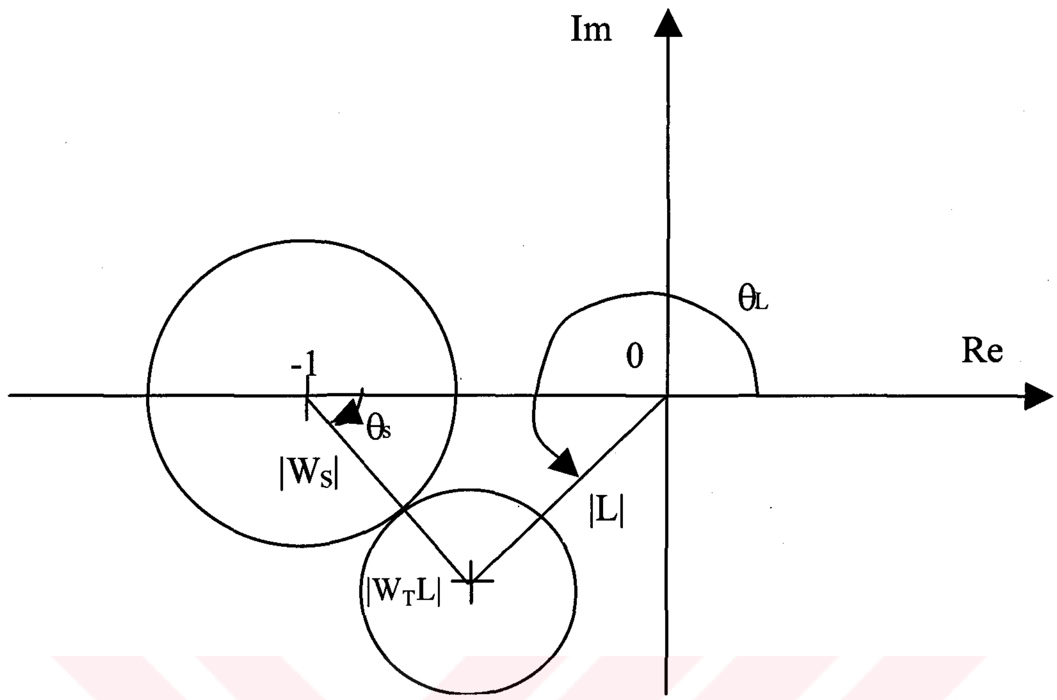

Figure 5.11 The point condition for mixed sensitivity

$$|L| = \frac{-\cos\theta_L + |W_S||W_T| \pm \sqrt{Disc}}{1 - |W_T|^2} \tag{5.33}$$

where

$$Disc = 1 + \cos^2\theta_L - 2|W_S||W_T|\cos\theta_L + |W_S|^2 + |W_T|^2 \tag{5.34}$$

The first part of the solution procedure for the loop gain L is formation of a grid of θ_L in (0:2π) and then solution of (5.33). Then, L is expressed in terms of a fictitious controller K as

$$L = KG = (K_R + jK_I)G \tag{5.35}$$

Solving (5.35) for the real and imaginary parts K_R and K_I of K and then solving

$$K_R + jK_I = \frac{Q}{G_n(1-Q)} = \frac{\tau_n s + 1}{K_n \tau_Q s} \tag{5.36}$$

for τ_n and τ_Q result in

$$\tau_n = -\frac{K_R}{K_I \omega} \tag{5.37}$$

$$\tau_Q = -\frac{1}{K_n K_I \omega} \tag{5.38}$$

which is the final step in the solution.

This solution procedure is repeated for all six of the marked operating conditions in Figure 5.4. The individual solution regions and the final solution region obtained by intersection in the controller parameter plane of all regions and the region for Hurwitz stability are shown in Figures 5.12 and 5.13, respectively. The final design point satisfying (5.29) for all six operating conditions is chosen as τ_n=0.16 sec and τ_Q=0.07 sec and is marked with a cross in Figure 5.13. The $|W_S S|+|W_T T|$ frequency domain plot shown in Figure 5.14 for this controller at all six operating conditions shows that constraint (5.29) is satisfied by this design.

A linear simulation study is performed next to assess the time domain performance that is achieved. Steering wheel and yaw disturbance step inputs are the two simulation maneuvers that were investigated. The steering wheel step input is normalized by the gain $K_n(v)$ for dry road (μ=1) in the simulations for easier comparison of the results. The simulation results shown in Figures 5.15-5.17 demonstrate the achievement of excellent disturbance rejection and good steering command tracking at all six operating points.

5.3.5 Solving Low Speed Problems

One relatively minor problem that one observes in the simulation result at the low velocity of v=10 m/sec and μ=1 (Figure 5.17) is that the steering wheel step input response is slower with the model regulator in place as opposed to the conventional car. This is undesirable as the model regulator should not force the acceptable conventional car response in this case to a slower one through its compensatory action. The main reason for this situation is that the steering wheel input response of the conventional car varies considerably with velocity. This variation is accommodated by the time constant τ_n in the desired model G_n of the model regulator. The problem mentioned above shows that τ_n should be selected smaller than its present value to match the fast conventional response at v=10 m/sec, μ=1.

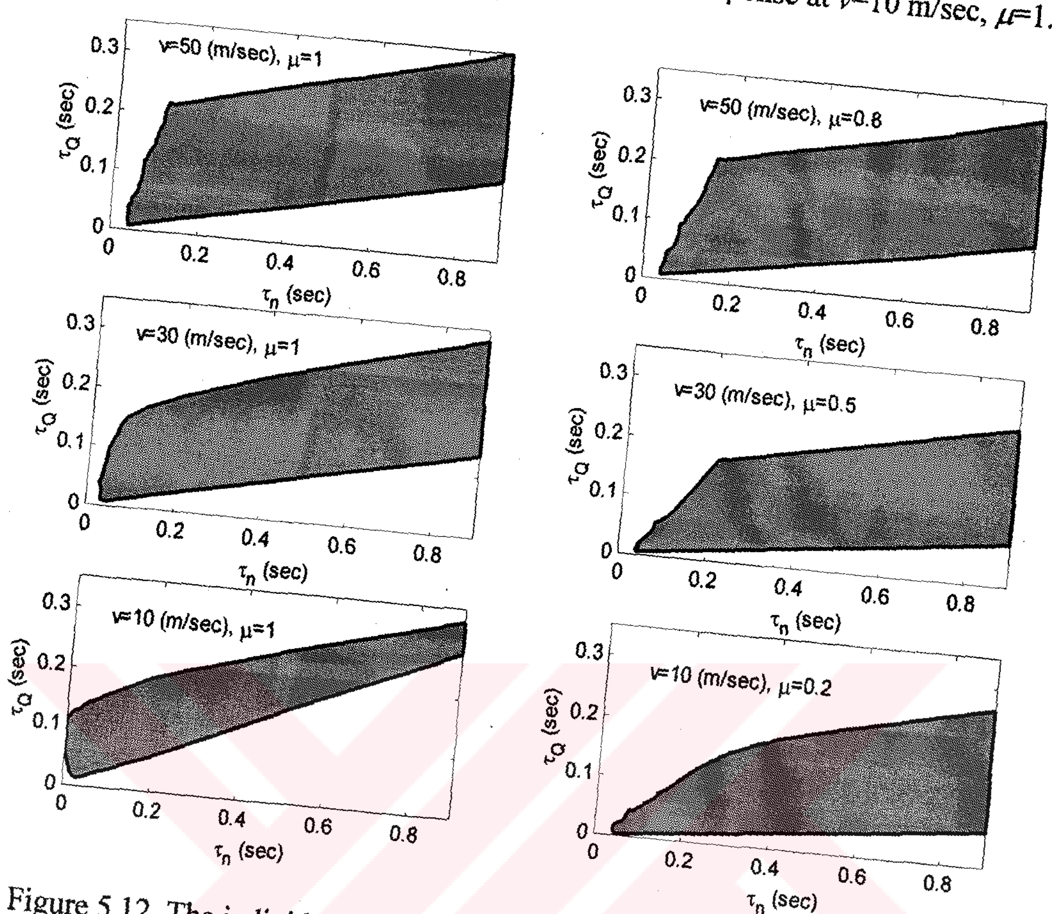

Figure 5.12 The individual solution regions in the controller parameter plane

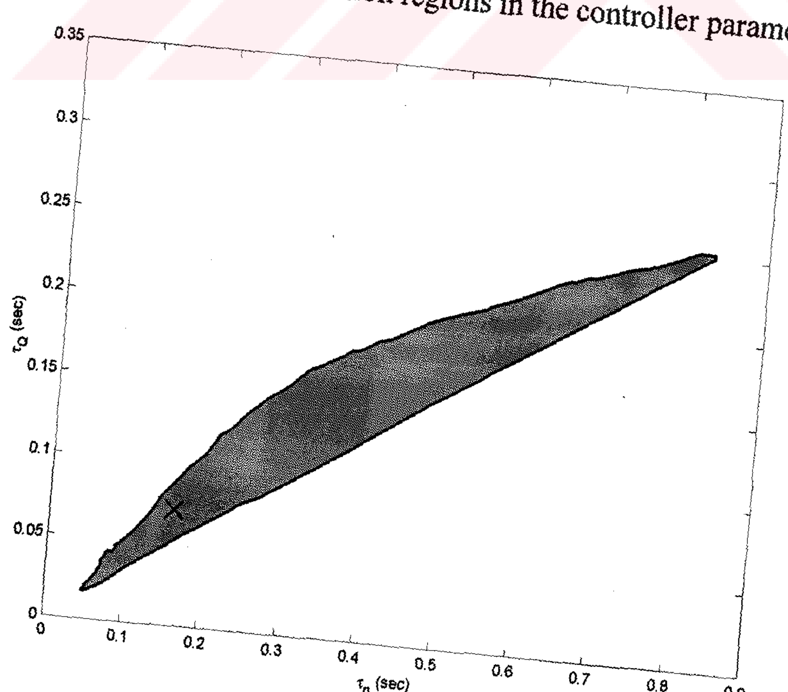

Figure 5.13 The overall solution region in the controller parameter plane

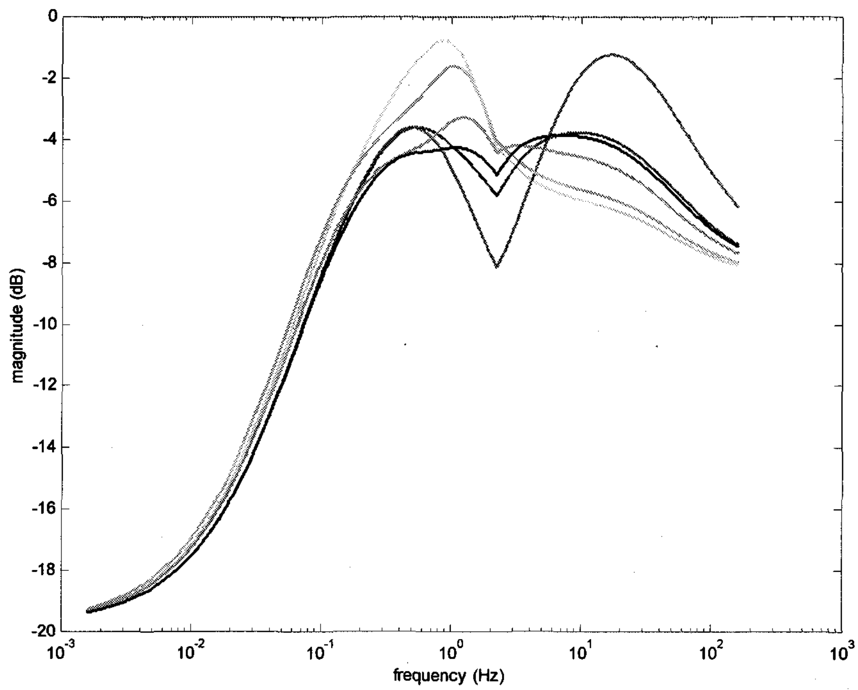

Figure 5.14 The $|W_S S|+|W_T T|$ frequency domain plot for all six operating points

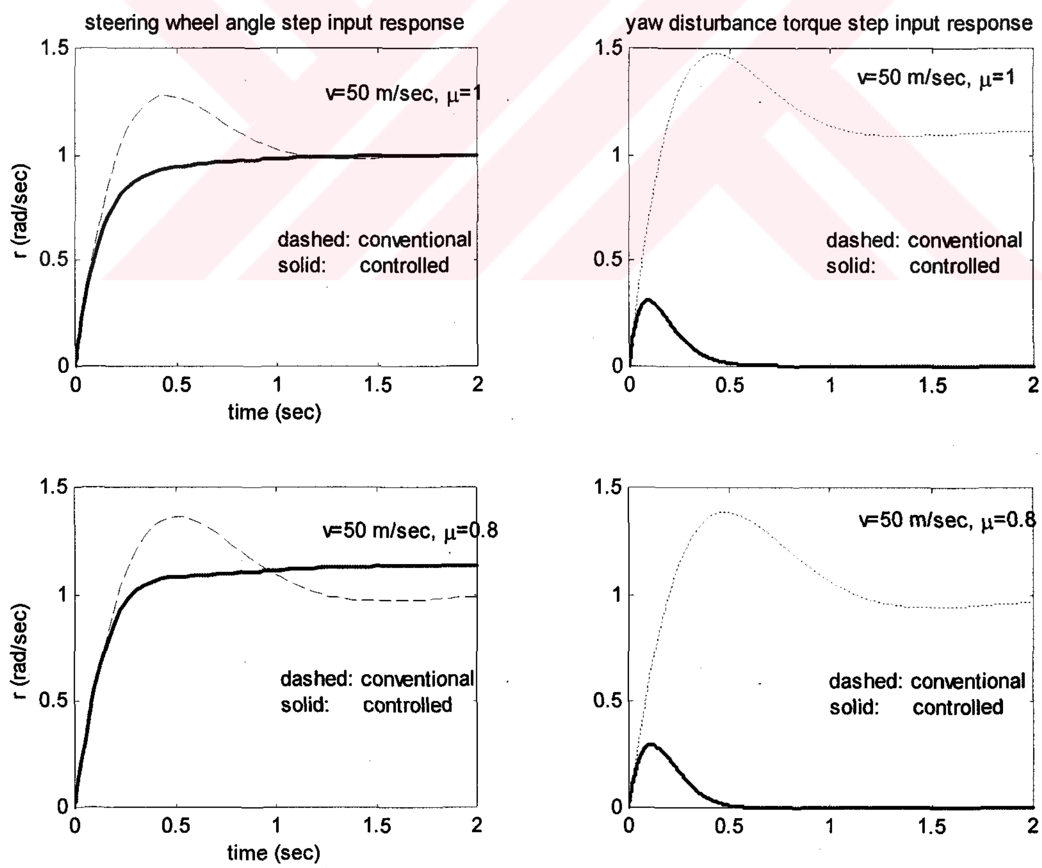

Figure 5.15 Linear simulations for the mixed sensitivity design at v=50 m/sec

While this is easily done, it results in unnecessarily fast response being imposed by the model regulator at high velocities. This contradicts the main principle that the steering controller should add its corrective actions only when necessary. So, the steering controller should avoid trying to increase the speed of response for a well damped and acceptable conventional response. A gain scheduling type remedy to this problem is presented in this section.

The time constant τ_n in the desired model G_n is also gain scheduled with velocity as

$$G_n(s) = \frac{K_n(v)}{\tau_n(v)s + 1} \tag{5.39}$$

to solve the low speed problem here. Note that the vehicle nominal single track model could also have been used for the same purpose. However, (5.39) is simpler to implement and results in well damped response. In an effort to find a suitable $\tau_n(v)$, the nominal conventional vehicle model is first re-expressed as

$$G(s) = \frac{K\omega_n^2(s+p)}{(s^2 + 2\zeta\omega_n s + \omega_n^2)} \tag{5.40}$$

and the average of the numerator time constant and the equivalent denominator time constant is evaluated as

$$\tau_n \to \frac{1}{(p + \zeta\omega_n)/2} \tag{5.41}$$

which after fitting data at v=10, 20, 30, 40, 50 m/sec results quite closely in

$$\tau_n(v) = \frac{0.0653v}{10} \tag{5.42}$$

This first rather crude guess has to be adjusted at every speed so that the response of $G_n(s)$ in (5.39) and the response of the nominal conventional car are very close at each speed. This results in

$$\tau_n(v) = (1.05 - 0.015v)0.00653v \tag{5.43}$$

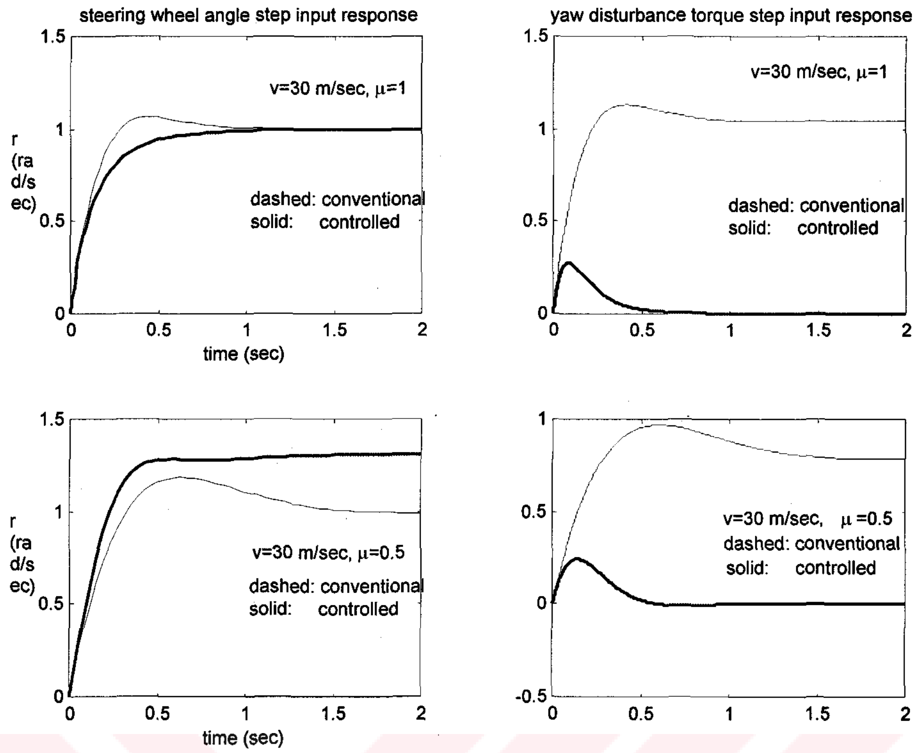

Figure 5.16 Linear simulations for the mixed sensitivity design at v=30 m/sec

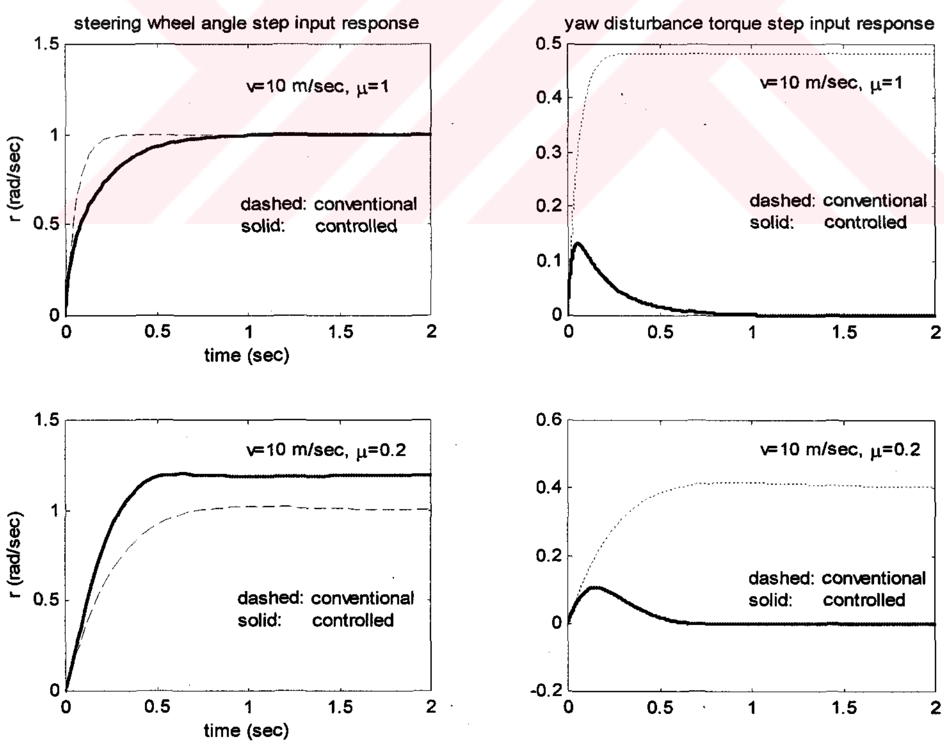

Figure 5.17 Linear simulations for the mixed sensitivity at v=10 m/sec

for the desired time constant and

$$G_n(s) = \frac{K_n(v)}{((1.05 - 0.015v)0.00653v)s + 1} \tag{5.44}$$

for the gain scheduled desired model itself. Corresponding simulation results displayed in Figures 5.18 and 5.19 demonstrate that the low velocity problem has been solved.

5.3.6 Limited Integrator Implementation

Another practical problem that needs to be addressed is one of man-machine interface. The task of the steering controller is to intervene during the panic reaction

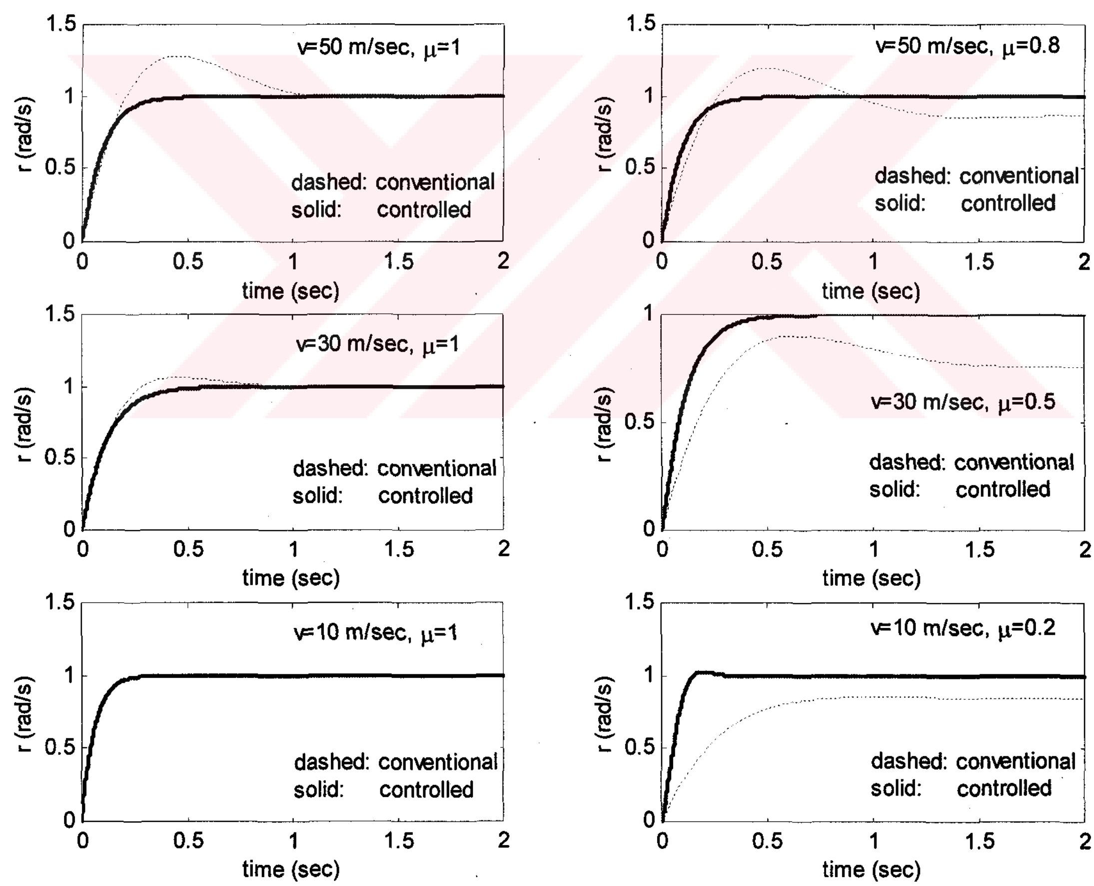

Figure 5.18 Linear simulations showing the solved low speed problem

time of the driver in catastrophic situations and then to hand over the steering task back to the driver afterwards. In control specific terms, the steering controller should only react to high frequency inputs outside the bandwidth of the driver. This is called short duration steering control here. Note that this effect can also be called the fading effect and is necessary when an auxiliary steering controller is used in order to avoid saturating the auxiliary steering actuator with a limited capability of steering wheel angle change. Two approaches that achieve this purpose of short duration steering intervention when necessary are presented in this and the next section. These approaches are most useful in the auxiliary steering actuator implementation.

Recall from Chapter 4 that the choice (5.19) for Q results in an integrator being incorporated into the loop gain, hence, resulting in zero steady state error in response to step reference and disturbance inputs. Short duration steering control can be achieved by using a low frequency limited integrator instead of an integrator in the loop. For this purpose, it is necessary to incorporate the low frequency limited integrator $K/(\tau s+1)$ instead of $1/s$ in the model regulator loop using

$$\frac{Q}{1-Q}=\frac{K}{\tau s+1}R(s)=\frac{K}{\tau s+1}\frac{n_R(s)}{d_R(s)}. \tag{5.45}$$

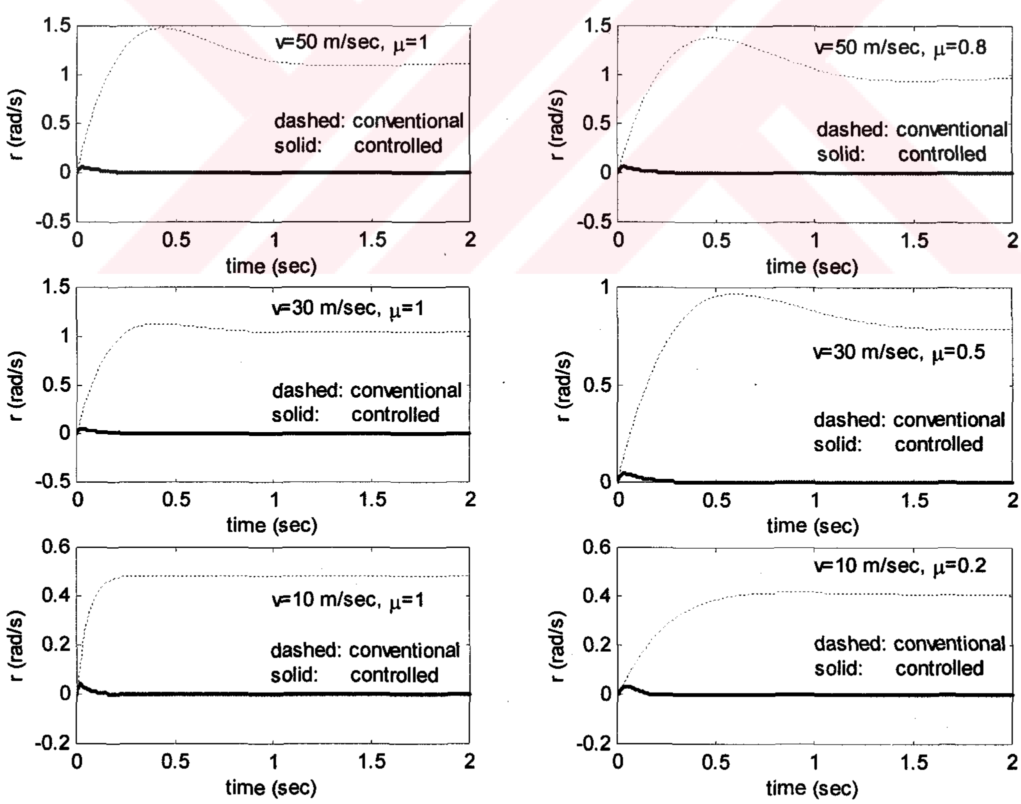

Figure 5.19 Linear simulations showing the solved low speed problem

Back solving for Q results in

$$Q = \frac{Kn_R(s)}{(\tau s+1)d_R(s)+Kn_R(s)} \tag{5.46}$$

Using the simplest possibility with $R=n_R=d_R=1$ results in

$$Q = \frac{K}{\tau s+1+K} = \frac{K/(1+K)}{\left(\frac{\tau}{1+K}\right)s+1} \tag{5.47}$$

The simulation results with (5.47) as Q, with K=10, τ=0.006 sec and with G_n given in (5.44) are shown in Figures 5.20 and 5.21. It is seen from an examination of these figures that the short duration steering intervention objective has been met. The

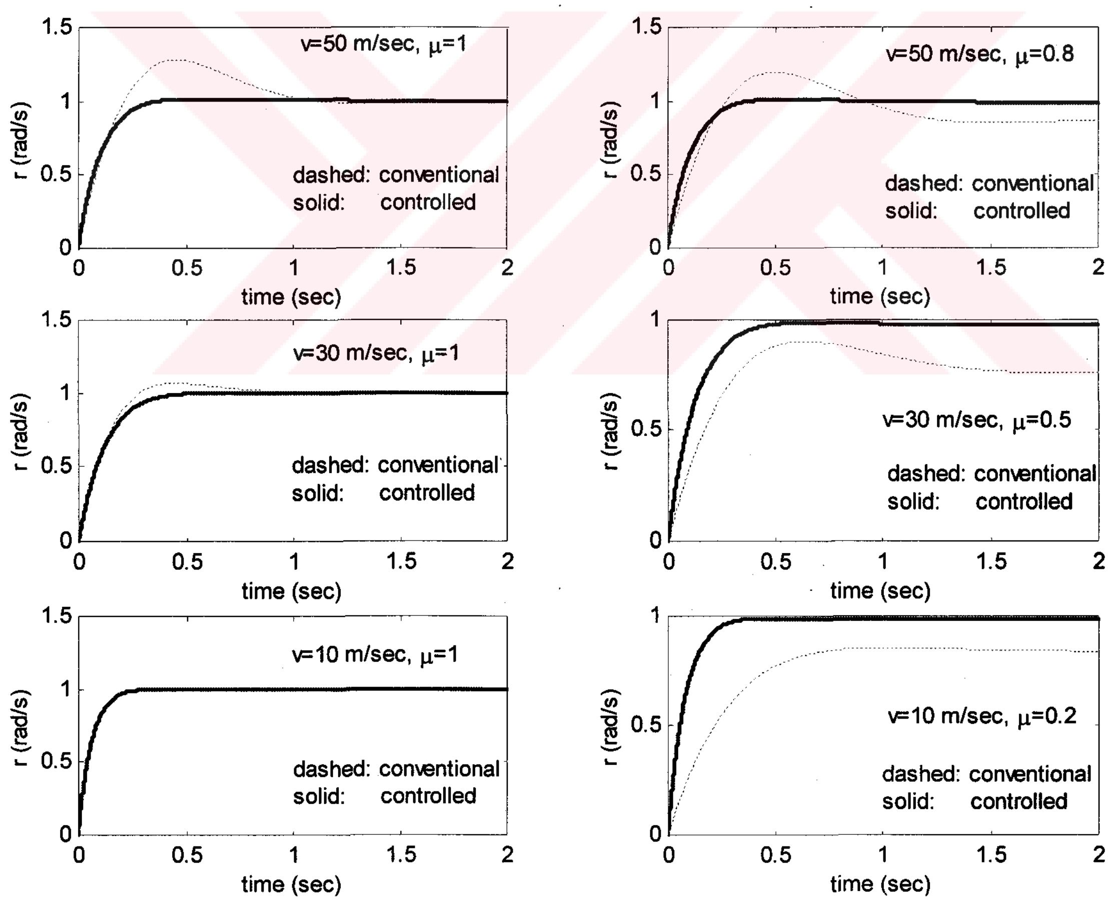

Figure 5.20 Linear simulations for the limited integrator implementation

disturbance rejection is very good with the model regulator with low frequency limited integrator action but a steady state error, which can easily be zeroed by the driver, remains.

5.3.7 Band Pass *Q* Filter

A more direct and better solution of the short duration steering intervention objective is to use a band pass Q filter in the model regulator. The Q filter should have unity gain and close to zero phase in its pass band. At low frequencies outside the pass band, Q should ideally be zero. These frequencies correspond to the working band of the driver. The simplest way of obtaining a band pass Q filter is by enhancing the previously designed low pass Q filter of (5.19) as

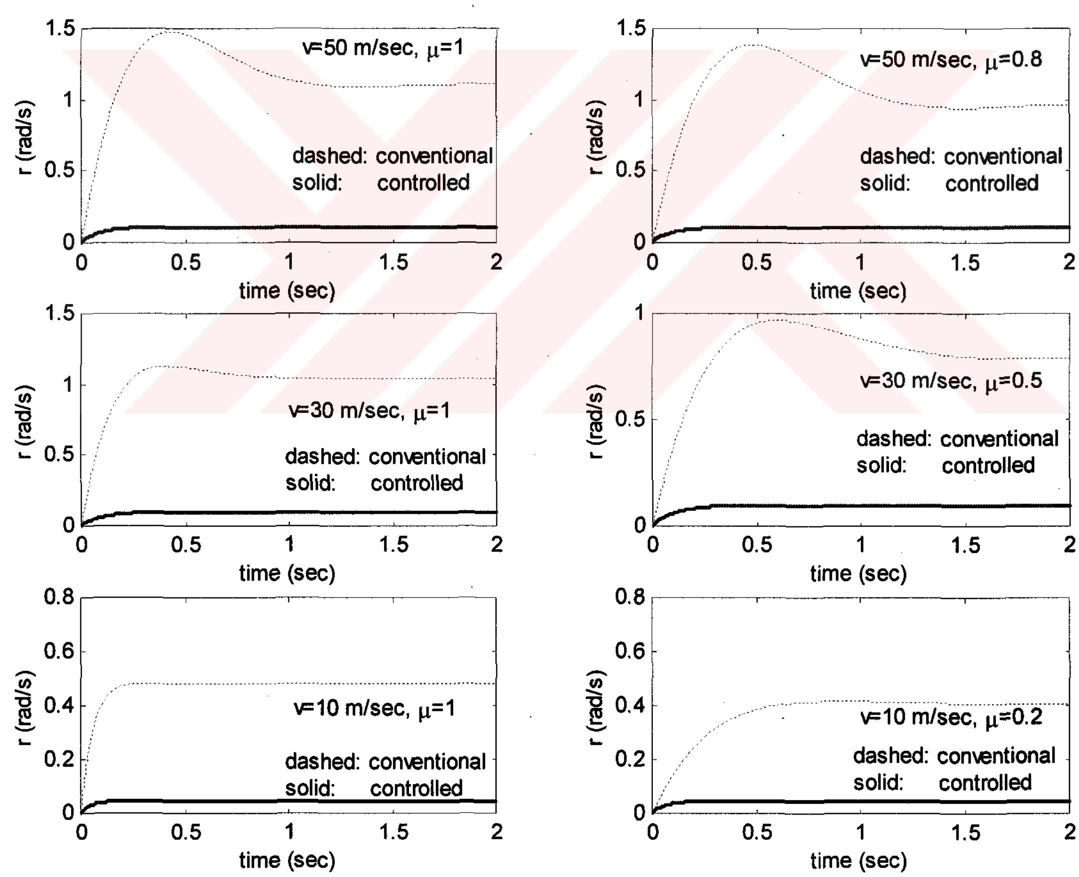

Figure 5.21 Linear simulations for the limited integrator implementation

$$Q = \frac{\tau_{bp} s}{(\tau_{bp} s + 1)(\tau_Q s + 1)} \tag{5.48}$$

Here, the pass band is chosen to be between 0.25 Hz and 26 Hz with τ_{bp} =0.637 sec and τ_Q =0.006 sec. The corresponding simulation results in Figures 5.22 and 5.23 demonstrate excellent short duration steering. It is evident from the yaw disturbance responses that the driving task is left to the driver who can easily handle the slow yaw rate change after his/her initial panic time during the course of which the steering controller minimizes the effect of the yaw disturbance.

5.4 Nonlinear Simulations

While the linearized single track simulation responses presented in the previous sections were quite useful in demonstrating the effectiveness of the steering controller presented in this chapter, these results should also be complemented by

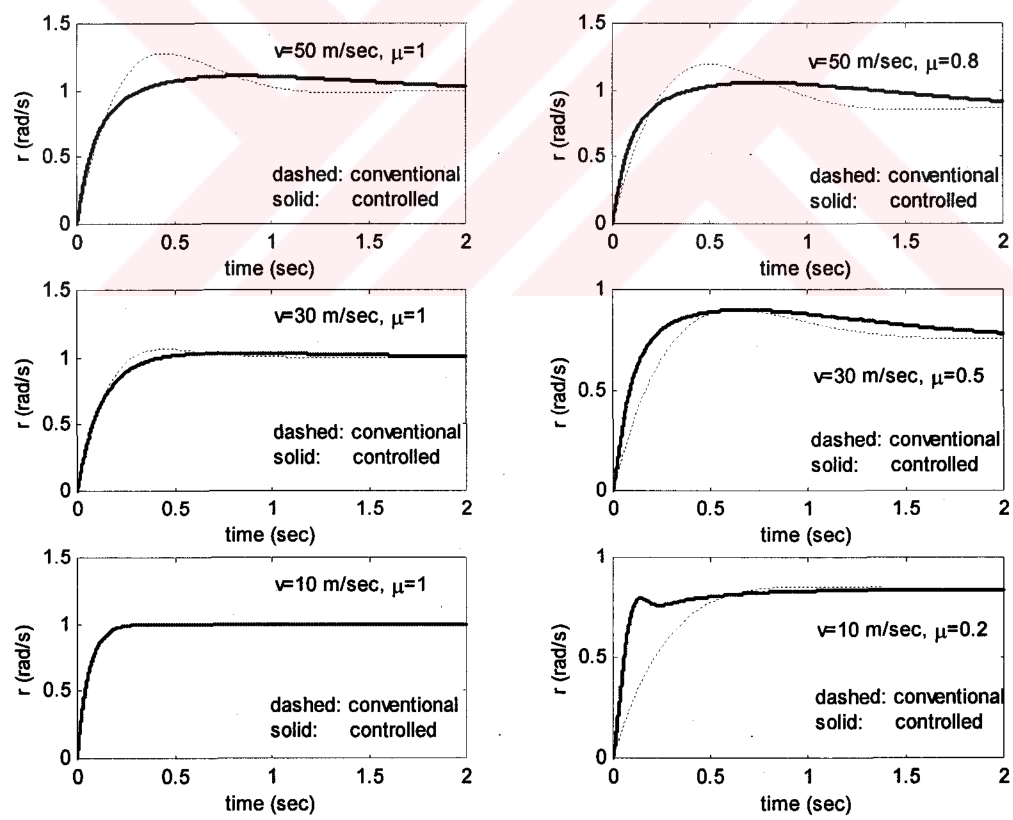

Figure 5.22 Linear simulations for band pass Q filter implementation

simulations using a nonlinear vehicle model. First, the nonlinear single track model of Figure 5.2 is used in this section to demonstrate that the model regulator works quite effectively when nonlinear plant behaviour is taken into account. It should be noted that unlike its linearized counterpart, velocity will not keep being constant in the nonlinear single track model when the steering angle δ_f is nonzero. In order to be able to compare results with the results that were previously reported here, the artificial cruise control system

$$(F_x)_{new} = F_x + K_p(v_d - v) \tag{5.49}$$

with a proportional controller with gain K_p=200,000 was used. v_d in (5.49) is the desired speed. The simulation results in Figure 5.24 for v_d=30 m/sec and μ=1 show that the model regulator works very well with the nonlinear model as well. Simulations at the other operating points in Figure 5.4 also exhibit excellent

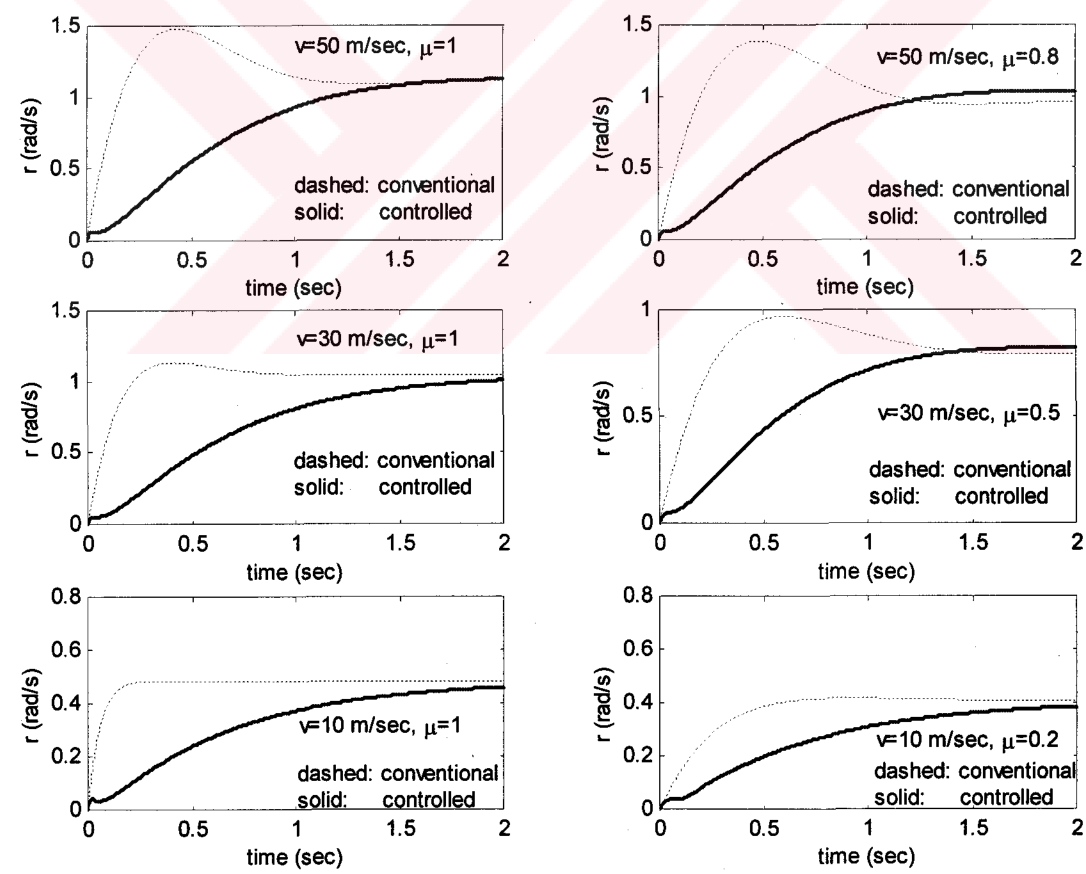

Figure 5.23 Linear simulations for band pass Q filter implementation

disturbance rejection and good command following even though they are not shown here.

Another quite useful feature of the nonlinear single track model with the cruise controller (5.49) is that it allows a desired velocity profile to be specified. In this manner, the operation of the gain scheduling feature of the model regulator type steering controller presented in this chapter can be tested in a variable velocity maneuver. The desired velocity profile ranging linearly from 10 m/sec to 50 m/sec and the corresponding simulation response are displayed in Figure 5.25. In this simulation, a lane change type of steering input followed by a yaw torque disturbance input are imparted to the system during its speed up phase. The results in Figure 5.25 demonstrate good command following and excellent disturbance rejection during this variable velocity maneuver.

Note that the gain scheduling implementation results in a nonlinear time varying system when the nonlinear model is used. Stability analysis of this system is quite difficult and one usually carries out a large number of simulations instead (Rugh and

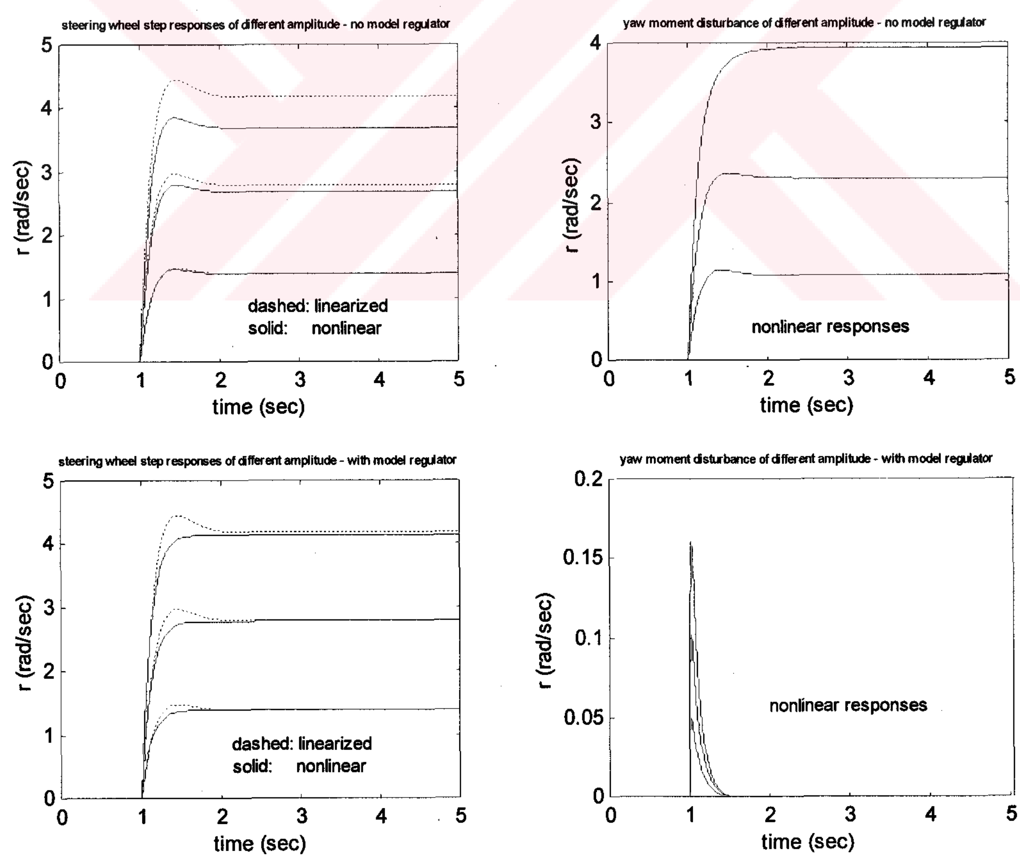

Figure 5.24 Nonlinear simulation results for v_d=30 m/sec and μ=1

Shamma, 2000). When the linear model is used with a gain scheduling type G_n, a linear time varying model is obtained . The stability analysis is easier to carry out in this case as the velocity v is the only parameter in the linear model that is time varying. An upper bound SSV analysis approach where all occurences of v are treated as uncertainty along with the other uncertainties in the system will result in a check of robustness of stability. Maximum value of the upper SSV bound being less than unity will guarantee robustness of stability based on the small gain theorem.

The second approach used in nonlinear simulations was to use a realistic nonlinear, higher order model that models the actual dynamics of the vehicle quite accurately. A commercially available program (Anon., 2000) that is also used by automotive companies in hardware in the loop simulation and rapid controller prototyping was chosen for this purpose. This program has a quite realistic model of a vehicle including tire, drive train, engine, suspension and transmission dynamics and coupling between its various subsystems. A μ–split maneuver during which the tires enter an ice patch on one side while the tires on the other side are on dry road was selected for the simulation. This is a very demanding maneuver in which the conventional (uncontrolled) vehicle becomes unstable. In contrast, the steering controller of this chapter works very well during this μ–split maneuver as is seen in Figure 5.26. This result shows that the steering controller of this chapter works quite satisfactorily in realistic situations also.

It should be noted that the model regulator type vehicle steering controller presented in this chapter can also be used on a disturbance triggered basis. This is useful when one has a good way of detecting the occurrence of a disturbance like a μ-split situation or a tire rupture.

5.5 Some Practical Aspects

Some practical and useful aspects of the model regulator based vehicle steering controller are discussed in this section. The first aspect has to do with the use of steering as the means of imparting vehicle yaw response corrective action. When the aim is vehicle yaw response stabilization or improvement, the yaw motion stabilizing/improving controller can use any means of creating a yaw moment for its

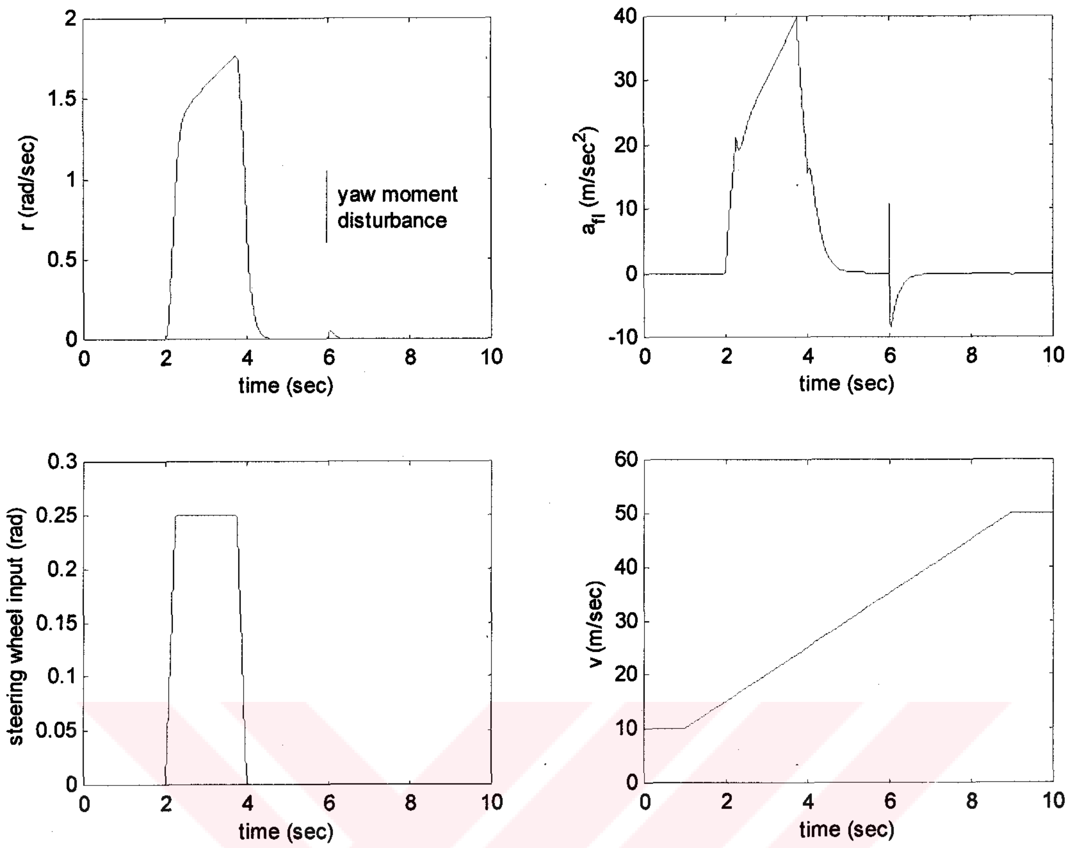

Figure 5.25 Simulations for the nonlinear single track model with the cruise controller

corrective actions. Consequently, the model regulator based yaw stabilizing/improving controller can also use individual wheel braking instead of steering for corrective action. It is also possible to use a combination of steering and individual wheel braking separately in different regions of operation or simultaneously. The model regulator design will be similar in these latter two cases.

In practical implementations, practical problems like sensor noise, actuator saturation, computational delay, finite word length effects etc. have to be considered. As a first rule of thumb, the bandwidth of the yaw rate sensor used in vehicle steering control should be at least twice as large as the Q filter's bandwidth. Moreover, significant yaw rate sensor noise should not occur up to about the five times the Q filter bandwidth to avoid amplification of this noise. Actuator saturation and bandwidth limitation will both degrade the performance of the model regulator based steering controller. However, the results will still be better than those achieved in its absence, i.e. the conventional vehicle.

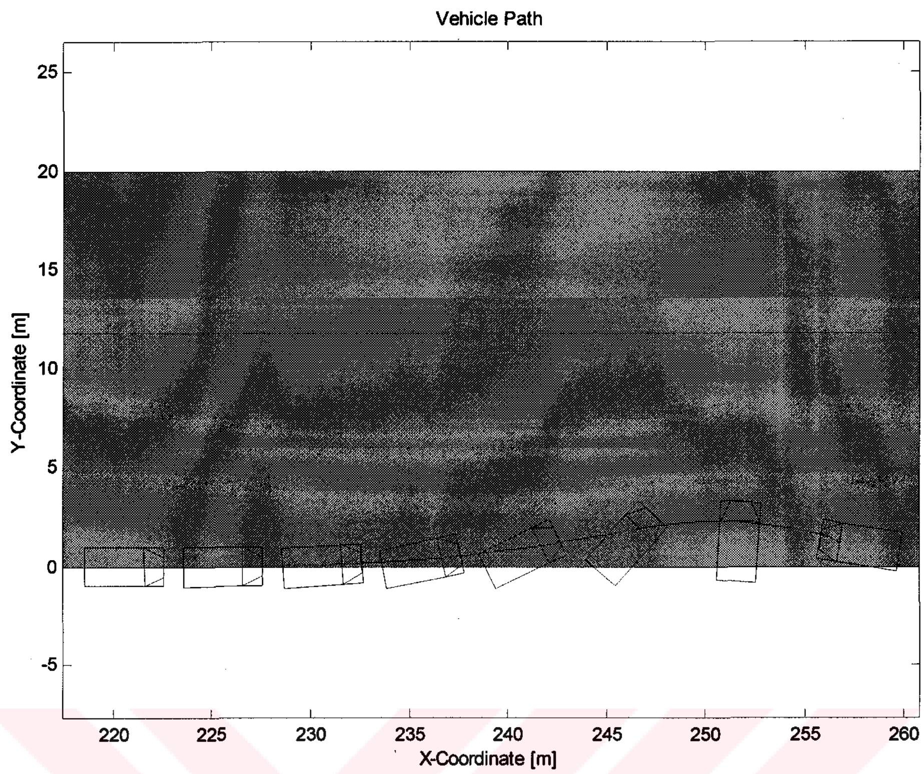

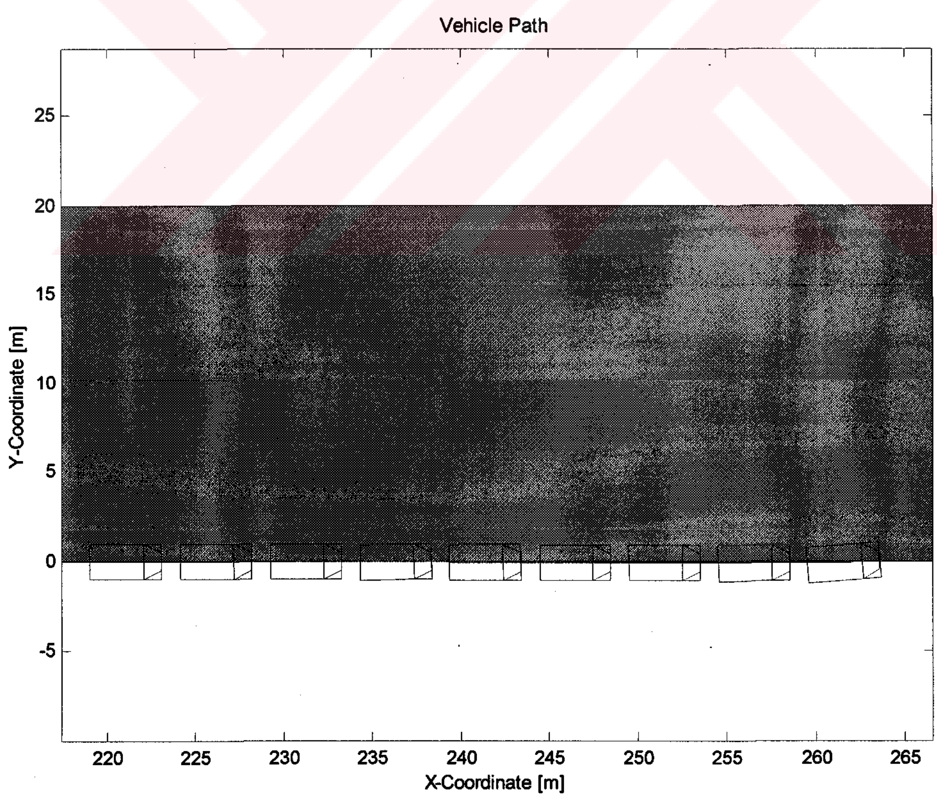

Figure 5.26 μ-split maneuver with higher order simulation model (top: conventional car, bottom: controlled car)

The electronic control unit (ECU) of the vehicle has several tasks with steering compensation being only one of them. In the presence of a network approach for communication like the control area network (CAN), the sensor signal may only be available after a delay time and the steering control action may only be available at certain intervals, for example. Of course, these implementation specific aspects will also degrade performance further. However, the model regulator is quite robust to model uncertainties and the level of performance degradation can be reduced by fine tuning the design. In an effort to see the effect of some implementation related problems on performance, the model regulator designs of the previous sections were subjected to an actuator with a bandwidth of 4 Hz and a steering controller update interval of 20 msec. In spite of the degradation in response, the results were much better than those achieved by the conventional (uncontrolled) vehicle, showing that even a design that is not fine tuned works quite satisfactorily.

6. ROBUST VEHICLE LATERAL CONTROL IN AUTOMATED PATH FOLLOWING

Automatic steering of vehicles is of practical importance for buses on separate, narrow lanes, for transport vehicles in factories and for highway automation. The main objective in automatic steering is to track a reference path with minimum tracking error. The deviation from the reference path, which may be specified by magnetic markers, is measured by a displacement sensor located in the front part of the vehicle. The steering controller, then, manipulates the front steering angle using this displacement information.

This chapter presents mainly the application of the robust two degree of freedom add-on controller, namely the model regulator, introduced in Chapter 4 to automatic path following. The vehicle considered here is the O305 city bus with the corresponding model data and design specifications being given in an IFAC benchmark problem (Ackermann and Darenberg, 1990) and in Ackermann et al (1995). The desired trajectory to be followed by the vehicle constitutes an external disturbance to be rejected for the controlled vehicle as the system output is taken as the deviation from this desired trajectory. The feedback controller for automatic steering designed in Ackermann et al (1995) is kept in place. This feedback controller uses yaw rate feedback for improved steering dynamics (Ackermann et al, 1995; Ackermann and Sienel, 1990). The two degreee of freedom add-on controller is used in this section for model regulation in the presence of model uncertainty, enhanced disturbance rejection in tracking a desired path and also to achieve satisfactory steering dynamics without the need for a yaw rate sensor. This latter feature is also useful for a fault tolerant design when the possibility of a yaw rate sensor failure is considered. Another useful feature of the model regulator based add-on controller that is demonstrated here is that it allows lower gain feedback controllers to achieve the design specifications in Ackermann et al (1995).

A human driver's behaviour can be divided into the open-loop pursuit and closed-loop compensatory parts. The pursuit part of the human control system which previews the future desired path generates the major part of the human driver action while the compensatory part, similar to the feedback controller in the automated scheme, merely reduces the remaining errors. Accordingly, a disturbance feedforward compensator is also considered here as an alternative add-on controller that can be used when preview of the reference trajectory is available.

6.1 Vehicle Steering Model, Specifications and Existing Feedback Controller

The linearized single track model illustrated in Figure 6.1 is used to model the steering dynamics.

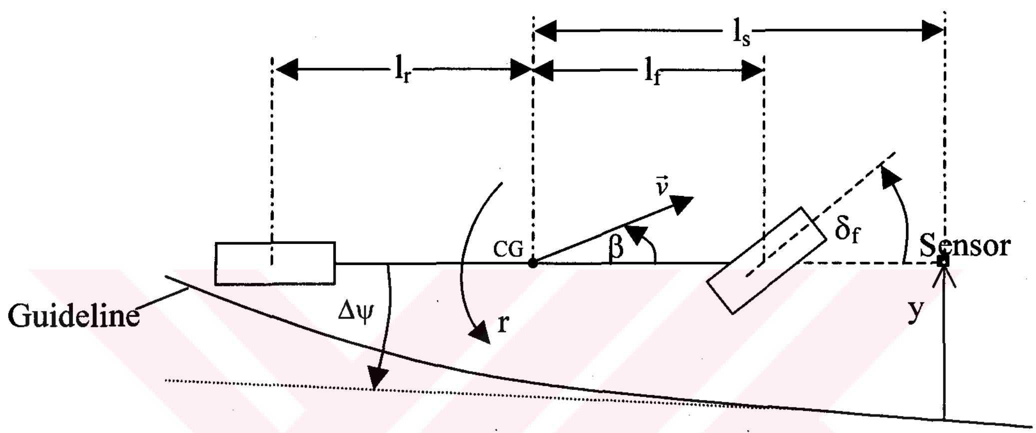

Figure 6.1 Single track model for automated path following

Together with the dynamics of the reference path and an actuator with integrating characteristics as in Ackermann et al (1995), the vehicle dynamics is described by

$$\begin{bmatrix} \dot{\beta} \\ \dot{r} \\ \Delta\dot{\psi} \\ \dot{y} \\ \dot{\delta}_f \end{bmatrix} = \begin{bmatrix} a_{11} & a_{12} & 0 & 0 & b_{11} \\ a_{21} & a_{22} & 0 & 0 & b_{21} \\ 0 & 1 & 0 & 0 & 0 \\ v & l_s & v & 0 & 0 \\ 0 & 0 & 0 & 0 & 0 \end{bmatrix} \begin{bmatrix} \beta \\ r \\ \Delta\psi \\ y \\ \delta_f \end{bmatrix} + \begin{bmatrix} 0 & 0 \\ 0 & 0 \\ 0 & -v \\ 0 & 0 \\ 1 & 0 \end{bmatrix} \begin{bmatrix} u_f \\ \rho_{ref} \end{bmatrix} \tag{6.1}$$

where l_s, v, β, r, $\Delta\psi$, δ_f and y are the sensor distance, speed at the center of gravity of the vehicle, sideslip angle, yaw rate, angle between centerline of vehicle and tangent to the guideline, front wheel steering angle and the deviation from the guideline at the sensor location, respectively. The other terms in (6.1) are given by

$$\begin{aligned}
a_{11} &= -(c_{r0} + c_{f0}) / \tilde{m}v \\
a_{12} &= -1 + (c_{r0}l_r - c_{f0}l_f) / \tilde{m}v^2 \\
a_{21} &= (c_{r0}l_r - c_{f0}l_f) / \tilde{J} \\
a_{22} &= -(c_{r0}l_r^2 + c_{f0}l_f^2) \tilde{J}v \\
b_{11} &= c_{f0} / \tilde{m}v \\
b_{21} &= c_{f0}l_f / \tilde{J}
\end{aligned} \tag{6.2}$$

where μ is the road adhesion factor, m is the vehicle mass and μc_{f0} and μc_{r0} are the cornering stiffnesses for the front and rear axles and $\tilde{m} = m / \mu$ and $\tilde{J} = J / \mu$ are the virtual mass and virtual moment of inertia respectively.

The curvature $\rho_{ref}=1/R_{ref}$ of the guideline is a measurable external disturbance. This external disturbance which is also the path to be followed comprises of circular arcs with the transition to a new curvature corresponding to a step input in ρ_{ref}. The data for the city bus O305 is taken from Ackermann et al (1995). The steering angle and steering angle rate are limited to 40 deg and 23 deg/sec, respectively. The maneuvers used in the simulations here are:

1) Transition from a straight line into a circle (R_{ref}=400m).

2) Transition from manual to automatic operation where the bus is assumed to drive in a distance of y=0.15 m parallel to the guideline when the control is activated.

3) Entering a narrow bus stop bay with a velocity of 2.5 m/sec or higher. The reference trajectory is shown in Figure 6.2. The displacement from the guideline should not exceed 0.15 m during the transient state and 0.02 m at steady state.

Two parameter space based robust controllers were designed in Ackermann et al (1995) using the operating ranges of v∈[1:20] m/sec, and $\tilde{m}$ ∈[9950:32000] kg for the velocity and virtual mass, the two parameters exhibiting the largest variation during operation. These feedback controllers are

$$G_{c_1} = 40^3 \frac{0.27s^2 + 1.3s + 1.9 + 0.75/s}{(s^2 + 48s + 40^2)(s + 40)} \tag{6.3}$$

$$G_{c_2} = 100^3 \frac{0.6s^2 + 13s + 10 + 3/s}{(s^2 + 100s + 100^2)(s + 100)} \tag{6.4}$$

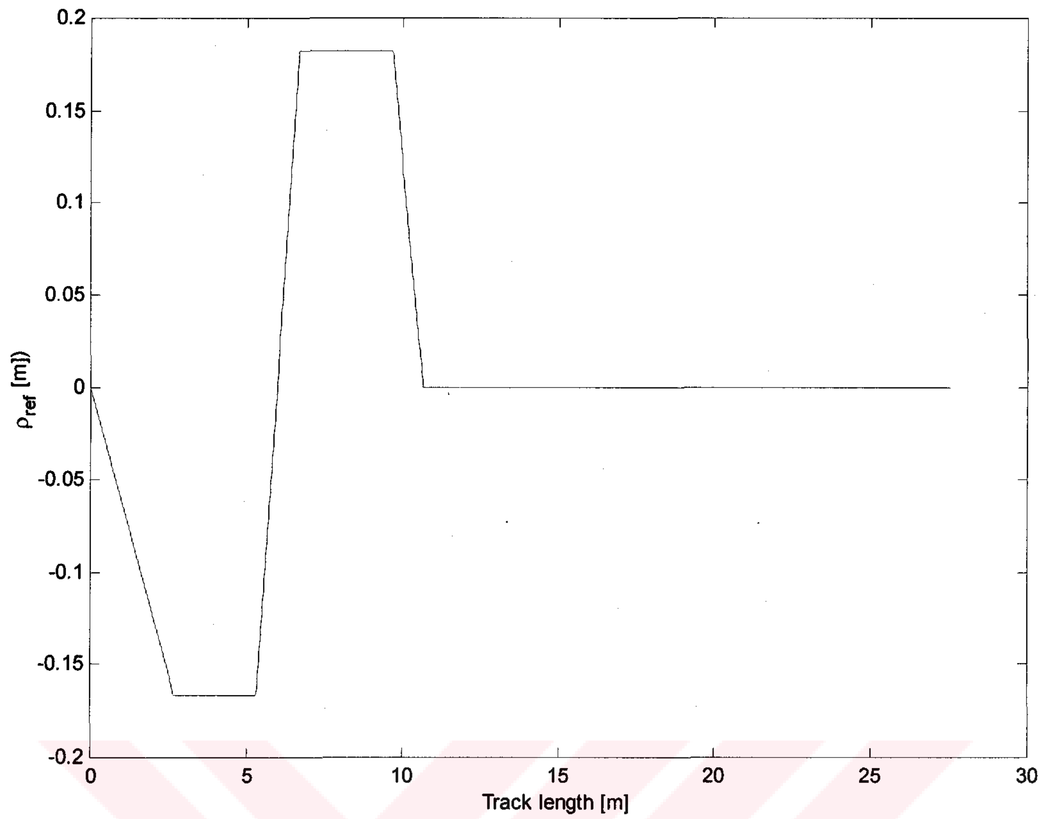

Figure 6.2 External disturbance ρ_{ref} for entering a narrow bus stop bay

While controller (6.4) satisfies all design requirements, the use of controller (6.3) results in a transient error in excess of 0.15 m while entering the bus stop bay at 2.5 m/sec. The vehicle model in (6.1) and (6.2) and the feedback controller (6.4) (in some cases (6.3)) are treated here as existing hardware and only add-on compensation is used in what follows.

6.2 Model Regulator Based Add-On Controller

A model regulator based add on controller is designed for the automated path following problem above in this section and shown to improve performance.

6.2.1 Yaw Rate Feedback

The use of yaw rate feedback and an integrating steering actuator with

$$\dot{\delta}_f = u_f - k_r r \tag{6.5}$$

were proposed in Ackermann et al (1993) to improve the steering dynamics. Yaw rate feedback with a gain of k_r =0.89 was determined and used in Ackermann et al (1995) to achieve improved steering system dynamics for the city bus example that is also considered here. With the aim of not having to rely on the yaw rate sensor to improve the steering dynamics, a model regulator is used here to demonstrate that similar dynamics can be achieved by using only the available output (y) and input (u_f) information. This model regulator based add-on controller can also be used as part of a fault tolerant design that will be activated in the presence of yaw rate sensor malfunction.

6.2.2 Model Regulator

Referring to Figure 6.3, the vehicle model can also be expressed as

$$y = G_{ua}u_f + d = (G_u + \Delta_u)u_f + d \tag{6.6}$$

where G_{ua} is the actual input-output relation between u_f and y where the lack of yaw rate feedback (k_r=0 in G_{ua}) is treated as model uncertainty and d is the external disturbance due to ρ_{ref}. Δ_u also includes modeling error in our nominal knowledge of the input-output relation denoted by G_u here.

The aim in model regulator design is to obtain

$$y = G_u u_{new} \tag{6.7}$$

as the input – output relation in the presence of model uncertainty Δ_u and external disturbance d. This aim is achieved in model regulator design by treating the external disturbance and model uncertainty as an extended disturbance *e* and solving for it as

$$y = G_u u_f + (\Delta_u u_f + d) = G_u u_f + e \tag{6.8}$$

$$e = y - G_u u_f \tag{6.9}$$

and using the new control signal u_{new} given by

$$u_f = u_{new} - \tilde{G}_u^{-1} e = u_{new} - \tilde{G}_u^{-1} y + \tilde{G}_u^{-1} G_u u_f \tag{6.10}$$

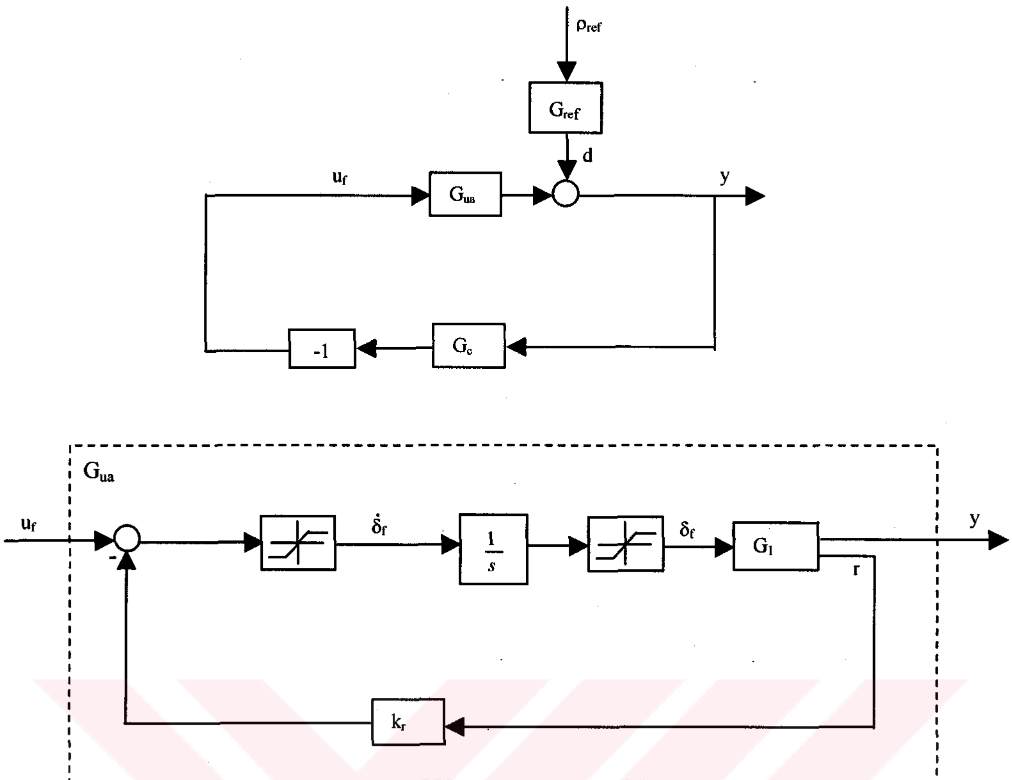

Figure 6.3 Feedback control architecture

to approximately cancel its effect in (6.8). $\widetilde{G}_u^{-1}$ is an approximate inverse of G_u and the input-output relation that is actually achieved in practice is

$$y = \underbrace{G_u u_{new}}_{desired\ I/O\ relation} + \underbrace{\left(1 - G_u \widetilde{G}_u^{-1}\right) e}_{\substack{undesired:\ due\ to\ model\ error \\ and\ external\ disturbance}} \tag{6.11}$$

The desired input-output relation (6.7) with u_{new} replacing u_f is, thus, obtained in frequency ranges where $G_u \widetilde{G}_u^{-1} \cong 1$, which is the basic model regulator design equation. (6.10) is used for implementation of the model regulator as shown in Figure 6.4.

In discrete time implementations of the model regulator, as is considered here, $\widetilde{G}_u^{-1}$ is designed using well known preview based compensation techniques like the zero phase error tracking (ZPET) method (Tomizuka, 1987) or extensions of this approach utilizing additional gain compensation zeros to achieve desired bandwidth of $G_u \widetilde{G}_u^{-1}$ (Menq and Xia, 1990; Menq and Xia, 1995).

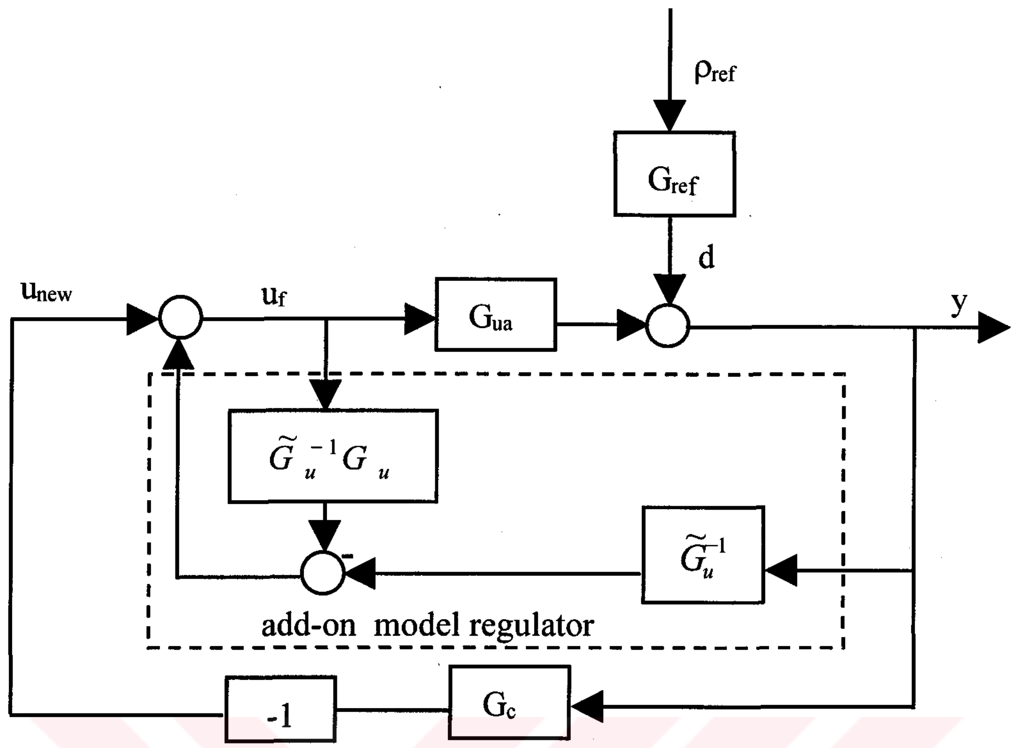

Figure 6.4 System with add-on model regulator

6.2.3 Sampling Rate Selection and Model Regulator Design

In contrast to feedforward control, preview information is not available in the model regulator. Hence, $\tilde{G}_u^{-1}$ has an l-step shift z^{-l} where l is the relative degree (3 here) of the discretized plant G_u, to make it causal. It turns out that this l-step shift is the major cause of performance degradation in a model regulator as it causes undesired phase lag (Güvenç and Srinivasan, 1994). This phase lag can be reduced by increasing the sampling rate but small values of the sampling time T_s:

1. May result in more nonminimum phase zeros with a corresponding and conflicting increase in computation time.

2. Processing power may be limited in a commercial product in comparison to the very high sampling rates that can be achieved in lab environments.

Figure 6.5 shows the location of zeros of G_u with v=20 m/sec and $\tilde{m} = 32{,}000\,\text{kg}$ with zero order hold discretization for different values of the sampling period T_s.

For $T_s < 0.0001$ sec, there are three NMP zeros, one of them lying on the negative real axis while the other two zeros lie on the unit circle at z=1. For $T_s \geq 0.0001\text{sec}$ the system has one real NMP zero. Trying to have only one NMP zero and trying to

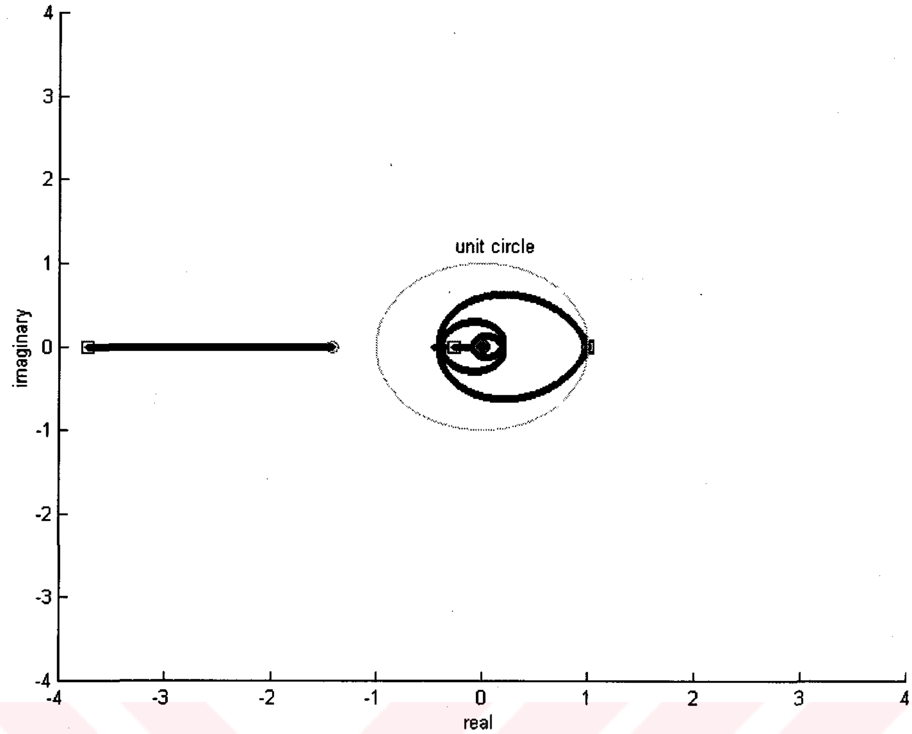

Figure 6.5 Effect of sampling period on open loop zeros (small T_s: □, large T_s: o)

increase the distance of some of the MP zeros from the unit circle, T_s=0.01 sec is chosen as the sampling period here. The corresponding NMP zero is $z_1 = -3.7257$. The optimal PTC (see Aksun Güvenç and Güvenç, 1999) based approximate inverse filter

$$\tilde{G}_u^{-1}(z) = z^{-3}\frac{10^6\left(-0.0316z^8 + 0.379z^7 - 1.39z^6 + 2.36z^5 - 2.01z^4 + 0.742z^3 + 0.0147z^2 - 0.0715z + 0.00835\right)}{3.16z^5 - 5.44z^4 + 1.45z^3 + 0.834z^2} \tag{6.12}$$

is designed for this system and the corresponding low pass filter $G_u G_u^{-1}$ is shown in Figure 6.6. The expression after the 3-step shift in (6.12) consists of the invertible part of $G_u(z)$ and the zero phase and gain error compensation terms.

6.2.4 Performance Evaluation of the Model Regulator

The magnitude frequency responses y/u_f (or y/u_{new} in the model regulator case) of the three cases of no yaw rate feedback, yaw rate feedback and no yaw rate feedback but forced to that behavior by the model regulator are displayed in Figure 6.7.

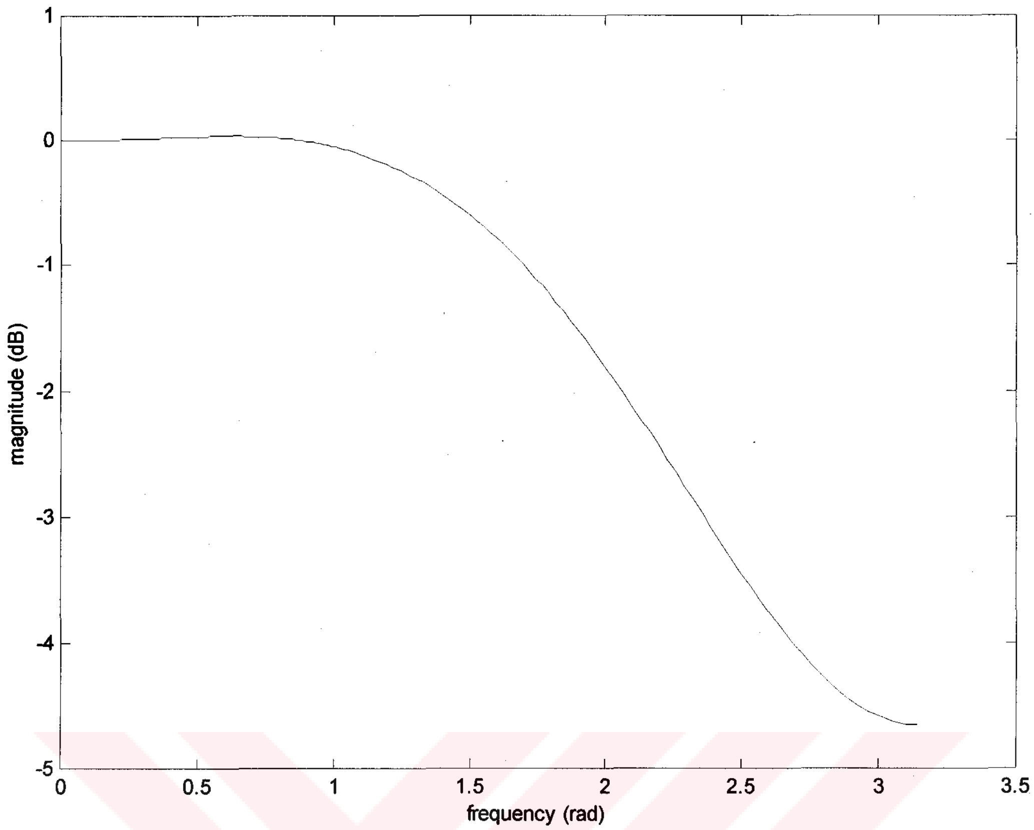

Figure 6.6 Magnitude frequency response of $G_u\tilde{G}_u^{-1}$

It is clear that the improved steering dynamics achieved in Ackermann et al (1995) by yaw rate feedback can also be achieved by the model regulator which does not require yaw rate information. This approach is useful for a fault tolerant design considering the possibility of yaw rate sensor failure.

The model regulator also regulates the input-output behavior to that of the desired model in the presence of model uncertainty and enhances disturbance rejection properties. This is evident in Figure 6.8 and Figure 6.9 where $|y/u_f|$ ($|y/u_{new}|$ with the model regulator) and $|y/\rho_{ref}|$, respectively, are plotted, for the four extremal plots at the corners of the uncertain parameter space v$\in$[1:20] m/sec, and $\tilde{m} \in$[9950:32000] kg.

Figure 6.8 demonstrates that deviations in $|\, y/u \,|$ between these four extremal plants are decreased significantly by the model regulator, especially at low frequencies. The corresponding decrease at low frequencies in $|\, y/\rho_{ref} \,|$ due to the model regulator seen in Figure 6.9 demonstrates the enhancement of disturbance rejection.

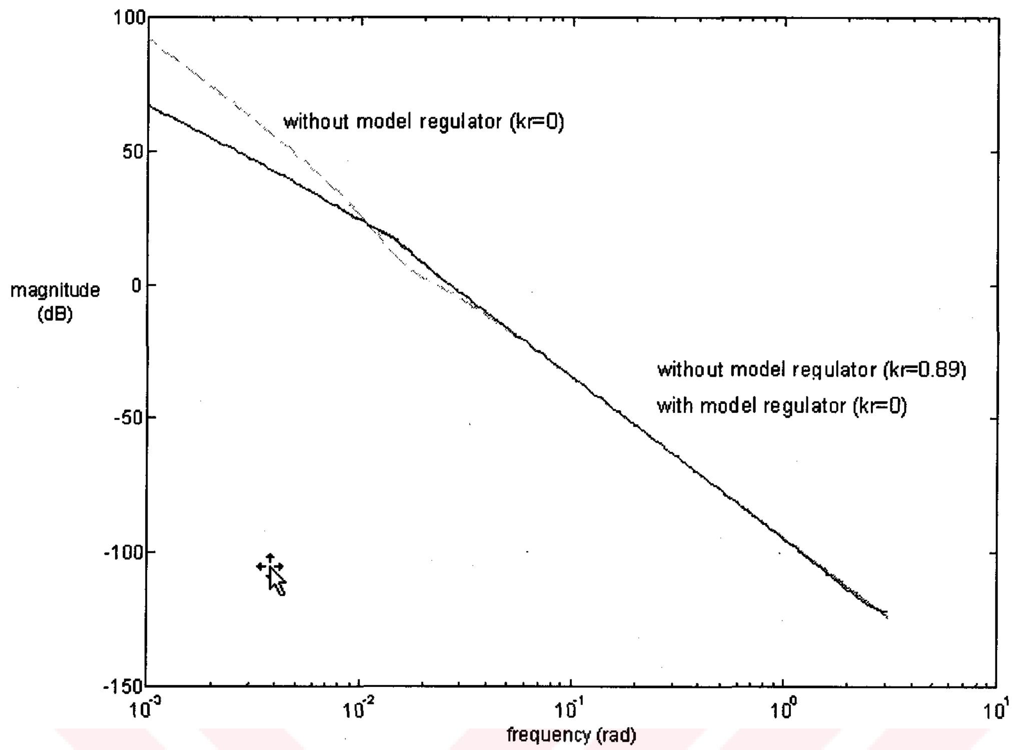

Figure 6.7 Effect of model regulator on $|y/u|$

6.3 Simulation Study

Time domain simulations for the three maneuvers in Section 6.1 are shown in Figure 6.10. Feedback controller (6.4) was used in these simulations. The dashed lines are responses of the yaw rate feedback system of Ackermann et al (1995) while the solid lines are obtained after the incorporation of the add-on model regulator. The results are satisfactory and are better than the results in the absence of the add-on model regulator. There is some difference between the two responses in the entering a circular arc maneuver but tracking error is decreased significantly in the entering a narrow bus stop bay maneuver.

The main limitation hindering much better results from being obtained with the model regulator is the presence of the actuator saturation for the steering angle rate. The steering angle rate saturates in the simulations here with the model regulator as it had done in Ackermann et al (1995) in its absence. The steering angle values δ_f, on the other hand, did not reach their saturation limit of 40 deg during any of the simulations reported in this chapter. The model regulator implementation had to be slightly modified by applying the $\dot{\delta}_f$ saturation to the $G_u \widetilde{G}_u^{-1}$ input in Figure 6.4 to account for the saturated input into the vehicle model.

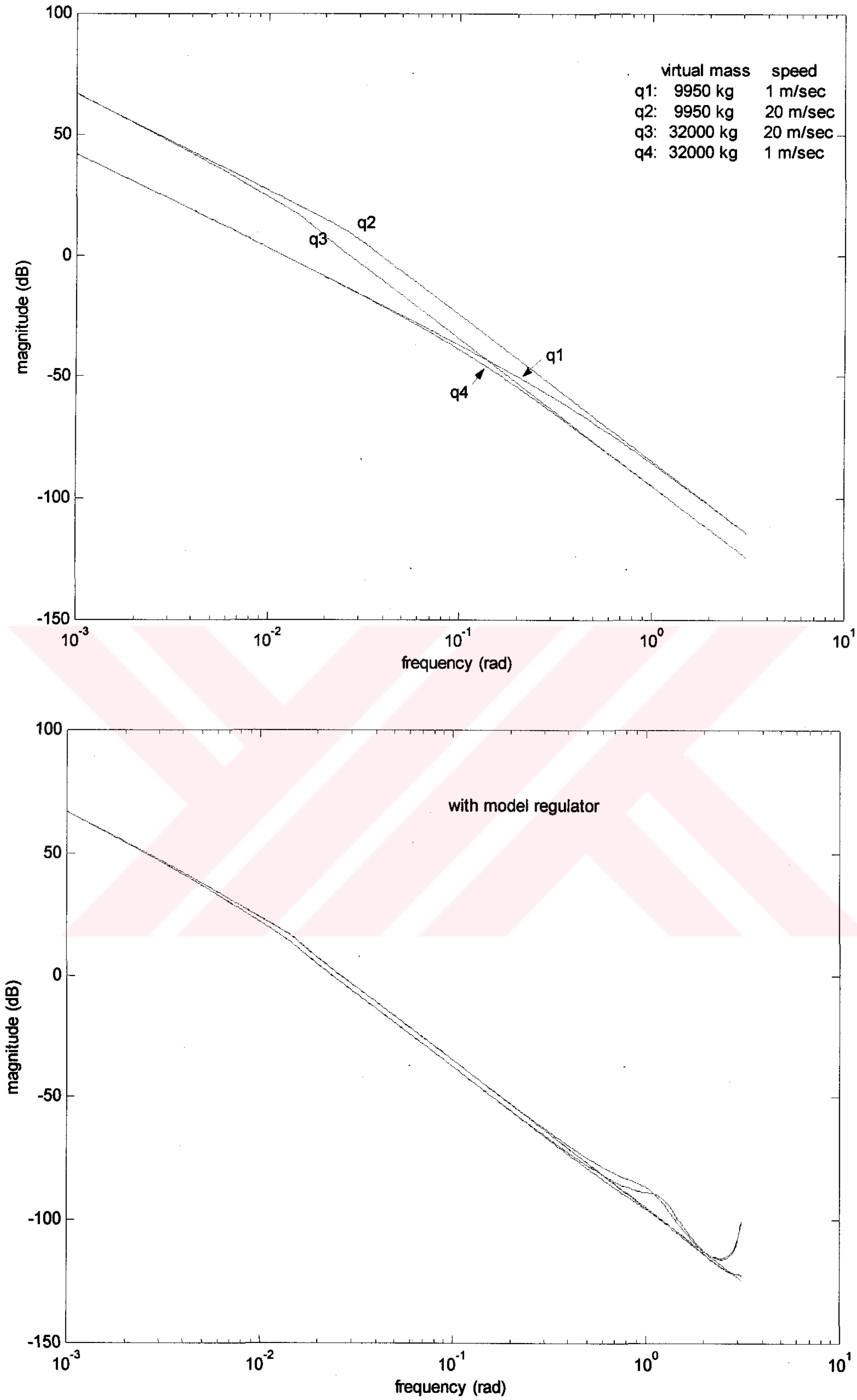

Figure 6.8 $|y/u|$ for the four extremal plants, without and with the model regulator

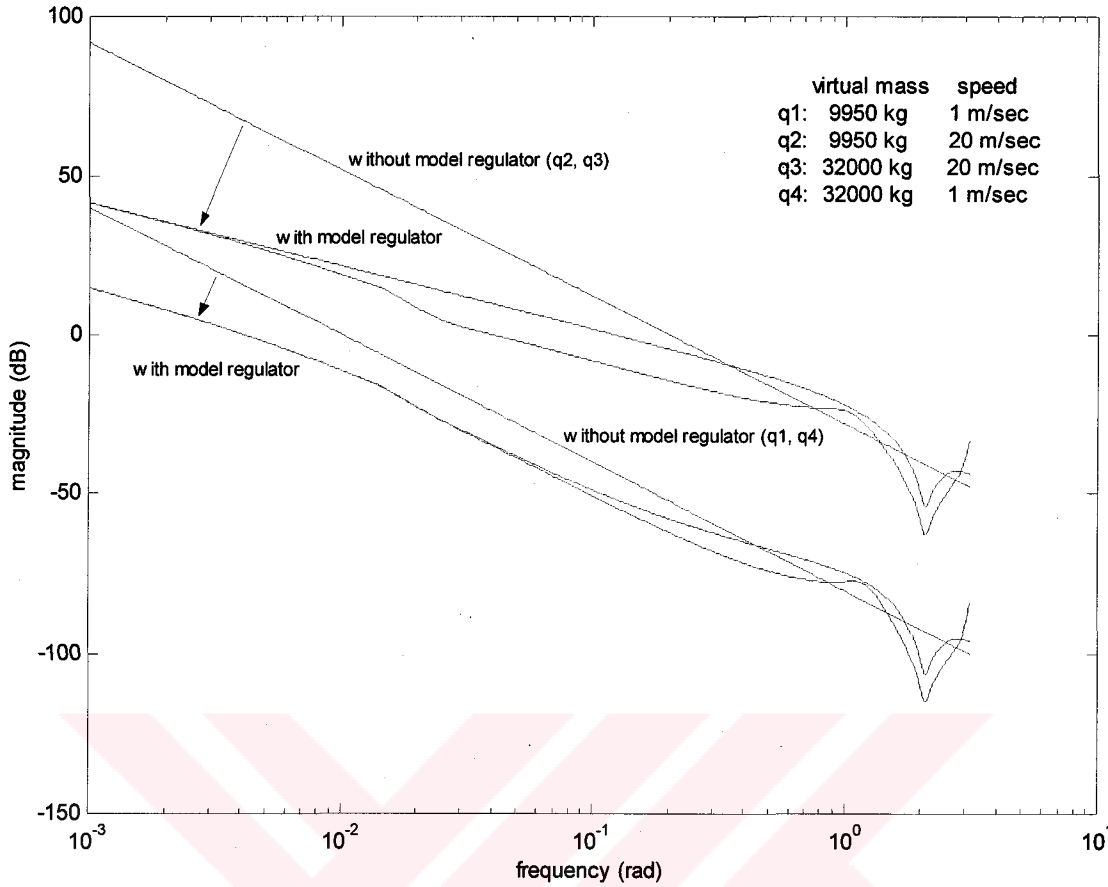

Figure 6.9 $|y/\rho_{ref}|$ for the four extremal plants with and without the model regulator

A performance enhancing measure will be to use a steering actuator with a higher steering angle rate limit ($\dot{\delta}_f > 23$ deg/sec). The entering a bus stop bay maneuver resimulated with a saturation limit of 38 deg/sec for $\dot{\delta}_f$ shown in Figure 6.11, for example, shows much improved and improved response with and without the model regulator, respectively.

The model regulator also allows lower gain controllers to be used without violating the design specifications. Feedback controller (6.3) which violates the transient error specification in the narrow bus stop bay maneuver at v=2.5 m/sec for instance satisfies this requirement in the presence of the model regulator as seen in Figure 6.12.

6.4 Model Regulator and Actuator Saturation

One point that makes the saturation in the steering angle rate $\dot{\delta}_f$ more difficult to handle here from the viewpoint of the model regulator is that it is followed by an

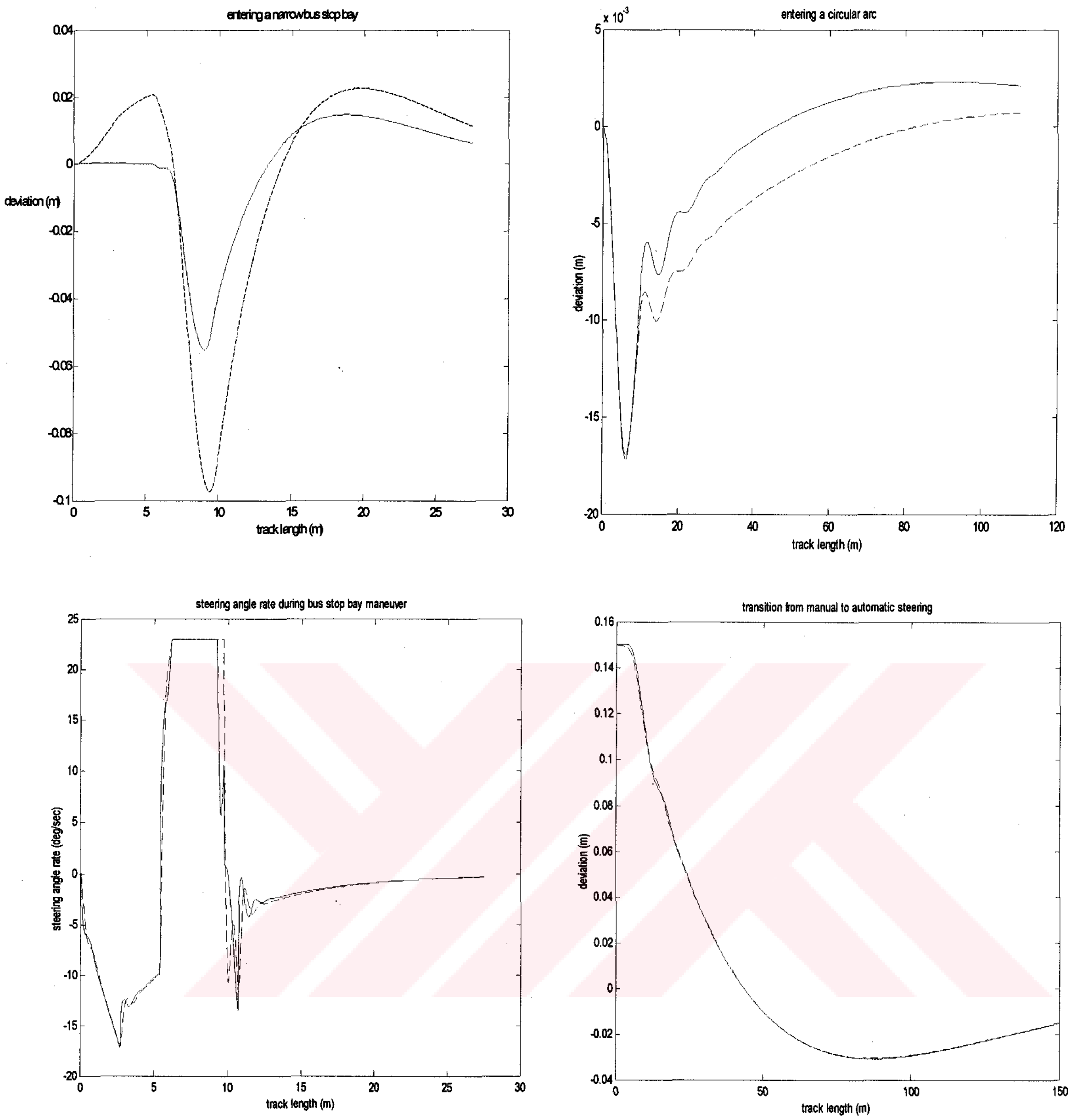

Figure 6.10 Simulation results with (solid) and without (dashed) model regulator

integrator. The effect of actuator saturation on model regulator performance will be investigated analytically in this part to demonstrate this point. Consider the system in Figure 6.13, which corresponds to the simulation study here with k_r=0 and the steering angle δ_f never saturating. u_r in Figure 6.13 is the actual, saturated steering angle rate signal entering the system.

The input-output relation (6.8) can be re-expressed as

$$y = (G_u + \Delta_u)u_r + d = G_u u_f + G_u(u_r - u_f) + \Delta_u u_r + d = G_u u_f + e_1 \qquad (6.13)$$

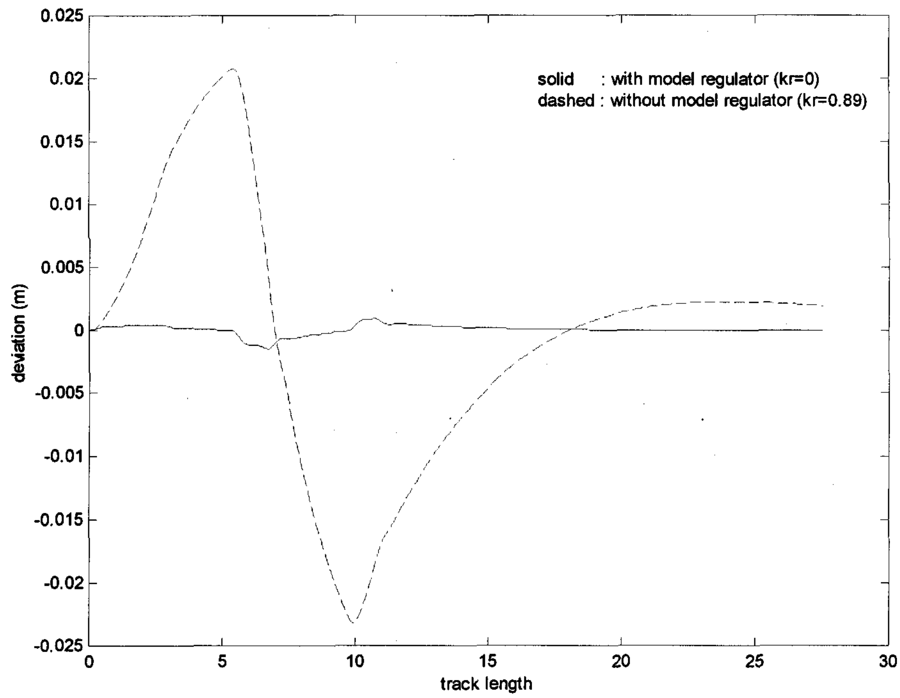

Figure 6.11 Bus stop bay maneuver simulation with increased saturation limit for $\dot{\delta}_f$

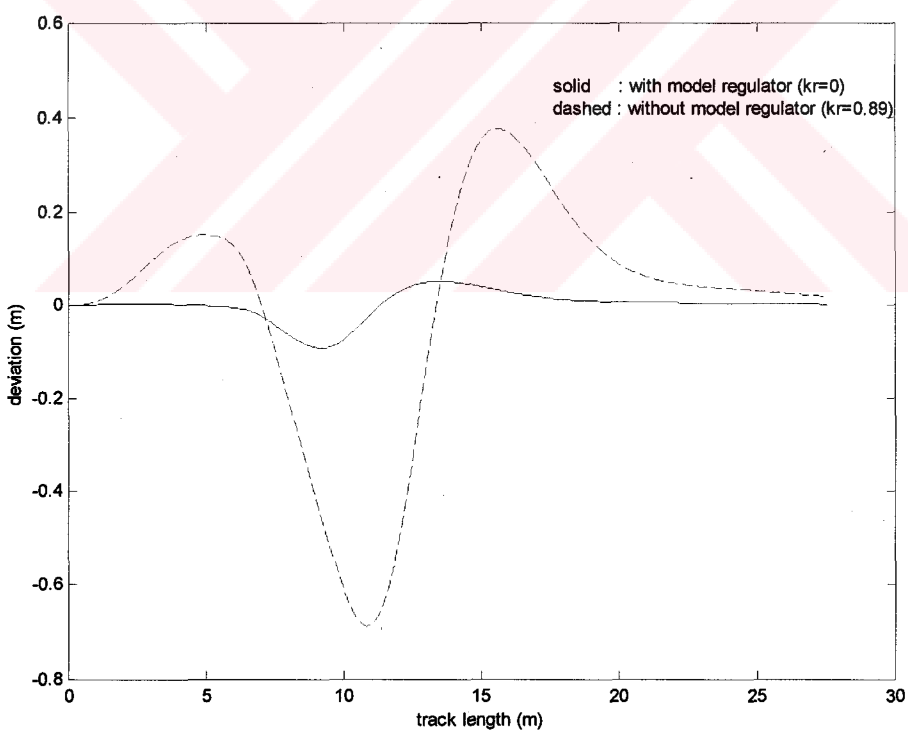

Figure 6.12 Bus stop bay maneuver simulation for low gain controller

where e_1 is the extended disturbance including saturation effects. The use of the model regulator implementation equation results in

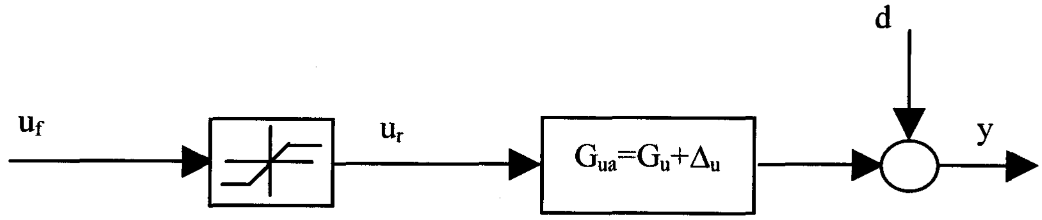

Figure 6.13 System with actuator saturation

$$y = \underbrace{G_u u_{new}}_{desired\ I/O\ relation} + \underbrace{\left(1 - G_u \tilde{G}_u^{-1}\right)e}_{\substack{undesired: due\ to\ model\ error \\ and\ external\ disturbance}} + \underbrace{\left(1 - G_u \tilde{G}_u^{-1}\right)G_u\left(u_r - u_f\right)}_{undesired: due\ to\ saturation} \tag{6.14}$$

as the input – output relation being achieved in practice. The first two terms in (6.14) are the same as before (see (6.11)) while the last term includes the effect of actuator saturation being represented in u_r-u_f, the difference between actual and saturated inputs, multiplied by $\left(1 - G_u \tilde{G}_u^{-1}\right)G_u$. Noting that the no model regulator case corresponds to $\tilde{G}_u^{-1} = 0$ in (6.14), the saturation term u_r-u_f is multiplied by G_u only, in this latter case. It is clear that, within its bandwidth, the model regulator helps alleviate problems due to the presence of actuator saturation by multiplying the $G_u(u_r - u_f)$ term by a small gain $\left(1 - G_u \tilde{G}_u^{-1}\right)$. This is illustrated in Figure 6.14 for the vehicle model considered here.

As seen from Figure 6.14, the presence of the integrator in the integrating actuator within the nominal system G_u results in large gains associated with the saturation effect at low frequencies here, thus significantly degrading performance. Thus, one approach to alleviation of the performance degradation due to actuator saturation, although not pursued here as the system in Ackermann et al (1995) is treated as existing hardware, is not to use an integrating actuator for steering.

6.5 Feedforward Compensation of the External Disturbance

Since the external disturbance ρ_{ref} can be previewed[3] during operation by using a look ahead sensor, it is also possible to use a disturbance feedforward compensator as illustrated in Figure 6.15 to cancel its effect.

[3] $\rho_{ref}(k+l)$ with l=3 here is available at sampling instant k.

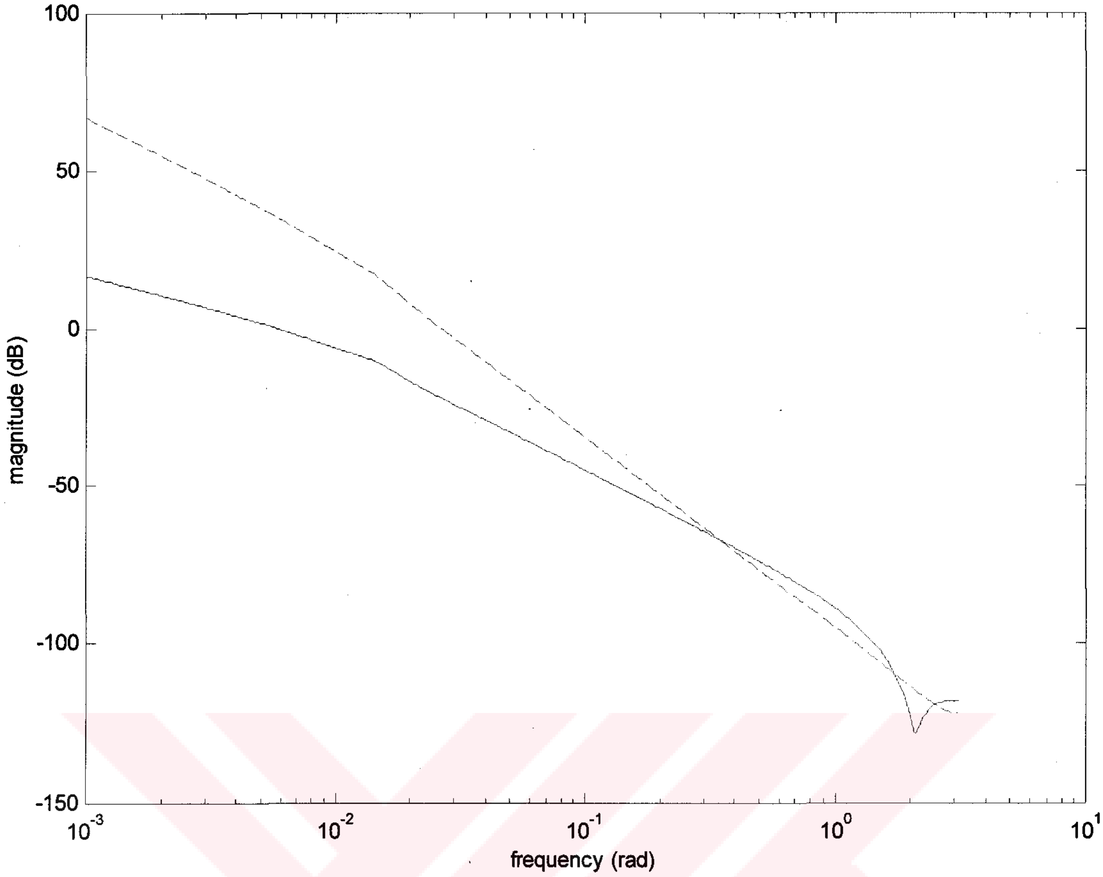

Figure 6.14 Effect of model regulator on actuator saturation ($G_u(z)$:dashed; $(1 - G_u(z)\tilde{G}_u^{-1}(z))G_u(z)$: solid)

The disturbance feedforward compensator is given by

$$G_{ffw}(z) = \tilde{G}_u^{-1}(z)G_{ref}(z) \tag{6.15}$$

Any one of a number of available discrete-time feedforward controller design techniques can be used to design $\tilde{G}_u^{-1}(z)$. $\tilde{G}_u^{-1}(z)$ given in (6.12) is used here except for the l-step delay (since preview is available). The simulation results displayed in Figure 6.16 as a solid line shows that the incorporation of the disturbance feedforward add-on controller improves response as compared to the results in Ackermann et al (1995) shown by the dashed line. The results are also slightly better than those obtained through the model regulator most probably due to the presence of the preview action. The steering angle rate saturates again during the simulations, thus degrading performance below what is theoretically achievable.

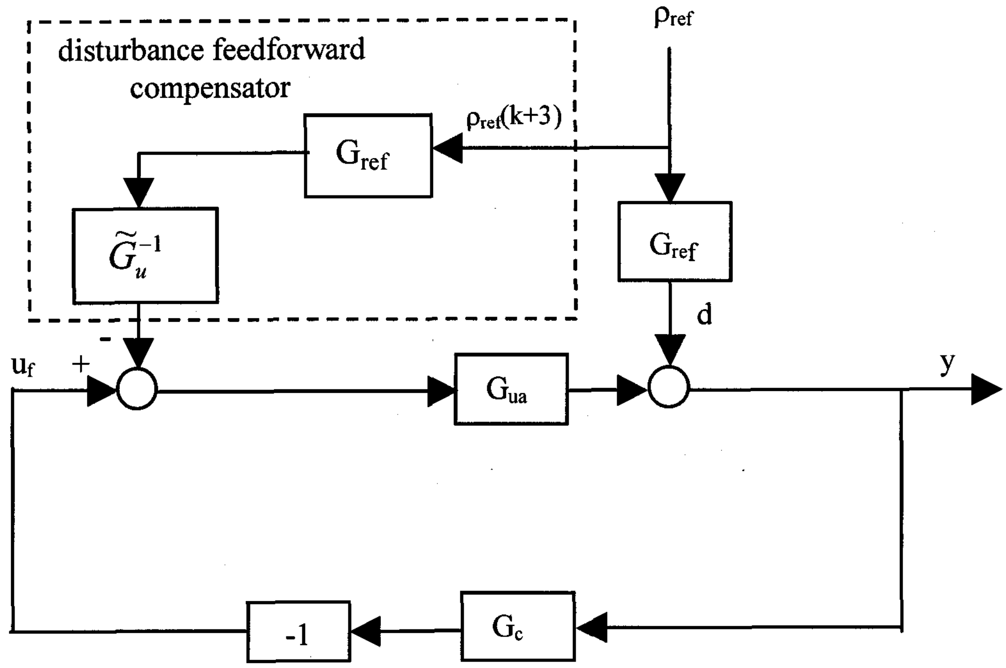

Figure 6.15 Disturbance feedforward add-on compensator structure

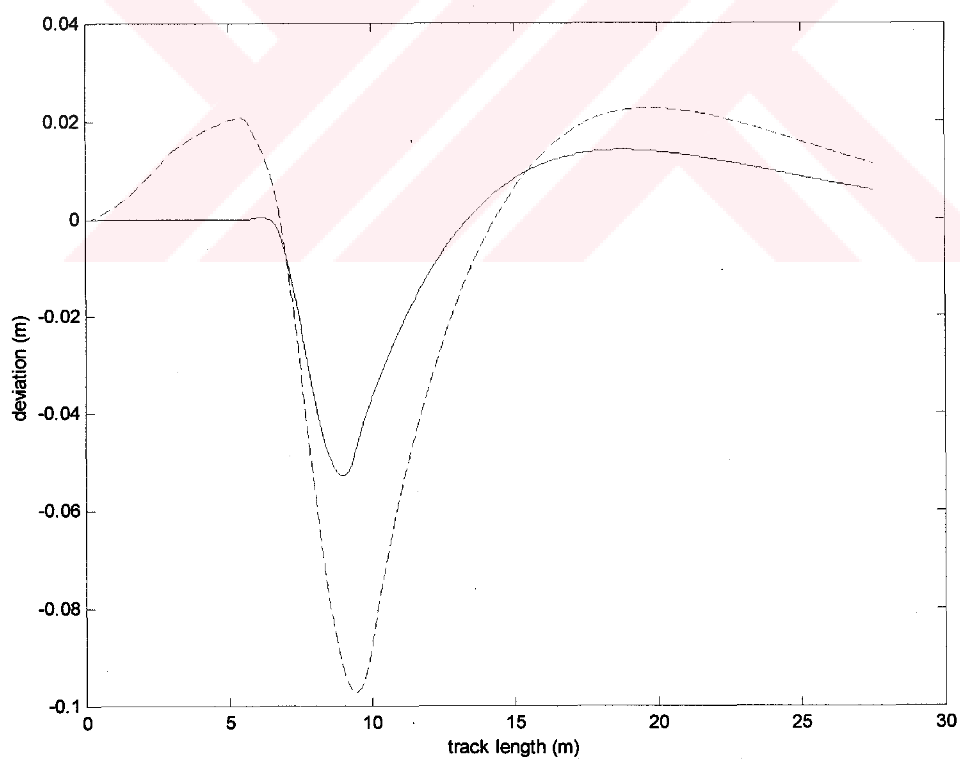

Figure 6.16 Bus stop bay maneuver simulation with feedforward add-on compensator

6.6 Discussion

A model regulator based add-on controller was used here for performance enhancement in automated path following. A disturbance feedforward based add-on compensator was also evaluated for the narrow bus stop bay maneuver. Both add-on compensators considered were implemented in discrete time. While the disturbance feedforward based add-on compensator was used only for improved disturbance rejection in following a well specified path, the model regulator based one was also able to do model regulation in the presence of model uncertainty and external disturbance and in particular achieve the desired yaw rate feedback dynamics without a yaw rate sensor. The data and simulation maneuvers were taken from Ackermann et al (1995) and correspond to a city bus. Both add-on compensators resulted in improved response as compared to the responses reported in Ackermann et al (1995) and were thus seen to be feasible for use in an actual system. One extra advantage of the model regulator based add-on compensator is that it requires no extra sensor for implementation. The disturbance rejection of the disturbance feedforward add-on compensator was slightly better due to its use of road curvature preview.

The performance enhancing effect of model regulator compensation in the presence of actuator saturation was also investigated analytically. However, steering angle rate saturation was still seen to be the major limitation hindering better results from being obtained with and without add-on compensation. Possible remedies are to use a steering actuator with a higher rate saturation value or not to use an integrating steering actuator.

7. ROBUST REPETITIVE CONTROL

A general architecture consisting of a reference feedforward control block and a model regulator was introduced as a robust motion controller in the previous chapters. Furthermore, this architecture was succesfully applied to several motion control problems, the most significant of them being vehicle steering control. There is a group of applications where the motion control problem addressed has periodic reference inputs or periodic disturbances. Motion controllers that take into account the periodic nature of the exogenous input work much better for such applications. Repetitive control is such a motion control scheme that has been developed specifically for handling systems with repetitive references/disturbances and will be treated in this chapter.

Repetitive control reduces error in systems with periodic reference inputs or disturbances with known period by introducing a highly frequency selective gain through a positive feedback loop containing a time delay element. The delay time is equal to the known period of the periodic reference/disturbance (see Figure 7.1). Significant improvements in the tracking accuracy or disturbance rejection characteristics of systems subject to periodic exogenous inputs can thus be achieved. Repetitive control was first used for rejection of periodic disturbances in a power supply control application (Inoue et al, 1981). Repetitive controllers have been shown to be effective and practical in a variety of applications including robot arm trajectory control (Omata et al, 1987; Sadegh et al, 1990), motor speed control (Kobayashi et al, 1990), friction dominated motion control (Tung et al, 1991), control of continuous steel casting (Jolly et al, 1993), control of material testing (Shaw and Srinivasan, 1993), machine tool motion control (Tsao and Tomizuka, 1994), control of cold rolling (Garimella and Srinivasan, 1996), disk drive track following control (Moon et al, 1998), CD player tracking control (Lee and Smith, 1998) and vibration attenuation of engineering structures (Prell et al, 1999).

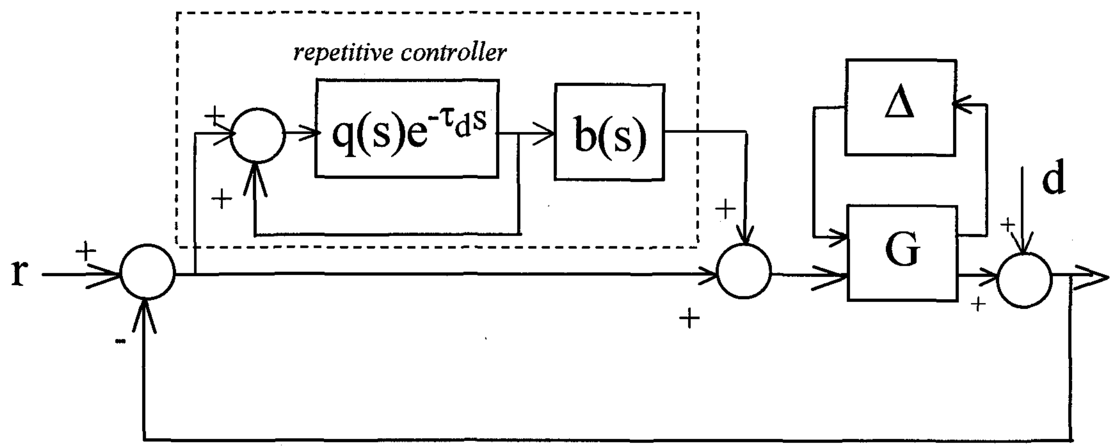

Figure 7.1 Repetitive control structure

Early theoretical developments relating to repetitive control systems had focused primarily on stability issues in continuous-time systems (Hara et al, 1988; Srinivasan and Shaw, 1991), and discrete-time systems (Tomizuka et al, 1989). In recent years, considerable research effort has been devoted to analysis and design for stability and performance robustness. Stability robustness of repetitive control systems in the presence of unstructured modeling error has been analyzed by Tsao and Tomizuka (1994). The robust repetitive controller design procedure of Srinivasan et al (1995) is based on Nevanlinna-Pick interpolation. Available robust control theory (e.g., Özbay, 1993) has been modified as appropriate and applied to repetitive control systems by Peery and Özbay (1997) on their work on repetitive controller design based on Youla parametrization. Moon et al (1998) have introduced a robust design method for parametric uncertainty in interval plants under repetitive control. A similar approach has been taken by Roh and Chung (1995). H_∞ controller design for MIMO repetitive control has been treated by Weiss and Häfele (1999). SSV-analysis has been used for assessing stability and performance robustness of SISO continuous time repetitive control systems by Güvenç (1996). SSV-synthesis has been applied to sampled data repetitive controller design by Li and Tsao (1998).

The repetitive controller design approach presented here is significantly different than those of the abovementioned references. Simple and, therefore, easily implementable repetitive controller filter architectures are fixed from the beginning and parameter values within these filters are tuned to satisfy frequency domain performance specifications, finally obtaining a region in controller parameter space where the desired specifications are met. Relevant basic information on repetitive control is presented in Section 7.1. The technique of mapping frequency domain performance specifications into controller parameter plane and its use in repetitive controller design is given in Section 7.2. A numerical example using a servohydraulic material testing machine application is used in Section 7.3 to demonstrate the effectiveness of the method.

7.1 Repetitive Controller Basics

Consider the repetitive control structure shown in Figure 7.1. Repetitive controller design involves the design of the two filters b(s) and q(s). Ideally, q(s) is desired to be unity as the positive feedback loop around the delay element becomes a generator of periodic signals with period τ_d in that case. This is not possible in practice, the main reason being that the repetitive control system is not robustly stable in that case (Weiss, 1997, Hara et al, 1988). q(s) is therefore chosen as a low pass filter with unity d.c. gain. Its cutoff frequency determination involves a trade-off between accuracy and stability robustness.

The main use of b(s) is to improve relative stability and steady state accuracy in combination with q(s). Consider the function of frequency given by

$$R(\omega) = \left| q(j\omega)\left(1 - b(j\omega)\frac{G(j\omega)}{1+G(j\omega)}\right)\right| \tag{7.1}$$

which is called the regeneration spectrum in Srinivasan and Shaw (1991). According to the same reference, $R(\omega)<1$ for $\forall\omega$ is a sufficient condition[4] for stability. Furthermore, $R(\omega)$ can be used to obtain a good approximation of the locus of dominant characteristic roots of the repetitive control system for large time delay, thus, resulting in a measure of relative stability as well. Accordingly, b(s) is designed to approximately invert G/(1+G) within the bandwidth of q(s) in an effort to minimize $R(\omega)$.

---

[4] becomes a sufficient and necessary condition as τ_d becomes large

Small time advances are incorporated into q(s) and b(s) here as

$$q(s) = q_1(s)e^{\tau_q s} \tag{7.2}$$

$$b(s) = b_1(s)e^{\tau_b s} \tag{7.3}$$

to improve performance. The loop gain of the repetitive control system and its sensitivity function are given by

$$L = G\left(1 + \frac{qe^{-\tau_d s}}{1 - qe^{-\tau_d s}} b\right) \tag{7.4}$$

$$S = \frac{1}{1+L} \tag{7.5}$$

The design procedure can be made more quantitative by specifying upper bounds on the sensitivity function magnitude at the fundamental frequency and its harmonics as

$$\left|S(j\omega)\right|_{\omega=\frac{2\pi}{\tau_d}k} < (S_{des})_k \; ; \; k = 1,2,\cdots,n \tag{7.6}$$

where n/τ_d is the largest frequency (in Hz) where significant tracking error reduction is desired. Note that requirement (7.6) can also be expressed as the weighted sensitivity (nominal performance) requirement

$$\begin{aligned} &\left|W_S(\omega)S(j\omega)\right| = \left|\frac{W_S(\omega)}{1+L(j\omega)}\right| < 1 \;\; or \;\; equivalently \\ &\left|W_S(\omega)\right| < \left|1 + L(j\omega)\right| \end{aligned} \tag{7.7}$$

where the weight W_S is a discontinuous weight corresponding to (7.6) at the fundamental frequency and its harmonics.

The plant under repetitive control is assumed to have unstructured modeling error (especially at high frequencies) here. So, the weighted complementary sensitivity (robust stability) requirement

$$\begin{aligned} &|W_T(\omega)T(j\omega)| = \left|\frac{W_T(\omega)L(j\omega)}{1+L(j\omega)}\right| < 1 \quad or \quad equivalently \\ &|W_T(\omega)L(j\omega)| < |1+L(j\omega)| \end{aligned} \tag{7.8}$$

should be satisfied.

7.2 Mapping Frequency Domain Specifications Into Controller Parameter Space

7.2.1 General Procedure

The aim in this section is to introduce the general technique of finding the region in the chosen controller parameter plane where design specifications (7.7) and (7.8) on sensitivity and complementary sensitivity are satisfied. These specifications are illustrated graphically in Figures 7.2 and 7.3. Initial work on the algebraic formulation for mapping of frequency domain performance specifications of the form (7.7) and (7.8) into controller parameter space can be found in Djaferis (1991), Saeki and Hirayama (1996) and Saeki and Kimura (1997). The main idea of solving (7.7) and (7.8) frequency at a time for a chosen pair of controller parameters within L is also used here.

Consider the robust stability problem (7.8). Consider Figure 7.3 which illustrates (7.8) with an equality sign (called the point condition here). Apply the cosine rule to the triangle with vertices at the origin, -1 and **L** in Figure 7.3 to obtain

$$|W_T L|^2 = |L|^2 + 1^2 + 2|L|\cos\theta_L \tag{7.9}$$

(7.9) is a quadratic equation in |L| and its solutions are

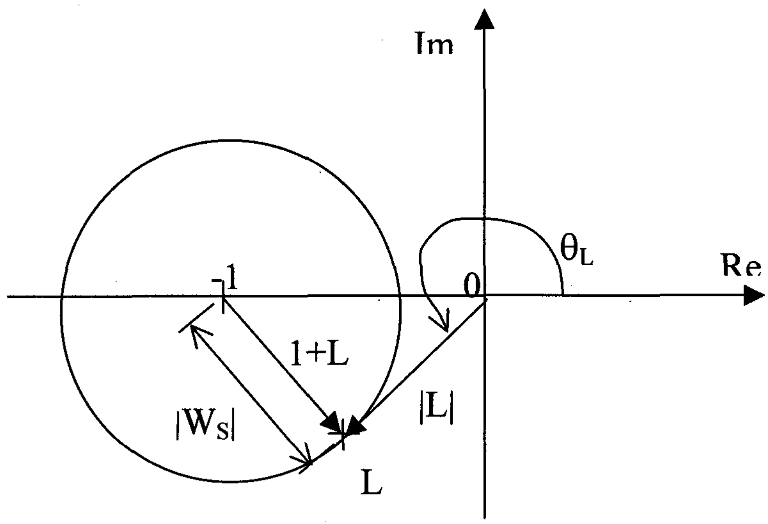

Figure 7.2 Illustration of the point condition (for nominal performance)

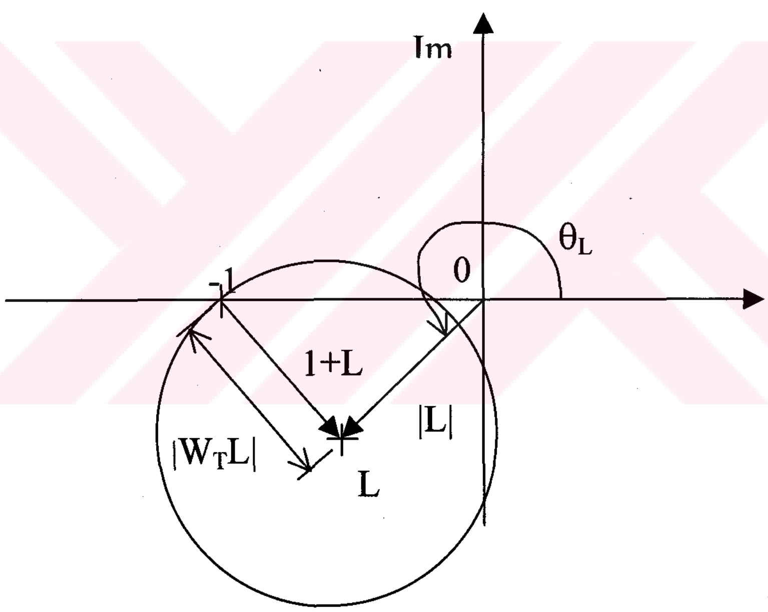

Figure 7.3 Illustration of the point condition (for robust stability)

$$|L| = \frac{-\cos\theta_L \pm \sqrt{Disc}}{1-|W_T|^2} \tag{7.10}$$

where

$$Disc = 1 + \cos^2\theta_L + |W_T|^2 \tag{7.11}$$

Only, positive and real solutions for |L| are allowed, i.e. *Disc*≥0 must be satisfied. Once L is determined, the loop gain equation has to be back solved at that frequency for the repetitive controller filter q(s) whose parameters will be tuned here. This back solution results in

$$q_1 = \frac{L-G}{L-G(1-b)} e^{(\tau_d - \tau_q)s} \tag{7.12}$$

The point condition solution procedure for robust stability is outlined below:

1. Choose a specific ω value. $|W_T|$, G and b at ω are all known after this choice.

2. Let $\theta_L \in [0:2\pi]$. Evaluate *Disc* using (7.11) and select the active range of θ_L where *Disc*≥0 is satisfied.

For all values of θ_L in the active range

3. Evaluate |L| using (7.10). Keep only the positive solutions.

4. Solve for the corresponding filter q_1 at the chosen frequency ω by using (7.12).

5. Using the specific structure of $q_1(s)$, back solve for the two chosen controller parameters.

6. Plot the closed curve in the chosen controller parameter plane. Either the inside (drawn with solid boundary) or outside (drawn with dashed boundary) of this curve is a solution of (7.8) at the chosen frequency.

7. Go back to Step 1 and repeat the procedure at a different frequency.

This procedure is easily programmable and quickly results in a graphical description of the solution of (7.8) at the chosen frequencies. The solution procedure for the nominal performance requirement (7.7) will not be presented here for the sake of brevity, as its derivation is quite similar to the derivation given above.

Application to Repetitive Control

Here, $q_1(s)$ is chosen as a multiplication of second order controllers given by

$$q_1(s)=\prod_{i=1}^{n}\frac{b_{2i}s^2+b_{1i}s+b_0}{s^2+a_{1i}s+a_{0i}} \tag{7.13}$$

Initially, n=1 is used and the design procedure in Section 7.2.1 is carried out. The back solution procedure in Step 5 of the solution procedure is performed using the relations

$$\mathrm{Re}(q_1)=\frac{(b_0-b_2\omega^2)(a_0-\omega^2)+a_1b_1\omega^2}{(a_0-\omega^2)^2+(a_1\omega)^2} \tag{7.14}$$

$$\mathrm{Im}(q_1)=\frac{b_1\omega(a_0-\omega^2)-a_1\omega(b_0-b_2\omega^2)}{(a_0-\omega^2)^2+(a_1\omega)^2} \tag{7.15}$$

where the subscript *i* in (7.13) has been dropped. If satisfactory performance is not obtained for n=1, the designed $q_1(s)$ is incorporated into the plant and a new second order form in (7.13) is tuned to improve performance.

7.3 Numerical Example

The servohydraulic material testing machine example of Srinivasan and Shaw (1991) is used here as a numerical example to illustrate the design method developed in the previous section. The plant is given by

$$G(s)=\frac{K}{s(\tau_{sv}s+1)\left(\frac{s^2}{\omega_h^2}+\frac{2\zeta_h s}{\omega_h}+1\right)} \tag{7.16}$$

where K=150 includes the effect of proportional control. The numerical values of the other parameters are τ_{sv} = 0.00187 sec, ζ_h = 0.4 and ω_h= 618 rad/sec. The repetitive controller filter b(s) used in Srinivasan and Shaw (1991) is

$$b(s) = e^{0.007s} \tag{7.17}$$

The filter q(s) is modified here into

$$q(s) = e^{0.001414s} q_1(s) = e^{0.001414s} \frac{a_0}{s^2 + a_1 s + a_0} \tag{7.18}$$

and regions in a_1 - a_0 controller parameter plane where the nominal performance and robust stability requirements in (7.7) and (7.8), respectively, are satisfied are computed.

The sensitivity constraint which is also specified in the discrete frequency formulation of (7.6) was evaluated for a high frequency and a lower frequency periodic command input with period τ_d corresponding to 0.04 sec and 0.1 sec, respectively. The specific numerical values used in the computations are given in Tables 7.1 and 7.2. The corresponding solution region is shown as the hatched region in Figure 7.4. A uniform weight for the stability robustness requirement for frequencies above 175 Hz is chosen here as $|T|<0.0546$ for $f>175$ Hz. Note that this corresponds to a discontinuous weight W_T. The corresponding region in the a_1 - a_0 controller parameter plane where robust stability and the nominal performance requirement (7.6) are both satisfied is shown as the hatched region in Figure 7.5.

The final design is completed by selecting a point in Figure 7.5. This choice is done rather arbitrarily here and the design point chosen is marked with a cross in Figure 7.5. Although not exploited here, this selection could also have been based on optimization of nominal performance or minimization of structured singular value for a parametric representation (see Güvenç, 1996). The simulation results of Figure 7.6 for triangular wave inputs with periods of 10 Hz and 25 Hz show the effectiveness of the design in reducing periodic error components. The physically implementable, equivalent form of the repetitive control system architecture shown in Figure 7.7 was used in the simulations.

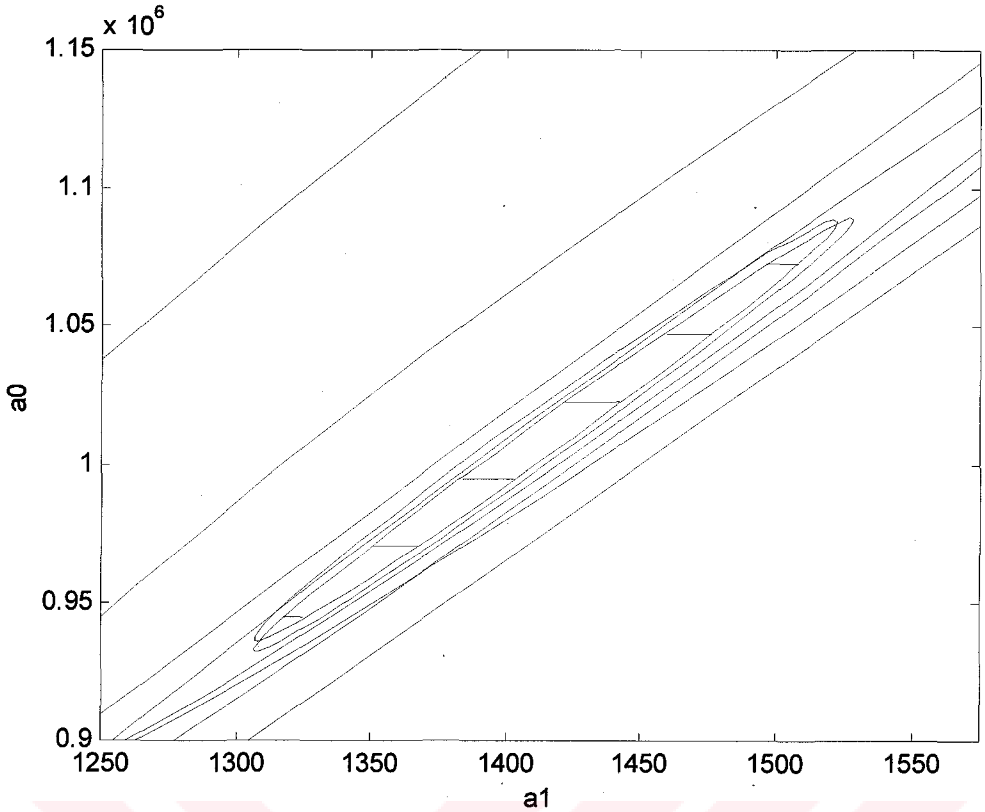

Figure 7.4 Solution region satisfying nominal performance requirement

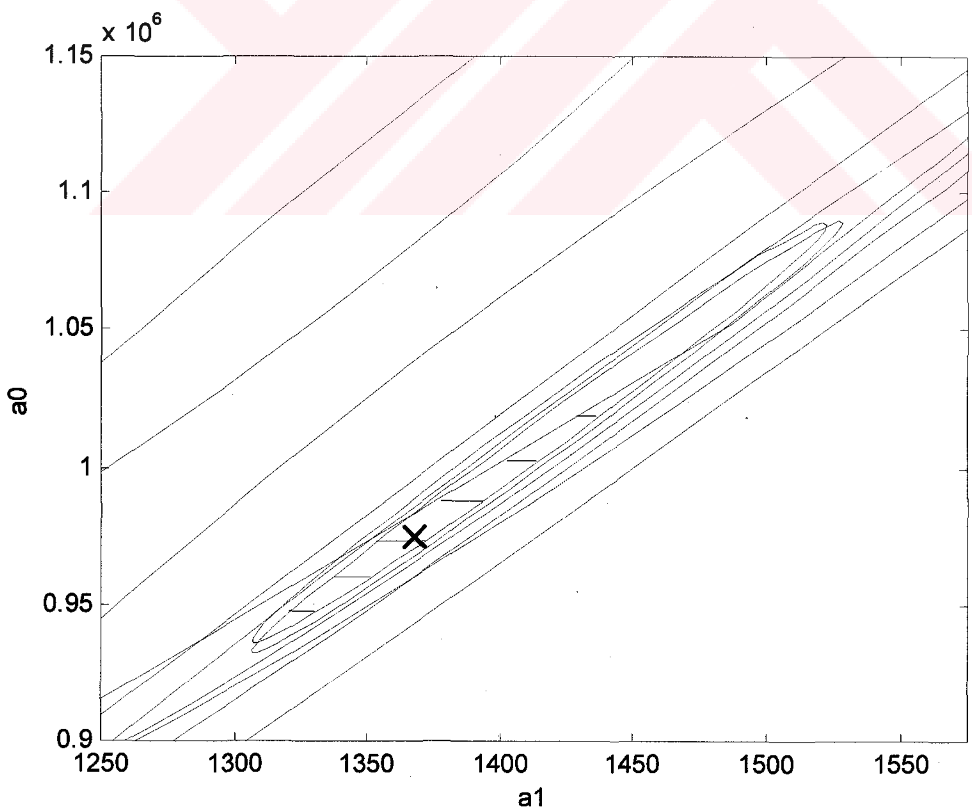

Figure 7.5 Region where both nominal performance and robust stability are satisfied

7.4 Summary

A method of robust repetitive controller design through mapping of frequency domain constraints (some of them being at discrete frequencies of interest) to controller parameter space was presented here. The main idea was to use a simple, easily implementable structure for the repetitive controller filter and find solution regions in the chosen controller parameter plane where the frequency domain specifications on nominal performance and robust stability are satisfied. The method was well suited to the structure of a repetitive control system with discrete frequencies of interest. The computations were also quite fast. It should also be noted that the time delay and the corresponding infinite dimensional nature of the repetitive control system pose no problems for the method introduced here. Using the method of this chapter, it is also possible to treat plants with time delay under repetitive control.

Fundamental and Harmonics		
k	$f=k/\tau_d$ (Hz)	S_{des}
1	25	1/500
2	50	1/30
3	75	1/6

Table 7.1 Desired sensitivity magnitude upper bounds at τ_d=0.04 sec

Fundamental and Harmonics		
k	$f=k/\tau_d$ (Hz)	S_{des}
1	10	1/1000
2	20	1/500
3	30	1/300

Table 7.2 Desired sensitivity magnitude upper bounds at τ_d=0.1 sec

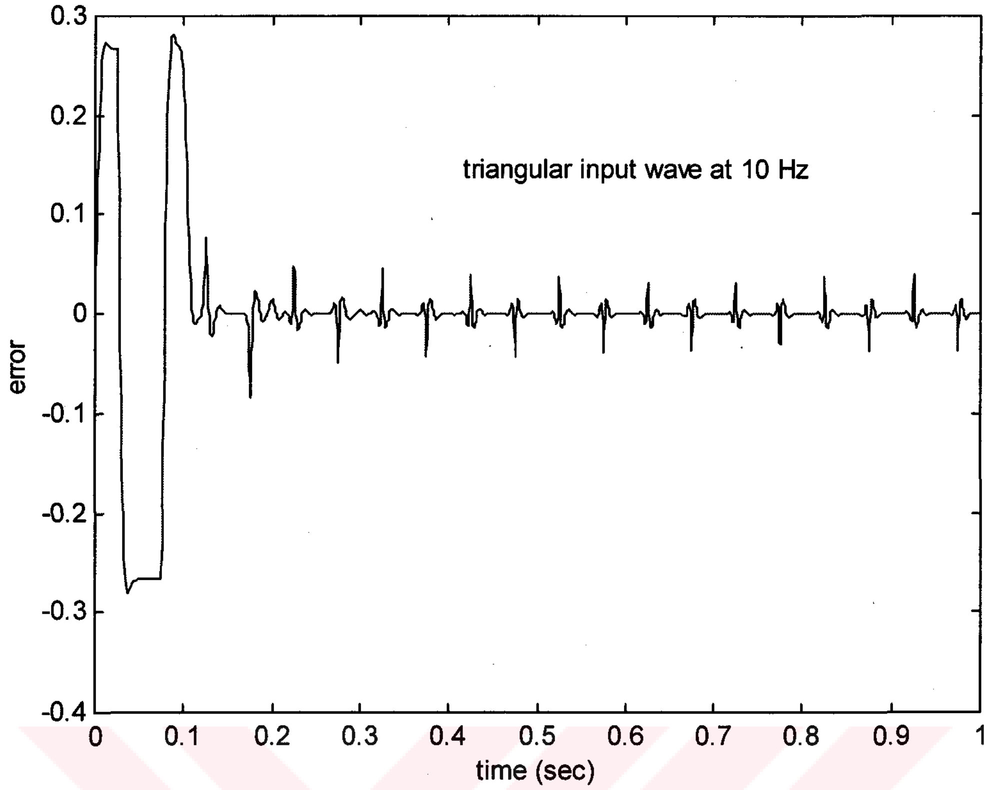

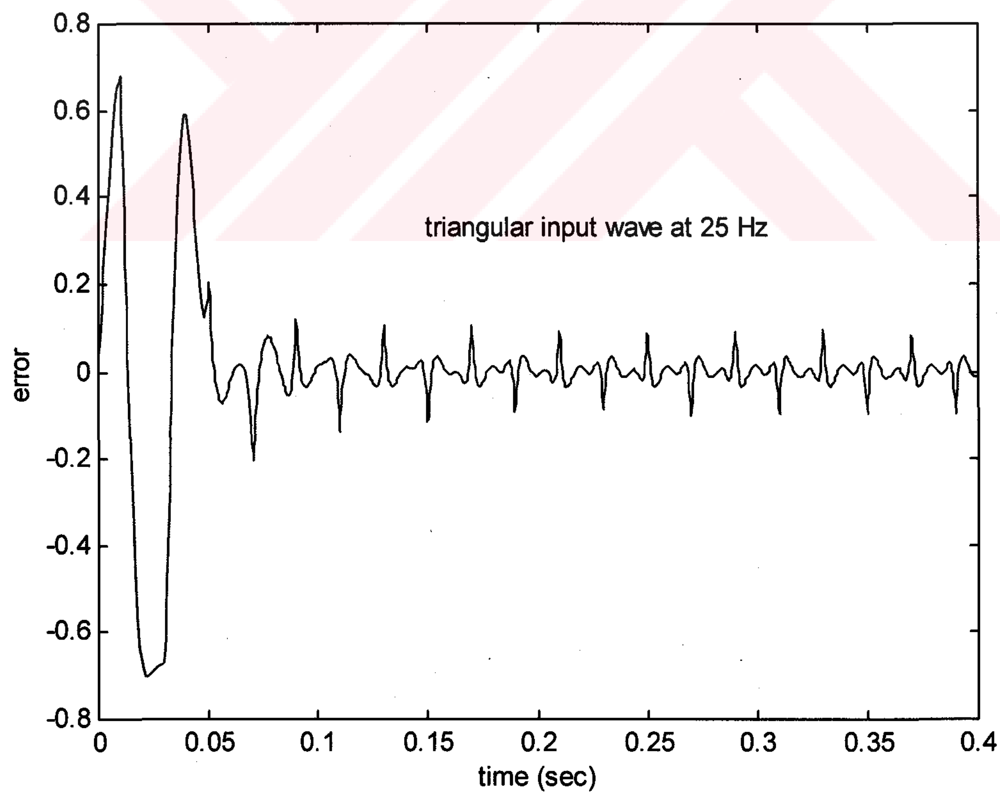

Figure 7.6 Simulation results

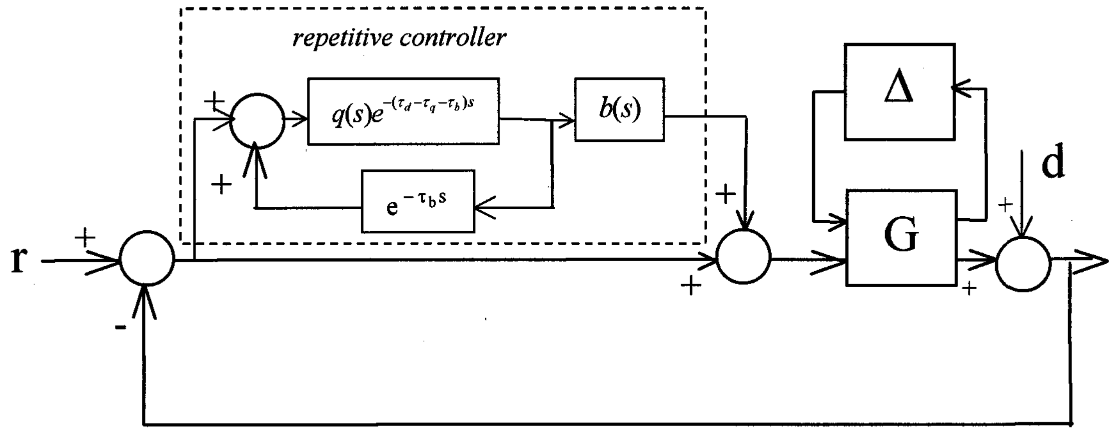

Figure 7.7 Repetitive control architecture for implementation

8. CONCLUSIONS

This thesis was on applied robust motion control. A generic robust motion control architecture consisting of an inner model regulator and a preview based feedforward controller was introduced for that purpose. Considering the possibility of periodic reference inputs or disturbances, as is typical of applications involving rotating machinery for example, a repetitive control architecture was also introduced and treated in this thesis. The main application examples treated in the thesis came from the field of vehicle dynamics control. Stability and performance robustness analysis was carried out using complex, mixed and real SSV methods. A mixed sensitivity measure for nonstandard robust performance was chosen as the design goal. An interactive graphical approach for robust performance design was developed and used to obtain the solution regions in the chosen plane of controller parameters.

In Chapters 2 and 3, preview based discrete time reference feedforward tracking control was analyzed in detail. The optimal precision tracking control method was developed for systems with and without complex non minimum phase zeros. This method was compared with several existing methods and found to be superior in performance and ease of design. The use of mixed SSV analysis was shown to be an effective method of assessing the performance robustness of preview based feedforward control schemes. The achievement and robust maintenance of the zero phase error property of such systems was also shown to be an important measure of (robust) performance. Preview based feedforward control schemes are most useful in high speed, high accuracy machining applications and a noncircular turning application was treated. In a later chapter, the developed method was also applied successfully to preview based rejection of the road curvature change disturbance in a vehicle path following application.

The main part of the thesis was on a two degree of freedom control structure known as the model regulator and its application to vehicle dynamics control problems. In Chapter 4, along with an introduction to the model regulator, its integral action capability and its applicability to open loop unstable plants were also demonstrated. The use of real SSV analysis was shown to be a much less conservative tool as compared to the standard small gain type test for stability robustness of the model regulator. Mixed SSV analysis was used to obtain a corresponding performance robustness analysis method for the model regulator. The developed SSV analysis method also showed that significant resonances of the regulated system should not lie at frequencies close to the bandwidth frequency of the model regulator.

The model regulator was applied to vehicle steering control with the aim of yaw stabilization and yaw response improvement. Both steer-by-wire and auxiliary steering actuation methods were treated. This novel application of the model regulator as a vehicle steering controller resulted in the development of significant application related architectural modifications. One of these architectural modifications, also used in Chapter 6, was for implementability in the presence of significant actuator saturation. A velocity based gain scheduling formulation of the model regulator was also developed for practical vehicle steering control over a wide range of operating speeds. Considering the man machine interface where the steering controller was desired to intervene only during the initial panic reaction time of the driver, fading implementations with a band pass filter formulation and with limited integrator action were formulated. Simulation results showed good steering command following and excellent disturbance rejection within the operating domain of the vehicle considered. Moreover, the results obtained were seen to be superior to results reported in the literature with other steering controllers. More realistic simulation studies also verified these statements on improved response. An interactive, graphical design method was also developed to solve the robust performance problem for the model regulator architecture and used in designing the vehicle steering controllers used.

An automated path following application was treated in Chapter 6. Both a model regulator and a preview based feedforward control architecture were successfully applied. The automated path following control of a city bus available in the literature was treated. A discrete time implementation was used to investigate the sampling related difficulties and to demonstrate the associated plant inversion type design techniques. The superior performance of the model regulator in the presence of actuator saturation was also shown. The results obtained were seen to be much better than previously reported results, available in the literature for this benchmark problem.

Considering the presence of a lot of motion control problems involving periodic reference inputs and disturbances, the repetitive control method was treated in Chapter 7. A combination of nominal performance and robust stability was chosen as the measure of robust performance. An interactive, graphical design method was developed to solve this problem for repetitive controller design. A unique feature of this design method was its capability of using discontinuous weights and hence concentrating only on chosen frequencies, a must for repetitive control. The design technique was successfully applied to a material testing machine application taken from the literature.

REFERENCES

Ackermann, J. and Darenberg W., 1990. "Automatic Track Control of a City Bus," *IFAC Theory Report on Benchmark Problems for Control Systems Design.*

Ackermann J. and Sienel W., 1990. "Robust Control for Automatic Steering," in *Proc. American Control Conference*, pp. 795-800.

Ackermann, J., Bartlett, A., Kaesbauer, D., Sienel, W. and Steinhauser, R., 1993. *Robust Control: Systems with Uncertain Physical Parameters*, Springer, London.

Ackermann J., Guldner J., Sienel W., Steinhauser R. and Utkin V.I., 1995. "Linear and Nonlinear Controller Design for Robust Automatic Steering," *IEEE Trans. on Control Systems Technology*, vol. 3, no. 1, pp. 132-143.

Aksun Güvenç, B., and Güvenç, L., 1999. "Optimal Precision Tracking Control of Discrete Time Nonminimum Phase Systems," *Proc. European Control Conference.*

Anonymous, 2000. *VEDYNA User Guide*, TESIS Dynaware GmbH, Munich.

Aström, K. J., Hagander, P. and Sternby, J., 1984. "Zeros of Sampled Systems," *Automatica*, vol. 20, pp. 31-38.

Balas, G.J., Doyle, J.C., Glover, K., Packard, A. and Smith, R., 1995. *μ-Analysis and Synthesis Toolbox*, Mathworks, Mass.

Barmish B., Khargonekar P., Shi Z. and Tempo R., 1989. "Robustness Margin Need Not Be a Continuous Function of the Problem Data," *System and Control Letters*, vol. 15, pp. 91-98.

Bünte T., Odenthal D., Aksun Güvenç B. and Güvenç L., 2001. "Robust Vehicle Steering Control Based on the Disturbance Observer," *IFAC Workshop on Advances in Automotive Control (AAC).*

Cannon R. H. and Schmitz, E., 1984. "Initial Experiments on the Control of a Flexible Manipulator," *International Journal of Robotics Research*, vol. 3, pp. 62-75.

Chiang R.Y. and Safonov M.G. 1992. *Robust Control Toolbox*, Mathworks, Mass.

Djaferis, T.E., 1991. "Representations of Controllers that Achieve Robust Performance for Systems with Real Parameter Uncertainty," *Systems and Control Letters*, vol. 16, pp. 329-339.

Doyle, J.C., 1982. "Analysis of Feedback Systems with Structured Uncertainties," *IEE Proceedings*, Part D, vol. 133, pp. 45-56.

Doyle, J.C., 1984. *Lecture Notes on Advances in Multivariable Control*, ONR/Honeywell Workshop, Minneapolis.

Doyle J.C., Francis B.A. and Tannenbaum A.R., 1992 *Feedback Control Theory*, Macmillan, New York.

Elgersma M., Freudenberg J. and Morton B., 1996. "Polynomial Methods for the Structured Singular Value with Real Parameters," *International Journal of Robust and Nonlinear Control*, vol. 6, pp. 147-170.

Fan, M.K.H., Tits, A.L. and Doyle, J.C., 1991. "Robustness in the Presence of Mixed Parametric Uncertainty and Unmodeled Dynamics," *IEEE Transactions on Automatic Control*, vol. AC-36, no. 1, pp. 25-38.

Fu, Y. and Dumont, G.A., 1989. "Choice of Sampling to Ensure Minimum-Phase Behaviour," *IEEE Transactions on Automatic Control*, vol. 34, no. 5, pp. 560-563.

Garimella, S.S. and Srinivasan K., 1996. "Application of Repetitive Control to Eccentricity Compensation in Rolling," *ASME Journal of Dynamic Systems, Measurement, and Control*, vol. 118, pp. 657-664.

deGaston R.R. and Safonov M.G., 1988. "Exact Calculation of the Multiloop Stability Margin," *IEEE Transactions on Automatic Control*, vol. AC-33.

Gross, E., Tomizuka, M. and Messner, W., 1994. "Cancellation of Discrete Time Unstable Zeros by Feedforward Control," *ASME Journal of Dynamic Systems, Measurement and Control*, vol. 116, no. 1, pp. 33-38.

Güvenç, L., 1996. "Stability and Performance Robustness Analysis of Repetitive Control Systems Using Structured Singular Values," *ASME Journal of Dynamic Systems, Measurement, and Control*, vol. 117, pp. 593-597.

Güvenç L., 1999. "Closed Loop Pneumatic Position Control Using Discrete Time Model Regulation," in *Proc. American Control Conference*, pp. 4273-4277.

Güvenç, L., Harib, K. and Srinivasan, K., 1995. "Extended Precision Tracking Control of Discrete-Time Nonminimum Phase Systems," *Proc. ASME International Mechanical Engineering Congress and Exposition*, San Fransisco, DSC-vol. 57-1, pp. 151-158.

Güvenç L. and Srinivasan K., 1994. "Friction Compensation and Evaluation for a Force Control Application," *J. of Mechanical Systems and Signal Processing*, vol. 8, no. 6, pp. 623-638.

Haack, B. and Tomizuka, M., 1991. "The Effect of Adding Zeros to Feedforward Controllers," *ASME Journal of Dynamic Systems, Measurement and Control*, vol. 113, no. 1, pp. 6-10.

Hara, S., Yamamoto, Y., Omata, T. and Nakano, M., 1988. "Repetitive Control System: A New Type Servo System for Periodic Exogenous Signals," *IEEE Transactions on Automatic Control*, vol.33, pp.657-667.

Inoue, T., Nakano, M. and Iwai, S., 1981. "High Accuracy Control of a Proton Synchrotron Magnet Power Supply," *Proceedings of the 8th World Congress of IFAC*, pp. 258-292.

Ishitobi, M., 1992. "Conditions for Stable Zeros of Sampled Systems," *IEEE Transactions on Automatic Control*, vol. 37, no. 10, pp. 1558-1561.

Jolly, T., Tsao, T.C. and Bentsman, J., 1993, "Rejection of Unknown Periodic Load Disturbances in Continuous Steel Casting Processes Using Learning Repetitive Control Approach," *IEEE Symposium on Intelligent Control Systems*.

Jury, E.I., 1964. *Theory and Application of the Z-Transform*, Wiley, New York.

Kempf C. J. and Kobayashi S., 1999. "Disturbance Observer and Feedforward Design for a High-Speed Direct-Drive Positioning Table," *IEEE Trans. on Control Systems Technology*, vol. 7, no.5, pp. 513-526.

Kobayashi, F., Hara, S. and Tanaka, H., 1990. "Reduction of Motor Speed Fluctuation Using Repetitive Control," *29th IEEE Conference on Decision and Control*, pp. 1697-1702, Hawaii.

Lee, R.C.H. and Smith, M.C., 1998. "Repetitive Control Experiments for a CD Player," *American Control Conference*, pp. 2682-2684.

Li, J. and Tsao, T.C., 1998. "Robust Performance Repetitive Control Design Using Structured Singular Values and Its Implementation," *ASME International Mechanical Engineer's Congress and Exposition*.

Liu C.-S.and Peng ,H., 2000. "Disturbance Observer Based Tracking Control," *ASME Journal of Dynamic Systems, Measurement and Control*, vol. 122, pp.332-335.

Menq, C. H. and Xia, J.Z., 1990. "Characterization and Compensation of Discrete-Time Nonminimum-Phase Zeros for Precision Tracking Control," *Symposium on Robotics Research*, DSC-vol. 26, pp. 15-23, ASME, New York.

Menq, C. H., and Xia, J.Z.,1995. "Precision Ttracking Control of Nonminimum-Phase Systems with Zero Phase Error," *Int. J. of Control*, vol. 61, no. 4, pp. 791-807.

Mita, T., Hirata, M., Murata, K. and Zhang, H., 1998. "H∞ Control Versus Disturbance-Observer Based Control," *IEEE Transactions On Industrial Electronics*, vol. 45, no. 3, pp. 488-495

Moon, J.H., Lee, M.N. and Chung, M., 1998. "Repetitive Control for the Track-Following Servo System of an Optical Disk Drive," *IEEE Trans. on Control Systems Technology*, vol. 6, no. 5, pp. 663-670.

Ogata, K., 1990. *Modern Control Engineering*, Prentice Hall.

Ohnishi K., 1987."A New Servo Method in Mechatronics," *Trans. Japanese Soc. Elect. Eng.*, vol. 107-D, pp. 83-86.

Omata, T., Hara, S. and Nakano, M., 1987, "Nonlinear Repetitive Control with Application to Trajectory Control of Manipulators," *Journal of Robotic Systems*, vol. 4, No. 5, pp. 631-652.

Owen, J. G.and Zames G., 1993. "Duality Theory of Robust Disturbance Attenuation," *Automatica*, vol. 29, no. 3, pp. 695-705.

Özbay, H., 1993. "H^∞ Optimal Controller Design for a Class of Distributed Parameter Systems," *International Journal of Control*, vol. 58, pp. 739-782.

Packard, A. and Doyle, J.C., 1993. "The Complex Structured Singular Value," *Automatica*, vol. 29, pp. 71-109.

Packard A. and Pandey P., 1991. "Continuity Properties of the Real/Complex Structured Singular Value," *IEEE Transactions on Automatic Control*, vol. AC-38, pp. 415-428.

Peery, T. and Özbay, H., 1997. "H^∞ Optimal Repetitive Controller Design for Stable Plants", *ASME Journal of Dynamic Systems, Measurement, and Control*, vol. 119, pp. 541-547.

Prell, A .P., Tsao, T. C. and Bergman, L.A., 1999. Application of Repetitive Control to Vibration Attenuation in Certain Engineering Structures," *Journal of Vibration and Control*, vol. 5, pp. 741-760.

Roh, C. L. and Chung, M. J., 1995. "Design of Repetitive Control System for an Uncertain Plant," *Electronics Letters*, vol. 31, no. 22, pp.1959-1960.

Rugh, J. W. and Shamma, J. S., 2000. "Research On Gain Scheduling", *Automatica* vol. 36, pp. 1401-1425.

Sadegh, N., Horowitz, R., Kao, W.W. and Tomizuka, M., 1990, "A Unified Approach to the Design of Adaptive and Repetitive Controllers for Robotic Manipulators," *Asme Journal Of Dynamic Systems, Measurement And Control*, vol. 112, pp. 618-629.

Saeki, M. and Hirayama, D., 1996. "Parameter Space Design Method of PID Controller for Robust Sensitivity Minimization Problem," *Transactions of the Society of Instrument and Control Engineers*, vol. 32, no. 12, pp. 1612-1619.

Saeki, M. and Kimura, J., 1997. "Design Method of Robust PID Controller and CAD System," *11th IFAC Symposium on System Identification*, pp.1587-1593.

Shaw, F. R. and Srinivasan, K., 1993, "Discrete-Time Repetitive Control System Design Using the Regeneration Spectrum," *Asme Journal Of Dynamic Systems, Measurement And Control*, vol. 115, pp. 228-237.

Skogestad, S. and Postlethwaite I., 1996. *Multivaribale Feedback Control*, John Wiley & Sons.

Srinivasan, K., Özbay, H. and Jung, I.S., 1995. "A Design Procedure for Repetitive Control Systems," *Proceedings of the ASME Dynamic Systems and Control Division*, DSC-vol. 57-1, pp. 581-593, 1995 ASME International Mechanical Engineering Congress and Exposition, San Francisco, Nov.

Srinivasan, K and Shaw, F. R., 1991. "Analysis and Design of Repetitive Control Systems Using the Regeneration Spectrum," *ASME Journal Of Dynamic Systems, Measurement And Control*, vol. 113, June, pp. 216-222.

Tomizuka, M., 1987. "Zero Phase Error Tracking Algorithm for Digital Control," *Journal of Dynamic Systems, Measurement and Control*, vol. 109, no. 1, pp. 65-68.

Tomizuka, M., Tsao, T.C. and Chew, K.K., 1989. "Analysis and Synthesis of Discrete-Time Repetitive Controllers," *ASME Journal of Dynamic Systems, Measurement, and Control*, Sept., pp. 353-358.

Tsao, T.C. and Tomizuka, M., 1994. "Robust Adaptive and Repetitive Digital Control and Application to a Hydraulic Servo for Noncircular Machining", *Journal of Dynamic Systems, Measurement and Control*, vol. 116, no. 1, pp. 24-32.

Tung, E., Anwar, G. and Tomizuka, M., 1991. "Low Velocity Friction Compensation and Feedforward Solution Based on Repetitive Control," *American Control Conference,* pp. 2615-2620, Boston.

Umeno T. and Hori Y., 1991. "Robust speed control of dc servomotors using modern two degrees-of-freedom controller design," *IEEE Trans. Ind. Electron.*, vol 38, no. 5, pp. 363-368.

Weiss G., 1997. "Repetitive Control Systems: Old and New Ideas," in C. Byrnes, B. Datta, D. Gilliam and C. Martin (Eds.), *Systems and Control in the 21st Century* (vol. 22, pp. 389-404), PSCT, Boston:Birkhäuser.

Weiss, G. and Häfele, M., 1999. "Repetitive Control of MIMO Systems Using H_∞ Design," *Automatica*, vol. 35, pp. 1185-1199.

Xia, J. Z. and Menq, C-H., 1990."Precision Tracking Control of Nonminimum Phase Systems and its Application to Noncircular Cutting," *Symposium on Automation of Manufacturing Processes*, DSC-vol. 22, pp. 95-99, ASME, New York.

Zhou, K., Doyle, J.C. and Glover, K., 1996. *Robust and Optimal Control*, Prentice Hall.

APPENDIX A

A.1 Properties of Structured Singular Value (SSV) μ

The first two properties of μ hold for both real and complex perturbations. The rest of the properties hold for only complex perturbations. The properties of μ are:

1. $\mu(\alpha M) = |\alpha| \mu(M)$ for any complex (or real) scalar α.

2. Let $\Delta = \mathrm{diag}\{\Delta_1, \Delta_2\}$ be a block diagonal perturbation (in which Δ_1 and Δ_2 may have additional structure) and let M be partitioned accordingly. Then

$$\mu_{\Delta}(M) \geq \max\{\mu_{\Delta_1}(M_{11}), \mu_{\Delta_2}(M_{22})\} \tag{A.1}$$

3. For a repeated scalar complex perturbation

$$\Delta = \delta I \ (\delta \text{ is a complex scalar}): \quad \mu(M) = \rho(M) \tag{A.2}$$

4. For a full block complex perturbation

$$\Delta \text{ full matrix}: \quad \mu(M) = \bar{\sigma}(M) \tag{A.3}$$

5. μ for complex perturbations is bounded by the spectral radius and the singular value (spectral norm)

$$\rho(M) \leq \mu(M) \leq \bar{\sigma}(M) \tag{A.4}$$

   This follows from (A.2) and (A.3), since selecting $\Delta = \delta I$ gives the fewest degrees of freedom for the optimization, whereas selecting Δ full gives the most degrees of freedom.

6. Consider any unitary matrix U with the same structure as Δ. Then

$$\mu(MU) = \mu(M) = \mu(UM) \tag{A.5}$$

7. Consider any matrix D which commutes with Δ, that is, $\Delta D = D\Delta$. Then

$$\mu(DM) = \mu(MD) \quad \text{and} \quad \mu(DMD^{-1}) = \mu(M) \tag{A.6}$$

8. Improved Lower Bound: Define $\mathcal{U}$ as the set of all unitary matrices U with the same block-diagonal structure as Δ. Then for complex Δ

$$\mu(M) = \max_{U \in \mathcal{U}} \rho(MU) \tag{A.7}$$

9. The result (A.7) is motivated by combining (A.5) and (A.4) to yield

$$\mu(M) \geq \max_{U \in \mathcal{U}} \rho(MU) \tag{A.8}$$

   The surprise is that this is always an equality. Unfortunately, the optimization in (A.7) is not convex and so it may be difficult to use in calculating μ numerically.

10. Improved Upper Bound: Define $\mathcal{D}$ to be the set of matrices D which commute with Δ (i.e. satisfy $D\Delta = \Delta D$). Then it follows from (A.6) and (A.4) that

$$\mu(M) \leq \min_{D \in \mathcal{D}} \bar{\sigma}(DMD^{-1}) \tag{A.9}$$

   This optimization is convex in D (i.e. has only one minimum, the global minimum) and it may be shown (Doyle, 1982) that the inequality is in fact an equality if there are 3 or fewer blocks in Δ. Furthermore, numerical evidence suggests that the bound is tight (within a few percent) for 4 blocks or more; the worst known example has an upper bound which is about 15% larger than μ (Balas et al., 1993).

11. Without affecting the optimization in (A.9), it may be assummed that the blocks in D to be Hermitian positive definite, i.e. $D_i = D_i^H > 0$ and for scalars $d_i > 0$ (Packard and Doyle, 1993)

   One can always simplify the optimization in (A.9) by fixing one of the scalar blocks in D equal to 1. For example, let D=diag$\{d_1, d_2, \ldots, d_n\}$, then one may without loss of generality set d_n=1.

12. The following property is useful for finding $\mu(AB)$ when Δ has the structure similar to that of A and B.

$$\mu_\Delta(AB) \leq \bar{\sigma}(A)\mu_{\Delta A}(B) \tag{A.10}$$

$$\mu_\Delta(AB) \leq \bar{\sigma}(B)\mu_{\Delta B}(A) \tag{A.11}$$

   Here the subscript ΔA denotes the structure of the matrix ΔA and $B\Delta$ denotes the structure of $B\Delta$.

CURRICULUM VITAE

Bilin AKSUN GÜVENÇ was born in Istanbul in 1972. She graduated from Terakki Vakfı Özel Şişli Terakki Secondary School in 1986 and Terakki Vakfı Özel Şişli Terakki High School with second ranking in 1989. She entered İstanbul Technical University, Department of Mechanical Engineering in 1989 and gained her bachelor of science degree in Mechanical Engineering in 1993. She entered the master program at İstanbul Technical University, Institute of Science and Technology, Department of Mechanical Engineering, Program of Robotics in September 1993 and gained her master of science degree in February 1996. She entered the Ph.D program at İstanbul Technical University, Institute of Science and Technology, Department of Mechanical Engineering, Program of Construction and Manufacturing in 1996. She passed her general exams on September 23, 1998. She worked as a guest researcher concentrating on her Ph.D thesis studies at the Institute of Robotics and Mechatronics at the German Aerospace Center at Oberpfaffenhofen (DLR-Oberpfaffenhofen) during the year 2000. She has been working as a research assistant at İstanbul Technical University's Department of Mechanical Engineering since January 1994. She is married. She speaks English and German.